NEUTRINO MASS AND OSCILLATION IN MATTER AND IN COSMOLOGY

By

Liguo Song

Dissertation

Submitted to the Faculty of the

Graduate School of Vanderbilt University

in partial fulfillment of the requirements

for the degree of

DOCTOR OF PHILOSOPHY

in

Physics

May, 2004

Nashville, Tennessee

Approved by

Prof. Thomas J. Weiler

Prof. Thomas W. Kephart

Prof. David J. Ernst

Prof. Akunuri V. Ramayya

Prof. Steven E. Csorna

To my parents, Baoqin Song and Jingfen Zhou

my brother, Liwen Song

and

my lovely girlfriend, Lin Tang

for their love and support.

ACKNOWLEDGMENTS

I would like to thank Dr. Thomas J. Weller and Dr. Thomas W. Kephart for the wonderful experience of studying and researching. Without their assistance, this thesis will never come into the current form. Dr. Weiler deserves specially appreciation as my mentor and friend both in physics and in life.

Special thanks are due to the other wonderful members of my Ph.D. committee: Dr. David J. Ernst, Dr. Akunuri V. Ramayya and Dr. Steven E. Csorna. Their invaluable advices and expertise are extremely helpful to improve this work.

Dr. Heinrich Päs, Mr. Marcin Jankiewicz, and Dr. Roman V. Buniy have all shared their insights with me in countless discussions. This work has benefited from the collaborations with Dr. Heinrich Päs, Dr. Ringwald, and Mr. Eberle significantly.

I also want to thank my friends the Department of Physics and Astronomy. Their companionship has made my lime in Vanderbilt University even more enjoyable. Dr. Hui Fang deserves special mention for his wonderful sense of humor and heated discussion.

My girlfriend, Lin Tang, has been my source of encouragement, support and happiness during the course of this work. Without her, my life would not be complete.

Finally, this work is specially dedicated to my parents, who have sacrificed so much to offer my brother and me the best opportunities.

TABLE OF CONTENTS

LIST OF TABLES

LIST OF FIGURES

CHAPTER I

INTRODUCTION
HISTORY AND CURRENT KNOWLEDGE OF THE NEUTRINO

1.1 Histories of Neutrino

The history of neutrinos, the knowledge of the thermal history of cosmological neutrinos and the discovery of neutrino properties, is a proud one for physicists, experimental and theoretical alike. Improvements in experimental techniques to study the universe and to measure neutrino oscillations offer more and more details to assist our understanding of neutrino properties. The analysis of data from the experiments, and the modeling of neutrino mass beyond the Standard Model (SM) are unveiling new physics for this new millennium.

1.1.1 Brief Thermal History of Neutrino

The thermal history of neutrinos is a relative simple one. After the birth of the universe, neutrinos are kept in equilibrium within the primordial plasma through reactions such as

$$\nu + \bar{\nu} \leftrightarrow e + e^{+},$$

$$\nu + e \leftrightarrow e + \nu.$$

About 1 second after the birth of the universe, when the temperature of the primordial plasma falls below 1 MeV, the rate for the above reactions becomes less than the expansion rate of the universe and the above reactions become too slow to keep neutrinos in equilibrium. Thus, neutrinos decouple from the primordial plasma. The neutrino mass, which is less than 1 eV, is much smaller than the decoupling temperature. So, the neutrino mass will not alter the decoupling temperature and the neutrino number density described in Reference [1] for massless neutrinos.

After decoupling, the neutrinos remain relativistic and free-stream through the universe. The free-streaming neutrinos will affect the power spectrum of the galaxy and the cosmic microwave background measured by the experiments such as WMAP [2], 2dFGRS [3], and SDSS [4].

The free-streaming neutrino becomes non-relativistic when the temperature of the universe drops below the mass of neutrino. This is about 50 thousands years after the birth of the universe. After the neutrino becomes non-relativistic, gravity begins to affect the distribution of relic neutrinos. This may result the local clustering of relic neutrinos around large cosmological structures. But detailed simulation revealed that the extent of the neutrino clustering is not significant [5, 6, 7, 8]. So, the neutrino number density from the standard cosmology will be used as the standard parameter.

To sum up, the mass of relic neutrinos will affect cosmic microwave power spectrum and the galaxy, which offers the inference of neutrino mass to the corresponding experiments. But, the tiny mass of relic neutrinos will not significantly affect their number density,

$$n_\nu = n_\nu^0(1+z)^3 = \frac{3}{22} n_\gamma^0 (1+z)^3$$

per flavor and per active spin state. Where the $n_\gamma^0 = 422$ cm^{-3} is the current number density of cosmic microwave photons obtained from

$$n_\gamma^0 = \frac{2\zeta(3)}{\pi^2} T^3,$$

where $\zeta(3) = 1.20$ is the Riemann zeta function of 3. With the current cosmic microwave background temperature $T_0 = 2.73$ K, consequently $n_\nu^0 = 56$ cm^{-3} is the current number density of relic neutrinos per flavors. Thus, we expect a total neutrino density of $3 \times 2 \times n_\nu^0 = 336$ cm^{-3}.

1.1.2 Brief History of Neutrino Studies

The history of neutrino discovery is a proud one for the theoretical physicists, not only because experimental verification followed theoretical prediction, but also because the discovery of neutrino saved one of the most precious conservation laws, the conservation of the energy.

Before the discovery of the neutrino, the observation of the continuous spectrum of the electron observed in beta decay experiments had raised the doubt about the conservation of energy, as the difference between the nucleon energy levels before and after the decay is not in agreement with the energy carried away by the electron, the only observed lepton

in the beta decay at that time. In 1930, to rescue the energy conservation, Pauli proposed in his letter to the attendees of a physics conference at Tübingen, Germany, that "neutral particles" named "neutron" also participated in the beta decay process and carried away the missing energy [9]. The neutron we know today was discovered later in 1932 [10], but it is too heavy to be Pauli's "neutron". So, in 1933, Fermi renamed Pauli's "neutron" to neutrino, a name which hints that the particle is neutral with small or even zero mass.

Twenty-six years after the naming of the neutrino, the neutrino was first detected in a nuclear reactor experiment by Cowan and Reines [11]. We now know this neutrino to be the electron neutrino ν_e. Then in 1962, the second neutrino type, the muon neutrino ν_μ, was observed by Dandy et al. [12]. The last known neutrino, the tau neutrino ν_τ, was not directly observed until 2001 by the DONUT Collaboration [13].

The determination of the neutrino mass is a more difficult task than the detection of the neutrino. Long before experiments could provide any valuable hints to the mass of neutrinos, the minimal Standard Model (SM) of particle physics provided a guess of zero mass. This "prediction" turned out to be not as successful as those of Pauli and Fermi. The first hint of neutrino mass was offered by the solar neutrino experiment begun in 1968, in which less than 1/3 of the theoretically predicted neutrino flux from the solar fusion cycles was observed [14]. This mystery was later dubbed the Solar Neutrino Puzzle. The first strong evidence for neutrino oscillation, thus neutrino mass, surfaced from the Super-Kamiokande experiment in 1998, which offered compelling data to support the oscillation of atmospheric muon neutrinos [15]. Earlier experiments, such as Kamiokande[1], had noticed the existence of an atmospheric neutrino-flavor "anomaly". Since the Super-Kamiokande, more neutrino oscillation experiments gathered data to support the oscillation of neutrinos.

1.2 Current Knowledge of Neutrino

During the past few years, many experiments have been carried out to study the properties of neutrinos, mainly the oscillation of neutrinos. The neutrino oscillation experiments include the solar, atmospheric and reactor-generated neutrino oscillation experiments.

[1]The predecessor of Super-Kamiokande experiment

Some of the successful solar neutrino oscillation experiments are Homestake [16], SNO [17], GALLEX [18], GNO [19], and SAGE [20], while some of the successful atmospheric neutrino oscillation experiments are Soudan2 [21] and MARCO [22]. The reactor neutrino oscillation experiments include CDHS [23], Bugey [24], CHOOZ [25], and KamLAND [26]. The controversial LSND [27] experiment uses a medium energy accelerator at Los Alamos National Lab to produce focused π^+ beams, whose decay produces neutrinos. The prestigious Super-Kamiokande experiment [28] observed both the atmospheric neutrino oscillation [15] and the solar neutrino oscillation [29]. In the ongoing K2K experiment [30], the Super-Kamiokande detector is the target for the neutrinos generated at the KEK accelerator in Japan. In the very near future, the two Fermi Lab experiments, MiniBooNE [31] and MINOS [32], will study oscillations at short and long baselines, respectively.

In addition to the above neutrino oscillation experiments, astrophysical experiments are also providing important information for properties of neutrinos. For example, WMAP [2], 2dFGRS [33], and SDSS [4] offered the best upper limit to the neutrino absolute mass. The light element abundance measurement from the big bang neucleosynthesis (BBN) provides the best astrophysical limit on the number of active flavor of neutrinos [34, 35].

Other experiments attempting to measure the absolute neutrino mass include the tritium beta decay and the neutrinoless double beta decay ($0\nu\beta\beta$). In tritium beta decay experiment, the neutrino mass will distort the endpoint of the electron spectrum. The upper limit of the neutrino mass square from the tritium beta decay experiments is

$$m_\nu^2 < 2.5 \text{ eV}^2,$$

while the best fit point to the data is a negative value [36]. This limit is more generous than the upper limit from the astrophysical experiments. The next generation tritium beta decay experiments, for example KATRIN [37], will be able to improve the limit down to the 0.3 eV^2 range [38].

The $0\nu\beta\beta$ experiment is very sensitive to the effective Majorana neutrino mass m_{ee} defined as

$$m_{ee} = \left| \sum_i U_{ei}^2 m_i \right|.$$

$0\nu\beta\beta$ experiments offer the upper limit on the effective Majorana neutrino mass $m_{ee} \leq$

0.55 eV [39]. But the result depends on the uncertain neutrino mixing matrix elements, and consequently is subjected to large systematic error. Reference [40] and the followup [41] have detailed reviews on the prospects of these two types of experiments.

The following is a summary of the neutrino properties gathered from the above experiments as discussed in References [42], [43], [44], [45], and [46].

1. Neutrino Mass-Squared Difference And Mixing Angles

   - Solar Neutrino Oscillation

     The Large Mixing Angle (LMA) region allowed by the solar experiment data at 3σ corresponds to

     $$\begin{aligned} 2.6 \times 10^{-5}\ \mathrm{eV}^2 \leq \quad & \delta m^2_{sol} \quad \leq 3.3 \times 10^{-4}\ \mathrm{eV}^2 \\ 0.26 \leq \quad & \tan^2\theta_{sol} \quad \leq 0.85. \end{aligned}$$

     The global best fit point locates at

     $$\begin{aligned} \delta m^2_{sol} &= 6.6 \times 10^{-5}\ \mathrm{eV}^2 \\ \tan^2\theta_{sol} &= 0.46. \end{aligned}$$

   - Atmospheric Neutrino Oscillation

     The global fit to the atmospheric neutrino oscillation data allows, at 3σ,

     $$\begin{aligned} 1.2 \times 10^{-3}\ \mathrm{eV}^2 \leq \quad & \delta m^2_{atm} \quad \leq 4.8 \times 10^{-3}\ \mathrm{eV}^2, \\ 0.3 \leq \quad & \sin^2\theta_{atm} \quad \leq 0.7. \end{aligned}$$

     The global best fit point occurs at

     $$\begin{aligned} \delta m^2_{atm} &= 2.1 \times 10^{-3}\ \mathrm{eV}^2 \\ sin^2\theta_{atm} &= 0.49. \end{aligned}$$

   - LSND Neutrino Oscillation

     The experiment data from the Liquid Scintillating Neutrino Detector (LSND) allow, at 90% C.L.,

     $$\begin{aligned} 0.2 \leq \quad & \delta m^2_{LSND} \quad \leq 2\ \mathrm{eV}^2 \\ 10^{-3} \leq \quad & \sin^2(2\theta_{LSND}) \quad \leq 3 \times 10^{-2} \end{aligned}$$

2. Number of Neutrino Flavors

   - Active Neutrinos

     The light element abundance measurement from BBN limits the total number of active neutrino flavors to be no more than 3 [34, 35].

   - Sterile Neutrino

     The three neutrino mass square differences of different orders, including the result from LSND, hint at the existence of a fourth neutrino. As the BBN constraint and the observed width of the Z^0 particle do not allow the fourth neutrino to participate in the weak interaction like the three active neutrinos, it is named "sterile" neutrino. The existence of the sterile neutrino is still a topic of heated debate.

3. Neutrino Absolute Mass

   - Heaviest Neutrino Mass

     The combination of the results from WMAP, 2dFGRS, and SDSS bounds the total mass of all relic neutrinos to [47]

     $$\sum m_i \leq 0.75 \text{ eV}.$$

     The total neutrino mass versus the heaviest neutrino m_3 in three-neutrino model is plotted in Fig. 1 [48]. It is allowed that at least one neutrino has mass of 0.24 eV's. The value of 0.2 eV will be used as the heaviest neutrino mass for the four-neutrino model in this work.

   - Neutrino Mass Spectrum

     There is currently not enough information to determine the neutrino mass spectrum because the signs of the neutrino mass-squared gaps have not be determined by the neutrino oscillation experiments. Moreover, the details of the mass spectrum are model dependent as will be briefly discussed later.

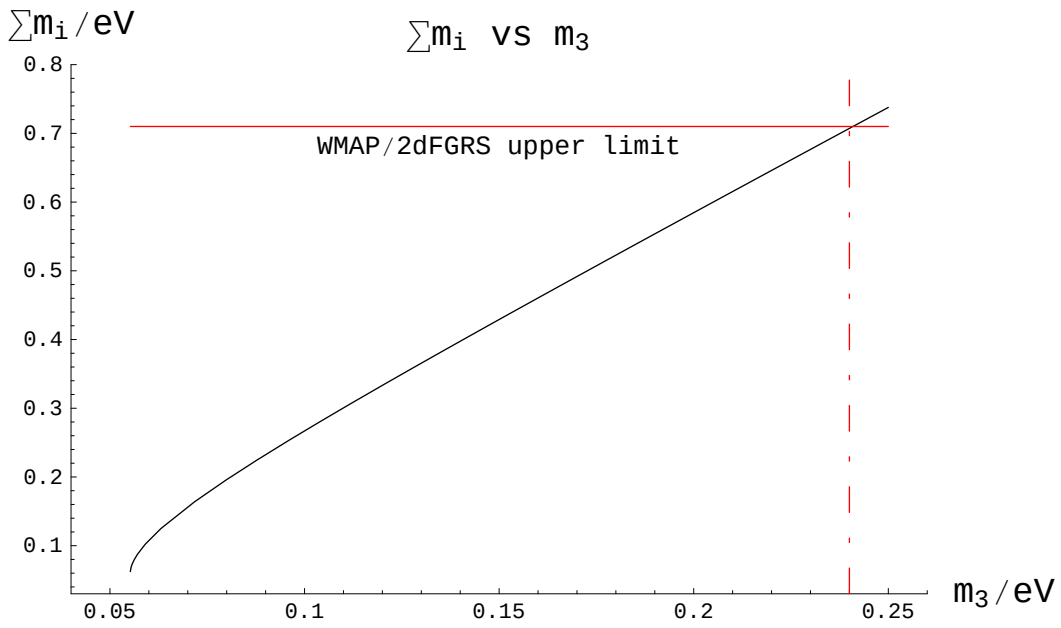

Figure 1: The Total Neutrino Mass versus The Heaviest Neutrino

PART ONE
NEUTRINO MASS AND Z-BURST MODEL

CHAPTER II

NEUTRINO MASS AND THE Z-BURST MODEL

2.1 The Original Z-Burst Model

The resonant annihilation of neutrinos from extremely high-energy neutrino cosmic rays (EHEνCR) on the big-bang relic cosmic neutrinos in the cosmic neutrino background (CνB) into Z-bosons (and vice versa), popularly known as Z-Burst Model, was originally proposed as an attempt to directly measure the big-bang relic neutrinos [49, 50], which only becomes possible with the recently proposed extremely-high energy cosmic ray detectors [51]. An even more challenging puzzle is the observation of the cosmic rays with energy much higher than the Greisen-Zatsepin-Kuzmin (GZK) cut-off energy, $E_{GZK} = 5 \times 10^{19}$ eV [52, 53, 54]. The nature and origin of these extremely-high energy cosmic rays (EHECR's) are still an unsolved mystery. Many models have been proposed to explain this controversial phenomena. Some are within the conventional physics [55, 56], and others involve new physics [57, 58]. Yet, the secondary particles in the Z-Burst process, which is caused by EHEνCR above the GZK cut-off energy, is one of the models to offer plausible explanations of this phenomena [59]. Recent studies comparing different proposals to measure the neutrino mass recommended the Z-Burst Model as one of the most promising ways to detect the CνB and measure the absolute neutrino mass in the near future [60, 61]. The recently proposed extremely high-energy cosmic ray observatories [62, 63, 64, 65] may offer enough statistics for the detailed study of Z-Burst Model's prediction in this decade.

The Z-Burst model was originally proposed in 1982 [49], with the matter dominated flat cosmology model. The progress in the measurement of the cosmological parameters, especially the recent results from WMAP experiment [66], depict a very different universe. Noticeably the large value of cosmological constant, Λ, will change the evolution history of the universe, thus introduces quite different signatures of the Z-Burst Model.

These new interests and new developments demand a revision of the original Z-Burst Model, which was proposed nearly two decades ago when massless neutrinos were firmly

planted in the Standard Model.

2.2 Improve The Z-Burst Model With New Cosmology Model

The original Z-Burst Model was proposed under the assumption of neutrino mass and the matter dominated flat standard cosmology model. The former has been proved by the neutrino oscillation experiments [15], while the latter was not as successful. Furthermore, the absorption dip, the major signal of the Z-Burst Model in the neutrino cosmic ray spectrum is very sensitive to the source density distribution of the EHEνCR. But the lack of information on the origins of the EHEνCR prevents us from any knowledge of the distribution of the sources.

The annihilation of a neutrino and a relic anti-neutrino has a resonance at the energy

$$E_Z^{res} = \frac{M_Z^2}{2m_\nu} = 4.16 \times 10^{21} \left(\frac{1 \text{ eV}}{m_\nu}\right) \text{ eV}, \tag{1}$$

where $M_Z = 91.2$ GeV [67] and m_ν is the mass of the neutrino.

Recent studies of the cosmological parameters, especially WMAP [66] and the more recent SDSS [68] experiment, favor a flat universe with $\Omega_M = 0.3$, $\Omega_k = 0$, and $\Omega_\Lambda = 0.7$. With this updated model of the universe and following the original work [49, 50], it is very easy to find the transmission probability of a neutrino cosmic ray starting at redshift z and arriving at earth with energy E_0

$$P(E_0, z) = \Theta\left(1 - \frac{E_0}{E_Z^{res}}\right) \Theta\left((1+z)\frac{E_0}{E_Z^{res}} - 1\right) e^{-\tau(E_0)}, \tag{2}$$

with

$$\Theta(x) = \begin{cases} 0, & \text{if } x < 0 \\ 1, & \text{if } x \geq 0 \end{cases} \tag{3}$$

and

$$\tau(E_0) = \frac{2\sqrt{2}\pi G_F n_\nu^0}{H_0} \frac{(E_Z^{res}/E_0)^3}{\sqrt{\Omega_M (E_Z^{res}/E_0)^3 + \Omega_k (E_Z^{res}/E_0)^2 + \Omega_\Lambda}}. \tag{4}$$

Where $G_F = 1.17 \times 10^{-5}$ GeV^{-2} is the Fermi coupling constant, n_ν^0 is relic neutrino number density at today, $H_0 = h \times 100$ km/s/Mpc is the present value of the Hubble constant, Ω_M, Ω_k and Ω_Λ are the ratio of present matter, curvature, and cosmological constant density to

the critical density. As mentioned earlier, the WMAP and SDSS experiments have provided conclusive measurements for these parameters. The default values for these parameters will be $\Omega_M = 0.3$, $\Omega_k = 0$, and $\Omega_\Lambda = 0.7$ [68, 66].

Eqn. 4 is the non-relativistic approximation discussed in the original work [49]. This is still good approximation even though the neutrino mass is not as big as expected then. As discussed earlier in Sect. 1.2, the heaviest neutrino will have a mass around 10^{-1} eV, which is still significant larger than the momentum, around 0.7 meV, of the relic neutrinos. So at least for the heaviest neutrinos, Eqn. 4 will still be very accurate.

2.3 Neutrino Cosmic Ray Spectroscopy

There is no credible information on the origins of the EHEνCR's due to the lack of observations of the EHECR's. Several large EHECR detectors have been proposed recently. These include the EUSO [62], IceCube [64], Pierre Auger Observatory [65], OWL [63]. The future data from these experiment may offer enough neutrino events to study the Z-Burst absorption dip. But as these experiments will only measure the observable spectrum of the EHEνCR's, it is necessary to have a look of all the contributing factors to the observable neutrino cosmic ray spectroscopy.

2.3.1 Extremely High-Energy Neutrino Cosmic Ray Emission Spectrum

It is well known that the spectrum of cosmic rays follows a power law, with only slight changes of the exponential coefficient at the knees [69, 70]. Thus, it is natural to propose that the extremely high-energy neutrino cosmic ray spectrum of a single source also follows this power law:

$$f(E, z) = E^{-\alpha}, \tag{5}$$

where z is the redshift at the source. Replacing the initial energy of the neutrino cosmic with the energy observed on earth, this becomes

$$f(E_0, z) = (1 + z)^{-\alpha} E_0^{-\alpha}. \tag{6}$$

This spectrum, Eqn. 10, is in arbitrary units and is scale invariant.

2.3.2 Source Distribution of Extremely High-Energy Neutrino Cosmic Rays

There is no enough information, from either experiments or theories, to determine the source distribution of EHEνCR's. But due to the important role that the source distribution plays in the observable neutrino cosmic ray spectrum, models of the source distribution will be proposed as guidelines for the future observation of the observable absorption spectrum.

The first model is a Gaussian distribution centered at z_0 with standard deviation of σ. Thus the source distribution can be described with

$$s'(z) = s_0 e^{-\frac{(z-z_0)^2}{2\sigma^2}}. \tag{7}$$

The unit of this source distribution is number per comoving volume. If converted to the physical volume, it becomes

$$s(z) = \frac{s_0}{(1+z)^3} e^{-\frac{(z-z_0)^2}{2\sigma^2}}. \tag{8}$$

This model is inspired by the observation of the galaxies and intergalactic matter clustering at high redshift [71]. The galaxies and intergalactic matter clustering can be described as a Gaussian distribution centered at $z_0 = 3.0$ with dispersion $\sigma = 0.25$ [72]. Also, this Gaussian distribution model can represent a whole class of source distributions, in which the neutrino cosmic ray sources are located mainly around a center at a specified redshift and the density decreases toward both lower and higher redshift. The contribution of the parameters in this model will be studied in details in latter sections.

The second model is a Step-function distribution model, just a simple rectangle distribution in the comoving coordinates, characterized by the two limits z_{min} and z_{max}. To ease the comparison with the Gaussian distribution, the two limits z_{min} and z_{max} can be replaced by the center of the source $z_0 = (z_{min} + z_{max})/2$ and the half-width of the source density distribution $w_{1/2} = (z_{max} - z_{min})/2$. The source distribution can be described as

$$s(z) = \frac{1}{(1+z)^3} \Theta(z - z_0 + w_{1/2}) \Theta(z_0 + w_{1/2} - z). \tag{9}$$

Again, the factor of $(1+z)^{-3}$ is coming from the conversion from comoving volume to the physical volume. This model also represents a whole class of source distributions, in which the the neutrino cosmic ray source density rarely changes at different redshift, except beyond the two cutoff limits.

The above two models will be used in the study of the EHEνCR spectroscopy in the following sections. Other models of interest have been investigated [51]. Together, these models of the source distribution of EHEνCR should span the possibilities for the Z-Burst absorption dip.

2.3.3 Relative Observable Spectrum of Neutrino Cosmic Ray

With all the information discussed above, the observable EHEνCR spectrum on earth can be calculated as following

$$F(E_0) = \int_0^\infty \frac{s(z)}{H(z)} f(E_0, z) P(E_0, z) dz, \tag{10}$$

where

$$H(z) = H_0 \sqrt{\Omega_M (1+z)^3 + \Omega_k (1+z)^2 + \Omega_\Lambda}.$$

Due to the complexity of the transmission probability, $P(E_0, z)$, there is no general analytic solution for the observable spectrum $F(E_0)$. Numerical method will be used to study the details of the observable spectrum $F(E_0)$.

The observable spectrum of the EHEνCR's on earth will still be a power-law spectrum, with an absorption dip starting at $E_Z^{res}/(1+z_{max})$ and ending at E_Z^{res}, where z_{max} is the maximum redshift of the EHEνCR sources. A typical power-law spectrum is shown in Fig. 2.

In this plot, the Z-Burst absorption dip is not very significant. One way to enhance the absorption dip is to plot the ratio of the observable spectrum with absorption against the observable spectrum without absorption of the neutrino cosmic ray, named Relative Observable Spectrum (ROS). The same absorption dip as in Fig. 2, but in Relative Observable Spectrum, is plotted again in Fig. 3. It is clear that this plot significantly enhances the absorption dip's visibility. Another reason to adopt the ROS is to compare the different source density distributions and the different spectra of neutrino cosmic ray. By using the ROS, there is no need to unify the source distributions and spectrum of neutrino cosmic ray. The differences in the ROS will be strictly coming from the contribution of the different source density distributions and the different spectra of the neutrino cosmic ray.

Some cautions have to be exercised when using the Relative Observable Spectrum to analyze the EHEνCR's data. First of all, the observable spectrum without absorption of the

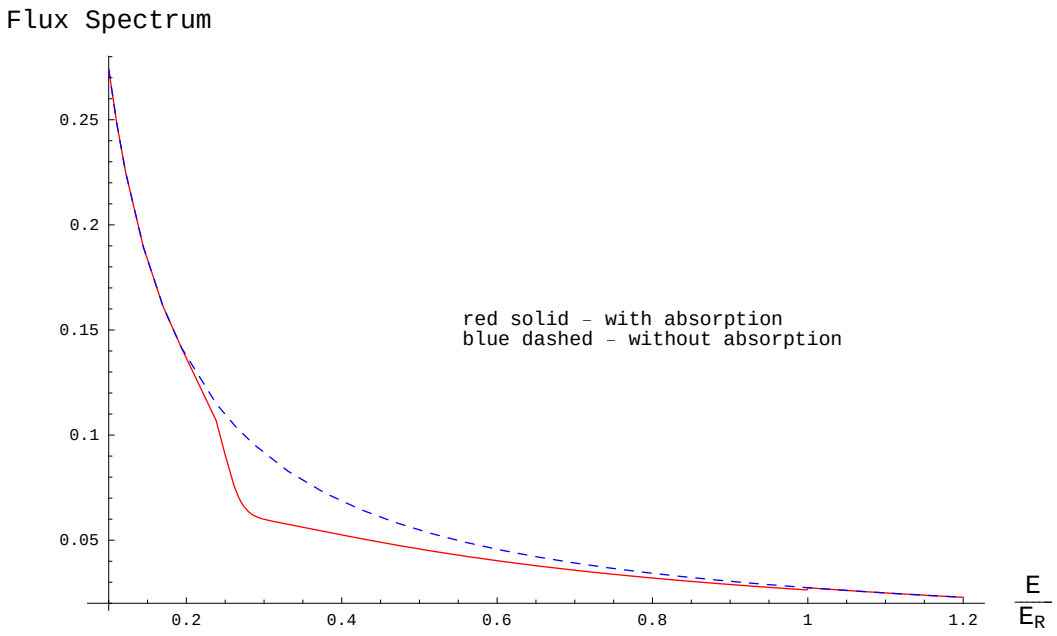

Figure 2: The Observable Spectrum of Neutrino Cosmic Ray

neutrino has to be deduced from the observed spectrum with the Z-Burst absorption dip. This has to use parts of the spectrum outside of the Z-Burst absorption dip. It is possible that there are also the "knee" structures like those in the cosmic ray spectrum at energy of 4 PeV and 400 PeV [69, 70]. In this case, the proper deduction of the observable spectrum will be tricky and has to be exercised with caution. Second, the statistical error at the high energy end will be much bigger than that at the low energy end of the Z-Burst absorption dip. This is a natural result of the power-law spectrum, which presents significantly less flux at the high energy end of the spectrum. This will reduce the significance of the absorption dip at the high energy end, so this part of the absorption dip has to be handled carefully. But the maximum of the Z-Burst absorption dip is usually located close to the low energy end. Thus, the step-up statistical error wouldn't downplay the role of the maximum in the Z-Burst absorption dip very much.

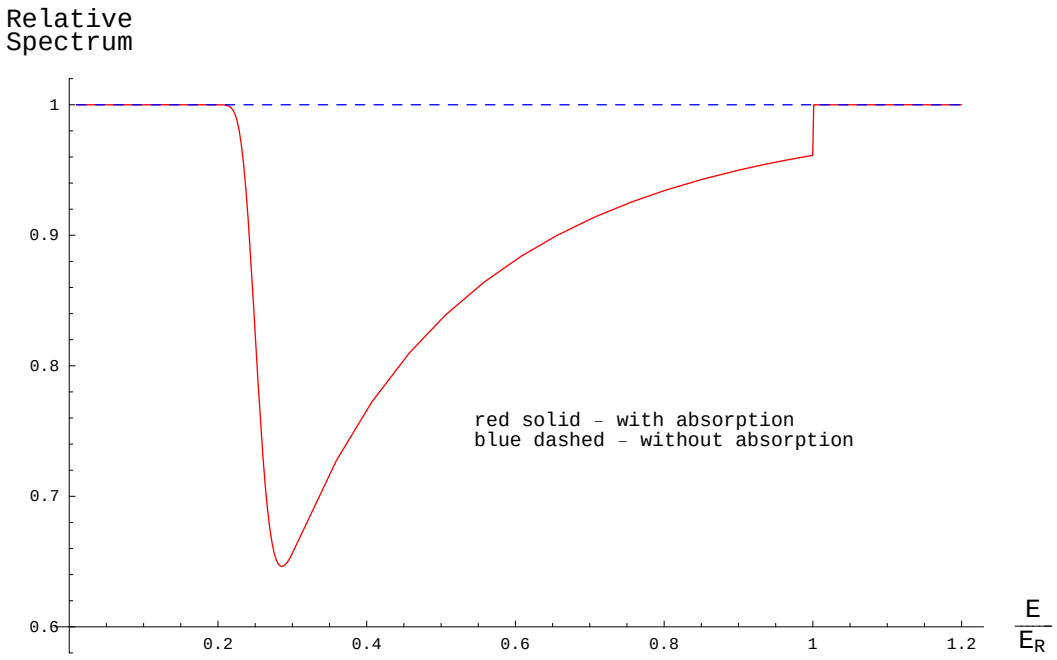

Figure 3: The Relative Observable Spectrum of Neutrino Cosmic Ray

2.4 Overview

The improved Z-Burst Model, with the new cosmology model and the reasonable models for the source density distribution of the extremely high-energy neutrino cosmic rays, makes is possible to study the Z-Burst absorption dip in the spectrum of the neutrino cosmic rays. The definition of the Relative Observable Spectrum (ROS) in Eqn. 10 is helpful to enhance the visibility of the Z-Burst absorption dip. It is extremely helpful in the study of the contributions from different parameters in the Z-Burst Model. The numerical calculation and the results of the relative observable spectrum of the extremely high-energy neutrino cosmic rays will be presented in the following chapter, and the contributions from different parameters will be studied in details.

CHAPTER III

NUMERICAL CALCULATION AND RESULTS OF THE Z-BURST ABSORPTION DIP

Using theoretical preparation of Relative Observable Spectrum of neutrino cosmic rays to study the Z-Burst absorption dip in the previous chapter, numerical calculation can now be carried out. We identify the major contributing parameters in the Z-Burst Model and the major signatures of Z-Burst absorption dip in the Relative Observable Spectrum of neutrino cosmic ray.

3.1 Overview of the Method and the Study

3.1.1 The Numerical Integration Method

Due to the complicated form of the transmission probability **T** of the neutrino cosmic ray described in Eqn. 2, it is impossible to calculate the final absorption spectrum analytically. So, numerical methods will be used to carry out the integration to achieve the final spectrum. All the numerical integration is carried out by the **NIntegrate** function, with the default setting, in Mathematica© 5.0 [73]. The **NIntegrate** function utilizes the adaptive Gauss-Kronrod method. The accuracy of this numerical integration method is sufficient for the study in this work.

For the Gaussian source distribution, the numerical integration is carried out in the range of redshift $z = 0 \sim 1000$. The upper limit of $z = 1000$ is sufficiently larger than the center of the Gaussian distribution. For the Step-function source distribution, the range of numerical integration is finite over the range $z = z_{min} \sim z_{max}$.

3.1.2 The Parameters of Z-Burst Model

In the calculation of the Relative Observable Spectrum of neutrino cosmic ray, there are a total of seven parameters involved. Some parameterize cosmology, such as the mass energy

fraction Ω_M, the curvature energy fraction Ω_k, the Hubble constant h, and the relic neutrino number density n_0, while others parameterize the properties of the neutrino cosmic ray source distribution, such as the center of the neutrino cosmic ray source distribution z_0, the half-width of the source distribution $w_{1/2}$ in the step-function case or the standard deviation σ of the Gaussian source distribution, and the coefficient of the power-law spectrum α. The different contributions of these parameters to the final results of the Relative Observable Spectrum of neutrino cosmic ray will be investigated in next section. The default values of these parameters, be used if not specified otherwise, are

$$\begin{array}{lll} \Omega_M = 0.3, & \Omega_k = 0, & h = 0.70, \\ z_0 = 3, & \alpha = 1, & n_0 = 56 \text{ cm}^{-3}, \\ \sigma = 0.25 & \text{or} & w_{1/2} = \sqrt{2\log 2}\sigma = 0.29. \end{array}$$

The Relative Observable Spectrum (ROS) with these standard parameters is plotted in Fig. 4.

3.2 The Non-Contributing Parameters

The parameters, Ω_k, Ω_M, h, and α, have relatively less significant contributions to the Relative Observable Spectrum of neutrino cosmic ray than the others. Uncertainties in their values barely affect the Z-Burst absorption dip in the Relative Observable Spectrum. We describe them now.

3.2.1 The Curvature Energy Fraction Ω_k

The curvature energy fraction Ω_k, the mass energy fraction Ω_M and the cosmological constant fraction Ω_Λ are confined by the relationship $\Omega_M + \Omega_k + \Omega_\Lambda = 1$. So, they cannot vary independently. In this study, only Ω_k and Ω_M will be explicit, while Ω_Λ will be defined by the above relation. Fig. 5 shows that the curvature energy fraction Ω_k has a very small contribution to the value of the transmission probability $\mathbf{T}$ of neutrino cosmic ray. So, it will not have any significant contribution to the Z-Burst absorption dip in the Relative Observable Spectrum of the neutrino cosmic ray. In recent years, the cosmological microwave background experiment WMAP [2] and the galaxy power spectrum experiment SDSS [4] have

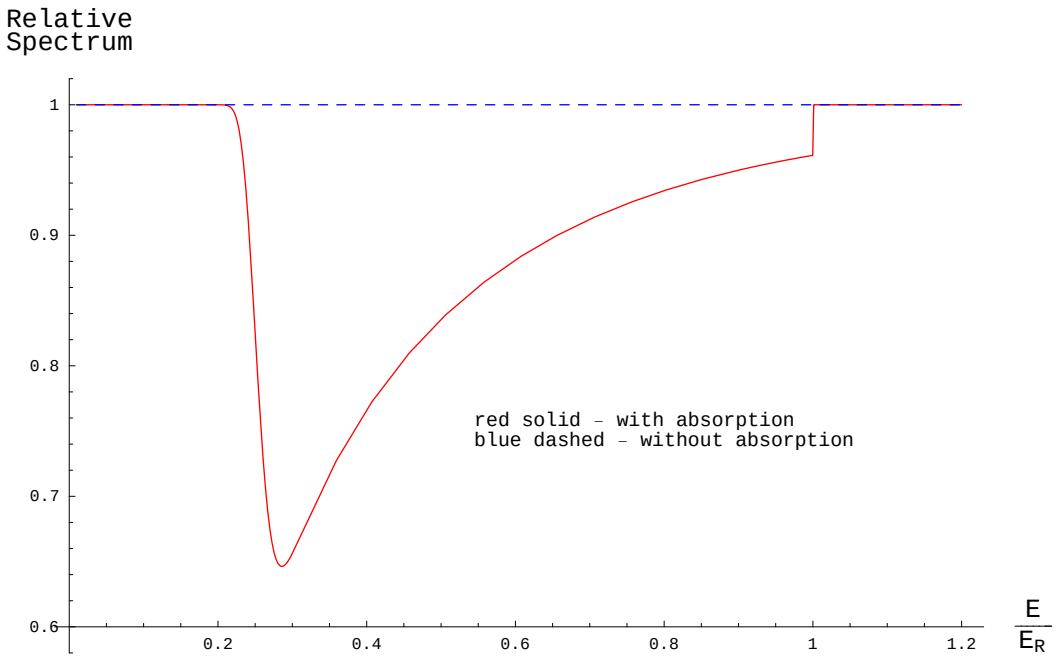

Figure 4: The Standard ROS of Neutrino Cosmic Ray

provided surprisingly accurate measurements of the flatness of our universe. Based on their results, $\Omega_k = 0$ will be used in all the numerical calculation of the Relative Observable Spectrum.

3.2.2 The Mass Energy Fraction Ω_M

The contribution of the mass energy fraction Ω_M to the neutrino cosmic ray transmission probability is shown in Fig. 6, and the contribution to the Relative Observable Spectrum of neutrino cosmic ray with a Gaussian source distribution is shown in Fig. 7. From these plots, it is obvious that Ω_M will significantly affect the Z-Burst absorption dip. But due to the relatively small uncertainty of the measured mass energy fraction density, $\Omega_M = 0.3$ [74] will be fixed in the numerical calculation and won't be treated as a contributing parameter.

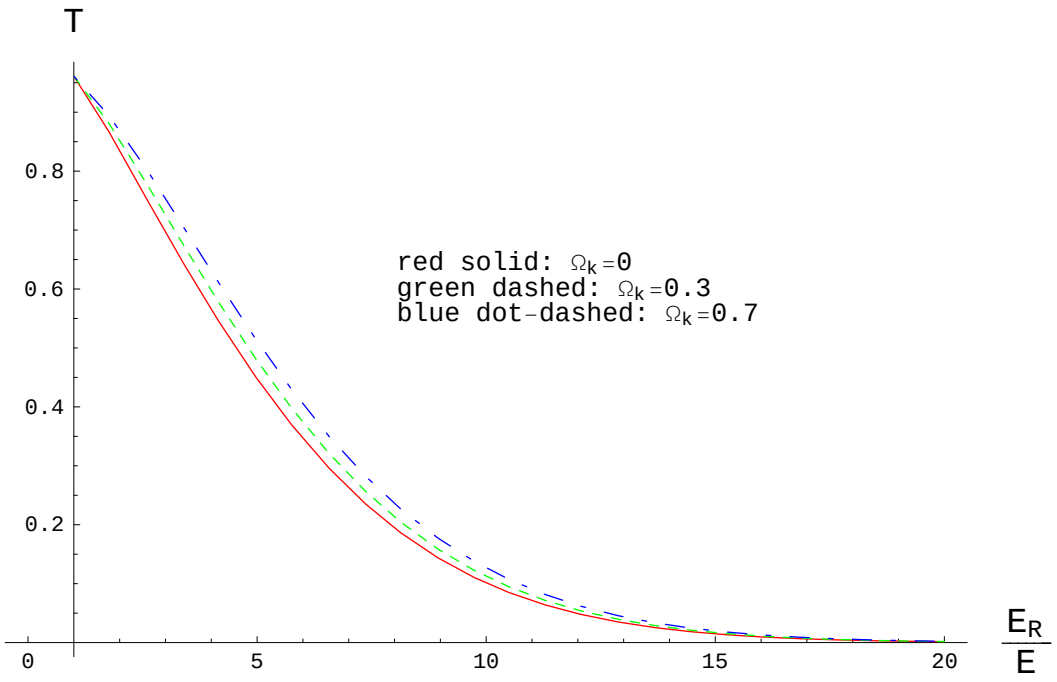

Figure 5: The Contribution of Ω_k to Transmission Probability $\mathbf{T}$

3.2.3 The Hubble Constant h

The contribution of the Hubble constant h to the neutrino cosmic ray transmission probability $\mathbf{T}$ is shown in Fig. 8, and the contribution to the Z-Burst absorption dip in the Relative Observable Spectrum of the neutrino cosmic ray from a Gaussian source distribution is shown in Fig. 9. Just like the mass energy fraction Ω_M, the Hubble constant's value does affect the Z-Burst absorption dip significantly. But due to the accurate measurement of the value of the Hubble constant h [74], the small uncertainty of h will not play a big role in the study of the Relative Observable Spectrum of neutrino cosmic ray.

3.2.4 Coefficient of the Power-Law Spectrum α

The coefficient of the power-law spectrum α plays a more complicated role to the Z-Burst absorption dip in the Relative Observable Spectrum of neutrino cosmic ray. In Fig. 10, the Relative Observable Spectra of neutrino cosmic ray with different power-law spectra

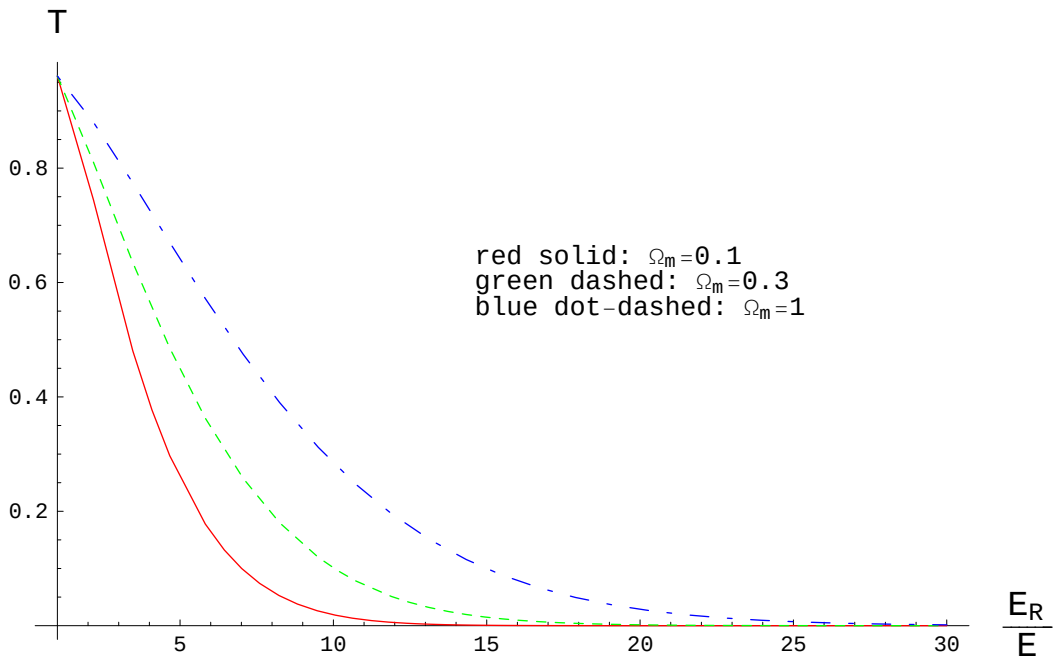

Figure 6: The Contribution of Ω_M in Transmission Probability $\mathbf{T}$

coefficient α from the same Gaussian source distribution are shown. It is quite obvious that the value of α doesn't make much difference here. In fact, the maximum difference of the Relative Observable Spectrum of neutrino cosmic ray between $\alpha = 1$ and $\alpha = 3$ is about 3%. But in our related work [51], it is shown that the value of α for a power-law source distribution, extended over $z_{min} = 0$ to $z_{max} \gg 1$. This source distribution produces a shallower absorption dip, in which the relative difference caused by the coefficient of the power-law spectrum α is more significant. It is worth pointing out that the power-law spectrum coefficient α only causes a difference of 3% in the depth of the absorption dips in both works. So in conclusion, the coefficient of the power-law spectrum will play a more significant role for an extended source distribution than for a localized source distribution. In this work, α will be treated as a non-contributing parameter as only localized neutrino cosmic ray source distributions will be studied.

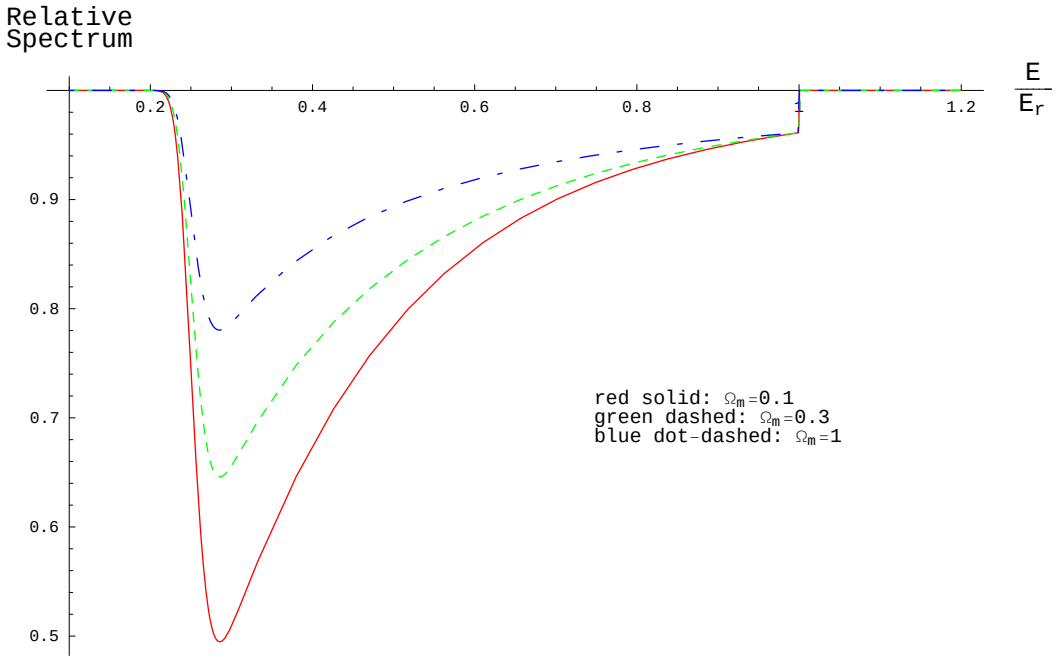

Figure 7: The Contribution of Ω_M to the ROS of Neutrino Cosmic Ray

3.3 The Contributing Parameters

The major contributing parameters are the mass of neutrino m_ν, the relic neutrino number density n_0, and the parameters describing the neutrino cosmic rays source distribution. The detailed signatures of these parameters in the Z-Burst absorption dip in the Relative Observable Spectrum of neutrino cosmic rays will be studied here.

3.3.1 The Mass of Neutrino

Determination of the absolute mass of neutrino is the major motivation in our study of the Z-Burst absorption dip. So it is vital to be able to Two methods can be used to extract the mass from the Z-Burst absorption dip in the Relative Observable Spectrum of neutrino cosmic rays.

The first one is to use the high-energy "edge" of the Z-Burst absorption dip. Fig. 11 shows the Z-Burst absorption dip in the Relative Observable Spectrum of neutrino cosmic

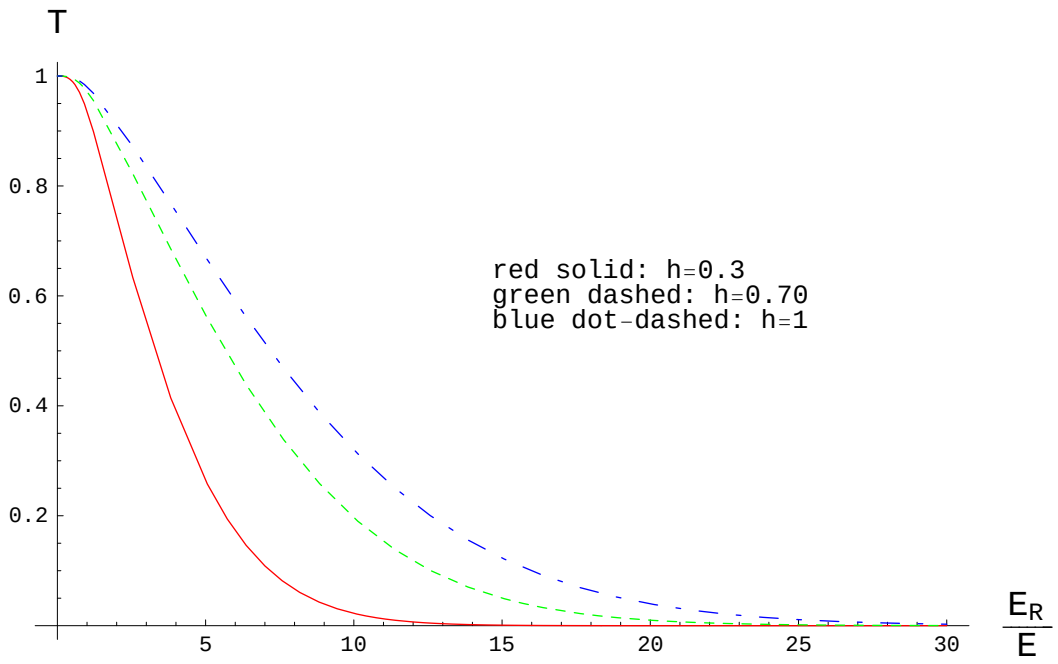

Figure 8: The Contribution of h to Transmission Probability $\mathbf{T}$

rays resulting from a Gaussian source, for a neutrino of mass $m_\nu = 0.2$ eV. The dip on the higher energy end is the "edge" corresponding to the Z-Burst resonant energy E_Z^{res} in Eqn. 1. The absolute neutrino mass is simply

$$m_\nu = \frac{M_Z^2}{2E_Z^{res}}.$$

But the fact that the "edge" is at the higher energy end reduces the practicality of this method. As discussed in Section 2.3.3, the power-law spectrum of cosmic ray energies will offer significantly less events at the higher energy end of the dip. This will reduce the statistics of the "edge". Also, the "edge" comes from the Z-Burst absorptions happening at nearby volume with $z \sim 0$. With the relic neutrino number density $n_\nu = n_\nu^0(1+z)^3$, this means small event number, thus the shallow edge. Eventually, with the improvement of the total number of observed events, the "edge" will lead to the ultimate result for the absolute mass of neutrino.

The second method is to get the neutrino absolute mass from the position of the maximum

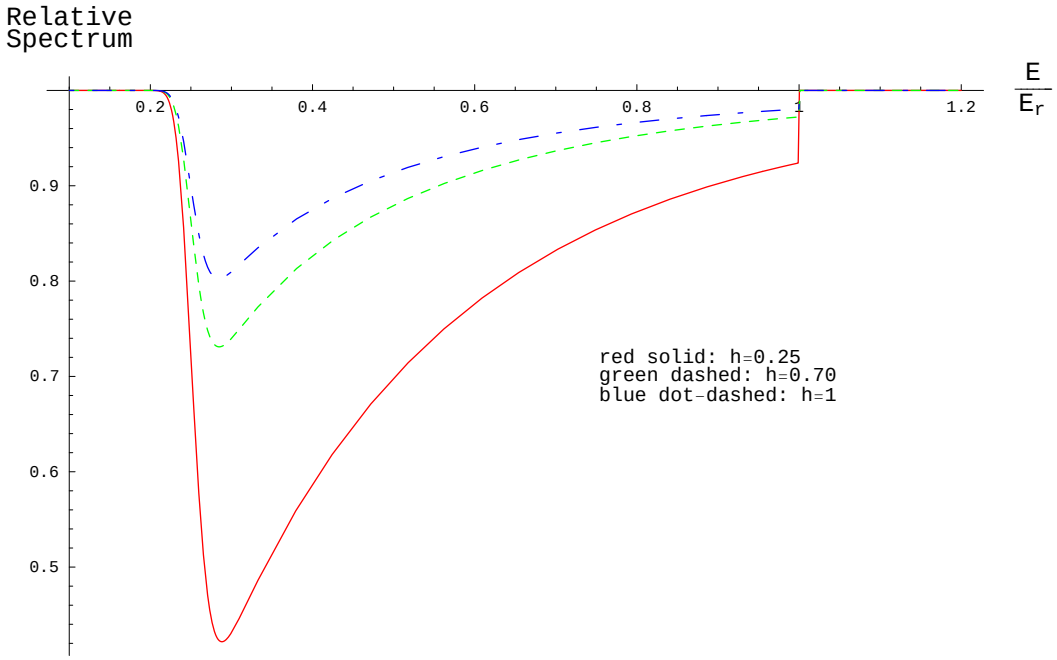

Figure 9: The Contribution of h to the ROS of Neutrino Cosmic Ray

of the Z-Burst absorption dip. Due to the depth of the absorption dip, nearly 20% in the case of Fig. 11, the maximum is much easier to identify than the edge in the Relative Observable Spectrum of neutrino cosmic ray with relatively few observed events. The maximum of the Z-Burst absorption dip usually locates between $0.2E_Z^{res}$ to $0.7E_Z^{res}$. The exact position is also determined by the source distribution of the neutrino cosmic rays. It would be possible to deduce the neutrino absolute mass within a order of magnitude of the neutrino absolute mass without any further information about the neutrino cosmic ray source distribution. More information of the neutrino cosmic ray source distribution will certainly help to improve the accuracy. This method is model dependent and has to be used with caution to infer the neutrino absolute mass.

Other helpful information that the Z-Burst absorption dip in the Relative Observable Spectrum of neutrino cosmic rays can offer is the mass spectrum of the neutrino. Fig. 12 and Fig. 13 show the Relative Observable Spectra for equal fluxes of the three different

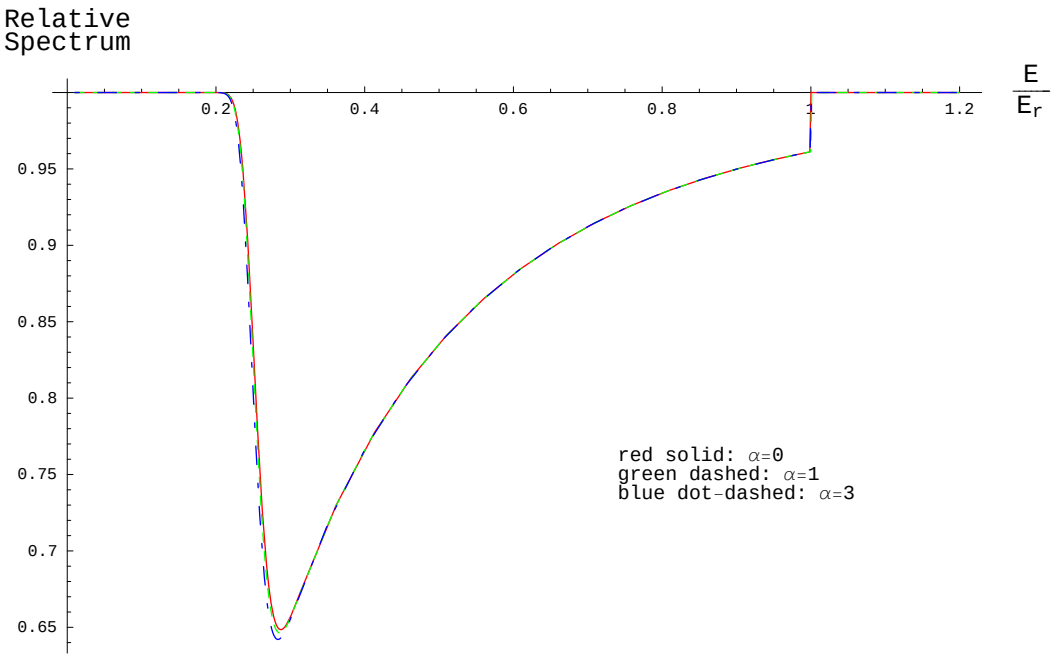

Figure 10: The Contribution of α to the ROS of Neutrino Cosmic Ray

neutrinos. Fig. 12 shows the case of the well-separated neutrino mass spectrum, in which all the masses are simply deduced from the measured solar, atmospheric and LSND mass square differences. In this case, the absorption dips of the different masses are well separated. But, the depths of the absorption dips are significantly reduced, about 1/3 of the neutrino flux with single mass eigenstate. This is due to the fact that the cosmic rays of the other two neutrinos will not be absorbed within the absorption dip of the third neutrino. This will significantly increased the number of events required to identify the absorption dips. Another difficulty in this case is the extremely high resonance energy for the light neutrinos. For neutrino mass of a few 10^{-1} eV, the resonance energy is between 10^{21} to 10^{22} eV. This energy scale is within the reach of the proposed extremely high-energy cosmic ray observatories [62, 63, 64, 65]. But for neutrino mass at much lighter scale, such as 10^{-3} eV, the resonant energy will be above 10^{24} eV. There is likely much less flux, and more aggressive experiments are needed to detect the Z-Burst absorption dip. These experiments are unlikely to exist in the next

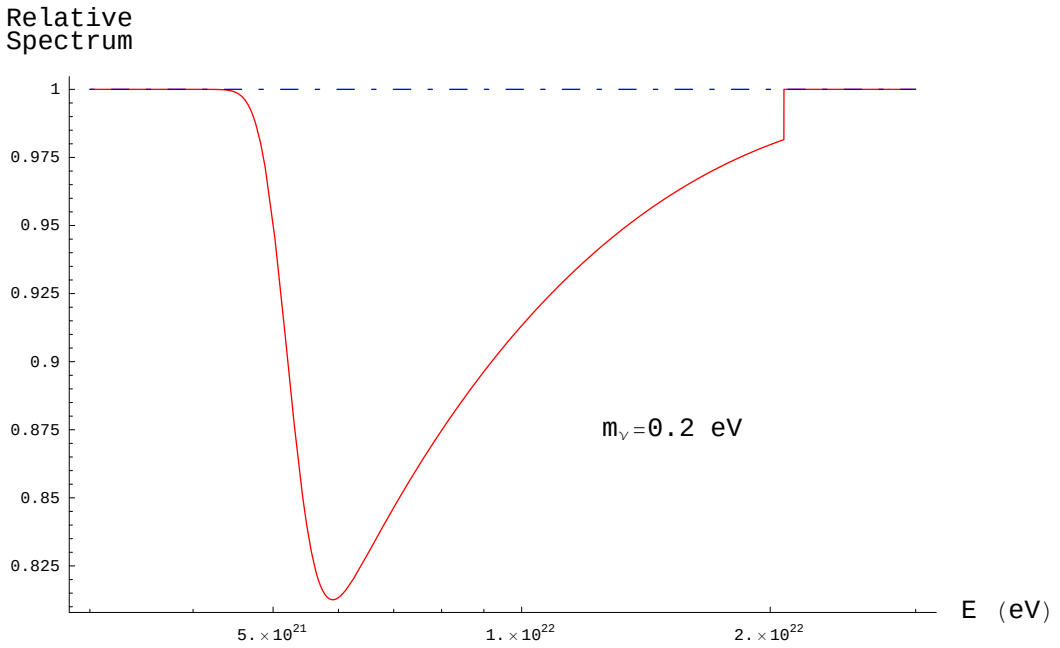

Figure 11: The ROS of Neutrino Cosmic Ray for neutrino mass $m_\nu = 0.2$ eV

couple of decades.

Another case is the degenerate mass spectrum, shown in Fig. 13. In this case, the measured solar and atmospheric mass gaps are small perturbations about a mean mass of a few 10^{-1} eV. Nearly the same absorption dip as for a single neutrino flux results, but with a slightly deformed "edge". It would be impossible to resolve the structure of the edge here, even if a considerable amount of events can be gathered. But the benefit of this degenerated spectrum is that absorption dip is deep.

Comparing these two possible mass spectra of neutrino, the degenerate mass spectrum will be more generous to the possible observation of the Z-Burst absorption dip. This hints that one would not be able to determine the mass spectrum of the neutrinos by the Z-Burst absorption dip alone. Ultimately, the neutrino oscillation experiments have to be used to establish the neutrino mass spectrum.

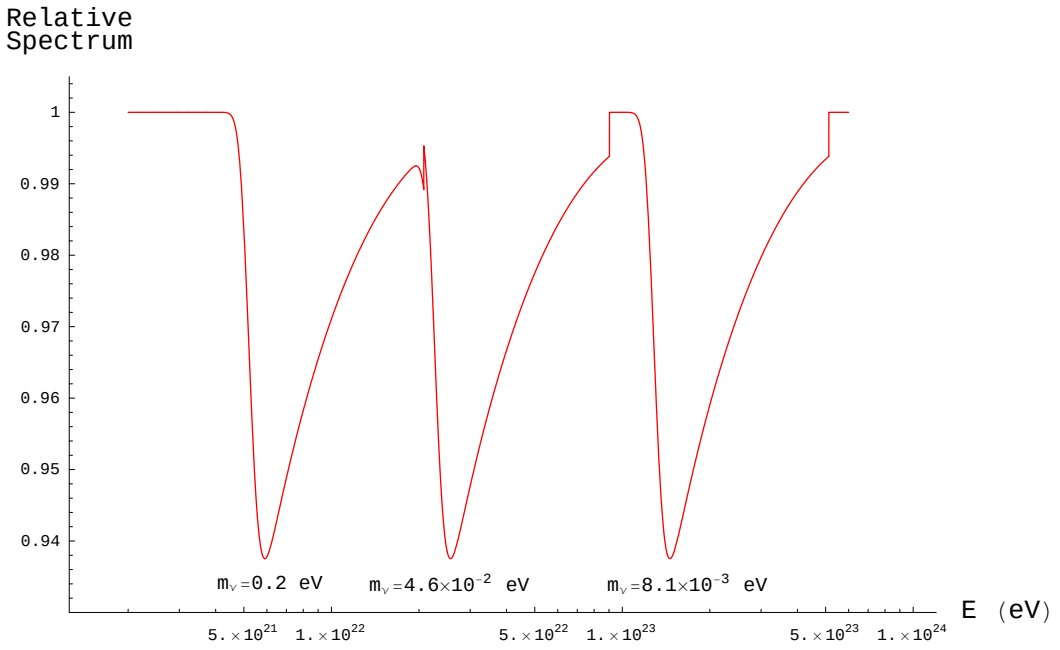

Figure 12: The ROS of Neutrino Cosmic Rays Composed of Equal Flux of Neutrinos with $m_{\nu_j} = 8.1 \times 10^{-3}$, 4.6×10^{-2}, 0.2 eV

3.3.2 Relic Neutrino Number Density n_0

Another factor that will significantly affect the Z-Burst absorption dip is the relic neutrino number density n_0. The hot Big-Bang cosmology is very successful at predicting the relic cosmic microwave background. It also leads to a very precise prediction for the number density of relic neutrinos. Yet, there is still no observation to back up this prediction, unlike the case of the cosmic microwave background.

Fig. 14 shows the relic neutrino number density n_0 will significantly affect the depth of the Z-Burst absorption dip. With this knowledge, it would be possible in principle to calibrate the relic neutrino number density and check the prediction of the hot Big-Bang cosmology.

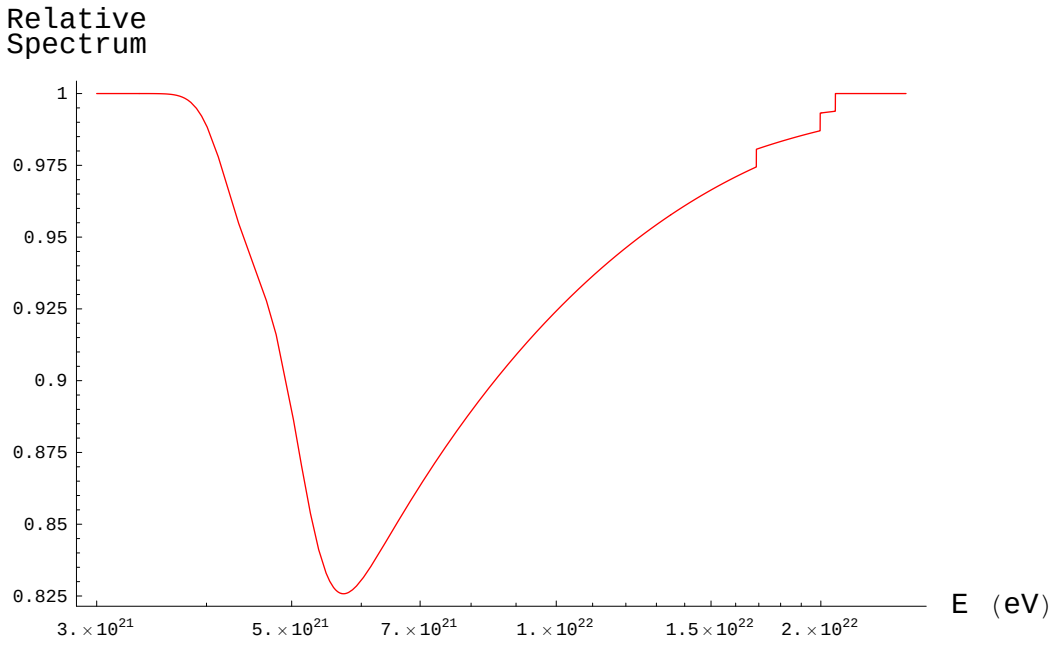

Figure 13: The ROS of Neutrino Cosmic Rays Composed of Equal Flux of Neutrino with $m_\nu = 0.2 + 0,\ +4.6 \times 10^{-2},\ +8.1 \times 10^{-3}$ eV

3.3.3 Source Distribution of Extremely High-Energy Neutrino Cosmic Rays

The source distribution of the extremely high-energy neutrino cosmic rays plays a vital role in the determination of the Z-Burst absorption dip. The source distribution can be described by the shape (Gaussian or step-function), the location, in redshift z, and the width, also in redshift z, of the source distribution. These factors will be studied in detail here.

The Shape of the Neutrino Cosmic Ray Source Distribution

The shape of the neutrino cosmic ray source distribution is determined by the evolutionary history of the source. Details of the shape depend highly on the model. In this section, the effects on the Z-Burst absorption dip the two models of the source distribution discussed in Section 2.3.2 will be compared. Another type of neutrino cosmic ray source distributions, the extended source distributions, has also been studied in our related work **??**.

The Gaussian distribution is characterized by the standard deviation σ about the mean. Bigger standard deviation σ means a more extended distribution, while smaller standard

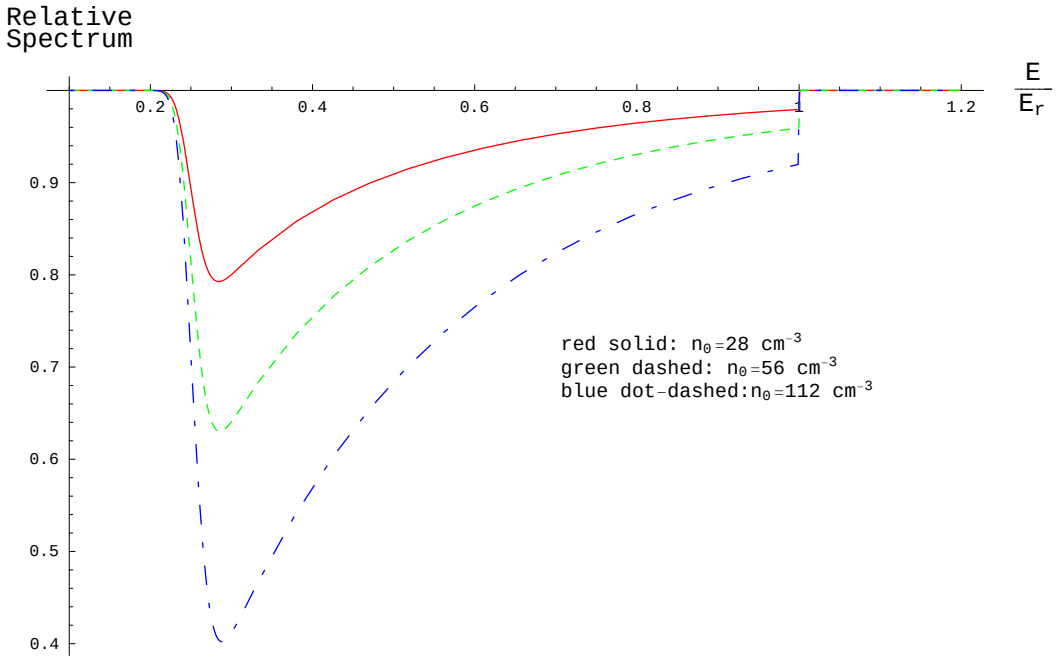

Figure 14: The ROS of Neutrino Cosmic Ray for Different Relic Neutrino Number Density n_0

deviation σ means a more localized distribution. Similarly, the step-function distribution is characterized by the half-width $w_{1/2}$. The two distributions are comparable to each other when the full width at half maximum (FWHM) of the Gaussian distribution $2\sqrt{2\ln 2}\sigma$ is the same as the full width $2w_{1/2} = z_{max} - z_m in$ of the step-function distribution. This leads to near equivalence at

$$w_{1/2} = \sigma\sqrt{2\ln 2}.$$

The Relative Observable Spectra of neutrino cosmic ray from the Gaussian source distribution and the step-function source distribution are plotted in Fig. 15 with the near equivalence as specified by the above equation.

From Fig. 15, it is obvious that the Z-Burst absorption dips of the two different source distributions are very close to each other. So it is easy to conclude that the shape of the source distribution doesn't affect the absorption dip very much. The similar shapes of the Z-

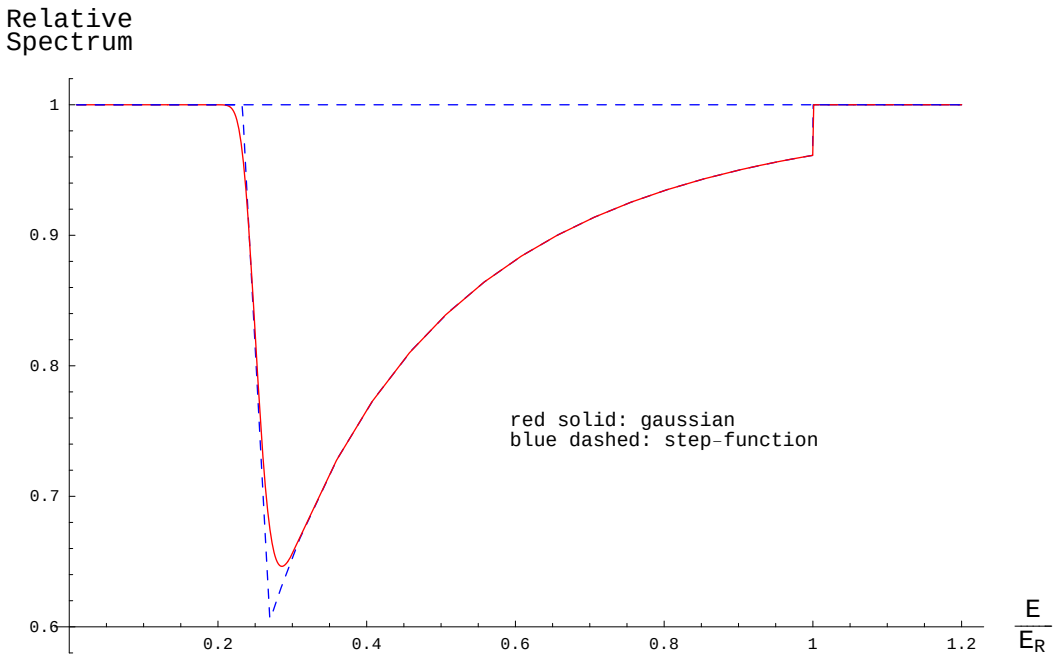

Figure 15: The ROS of Neutrino Cosmic Rays from Gaussian and Step-function Sources

Burst absorption dips from our related work with a different source distribution model [51] also support this conclusion. This is a good news for the future studies of the Z-Burst absorption dip, as the conclusions of these studies will be nearly model independent. This is also the reason why the Gaussian distribution has been used and will be use to study the contributions of the other parameters, including the location and the width of the source distribution, to the Z-Burst absorption dip in this work.

The Location of the Extremely High-Energy Neutrino Cosmic Ray Source

The location of the extremely high-energy neutrino cosmic ray sources is vital information. This information will reveal the era in which the extremely high-energy cosmic rays are generated. It would also discriminate among the models of the extremely high-energy neutrino sources. This section will study the effects that the location of the sources will have on the Z-Burst absorption dip.

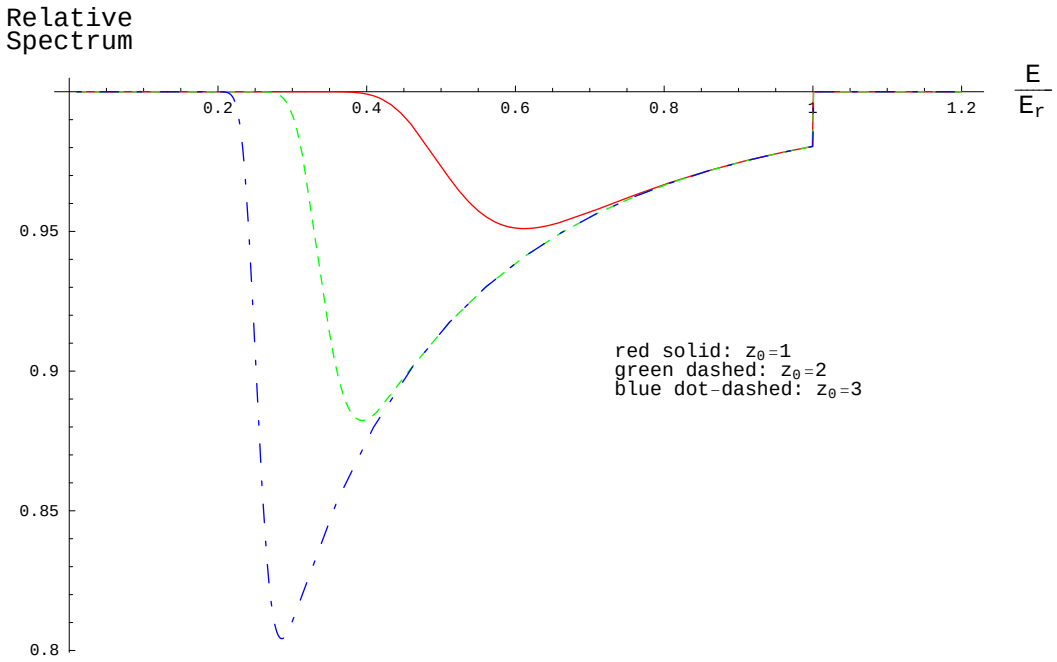

Figure 16: The ROS of Neutrino Cosmic Rays from a Gaussian Distribution Centered at $z_0 = 1, 2, 3$.

Fig. 16 shows the Relative Observable Spectrum resulting from a Gaussian source distribution with different mean values for z. From this figure, it is obvious that the further away the sources are from earth, the lower is energy the maximum of the absorption dip. This is due to the bigger redshift that the neutrino cosmic rays experienced. Also interesting, the further away the source is, the deeper the absorption dip is. The enhanced depth of the absorption dip is due to the higher physical density of the relic neutrino or anti-neutrino at higher redshift. Thus the neutrino cosmic rays from higher redshift experienced more absorption than the neutrino cosmic rays from a source at lower redshift.

As discussed in Section 3.3.1, the position of the maximum of the absorption dip can be used to learn the absolute mass of the neutrino. But the fact that the position of the maximum of the absorption dip also depends on the mean location of the neutrino cosmic ray sources complicates the case. The fact that the neutrino cosmic ray's direction will not change during its journey from the source to earth mitigates the complications. With the

help of associated observations, the redshift of the sources can be determined, thus fixing the mean location of the sources. With the mean so determined, it would be straightforward to find the absolute mass of the neutrinos from the position of the maximum of the Z-Burst absorption dip. Even if the mean location of the neutrino cosmic ray sources is not available, the absolute neutrino mass can still be estimated with accuracy up to one order of magnitude around the real mass.

The Width of the Neutrino Cosmic Ray Source Distribution

The standard deviation σ of the Gaussian distribution parameterizes the localization of the sources. Smaller σ corresponds to a more localized source distribution, while larger σ means more a extended source distribution. With a sufficiently large σ, the Gaussian distribution can even represent a nearly flat source distribution. How will the width of the source distribution affect the Z-Burst absorption dip? This question will be answered in this section.

The Z-Burst absorption dips from three Gaussian distributions, with $\sigma = 0.25$, 1, 2, are shown in Fig. 17. It is clear that the more extended the sources are, the shallower the Z-Burst absorption dip is. This is a natural result of the source location's contributions briefly discussed in the previous section. For an extended source distribution, there will be relatively more sources at both lower redshift and higher redshift than a localized source distribution. Based on the discussion in the previous section, the sources at higher redshift will produce deeper absorption dips, while the sources at lower redshift produce shallower absorption dips. But the maximum of the absorption dips from different redshifts are at different energies. When combining these absorption dips together, all the absorption dips will become shallower. The more sources at the lower redshift, the shallower the absorption dip will become, even though there will also be more sources at higher redshift. This results a shallower absorption dip for the extended source distribution than the localized source distribution.

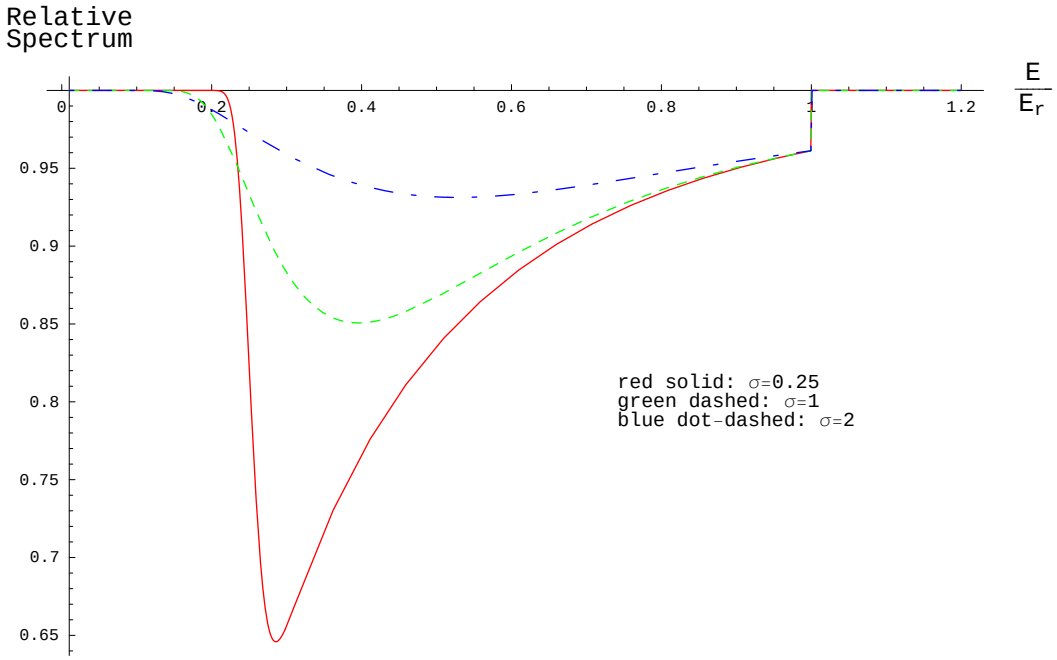

Figure 17: The ROS of Neutrino Cosmic Rays from Gaussian Distributions with σ = 0.25, 1, 2

3.4 Discussion and Conclusion

3.4.1 Neutrino Flavors

In the current study, both the relic neutrinos and the extremely high-energy cosmic ray neutrinos are treated simply as pure mass eigenstate, except in Fig. 13. The main reason for this simplification is that the relic neutrinos are in the decoherent mass eigenstates. So, it is more straightforward and instructional to work in the mass eigenstates when studying the resonant annihilation between the relic neutrinos and the extremely high-energy cosmic ray neutrinos.

The neutrino flavors do introduce some intriguing questions because the neutrinos are generated and will interact with other particles in flavor eigenstates. The first one of these questions is the ratio of the different flavor eigenstates, thus the ratio of the different mass

eigenstates, in both the relic neutrinos and the extremely high-energy cosmic rays. The answer to this question is really model dependent and worth a full separated investigation of its own. The second question is the effect of the neutrino oscillation on the detection of the Z-Burst absorption of the extremely high-energy neutrino cosmic ray. The extremely high-energy neutrino cosmic rays from cosmically distant sources will not become the decoherent mass eigenstates, because the neutrino decoherence length is [51]

$$D_{decoherence} = 0.5 \left(\frac{h}{0.7}\right) \left(\frac{\tau_\Psi}{3\ \mathrm{m}}\right) \frac{E_{22}^2}{\delta m_{-3}^2} D_H \times 10^{20}, \tag{11}$$

where $\delta m_{-3}^2 \equiv \delta m^2/10^{-3}\ \mathrm{eV}^2$, $E_{22} \equiv E/10^{22}\ \mathrm{eV}$, the Hubble distance $D_H \equiv c/H_0 = 4.2(0.7/h)$ Gpc, and $c\tau_\Psi$ is the natural length of the wavepacket. For neutrino cosmic ray with energy 10^{22} eV, the decoherence will never happen. The effect of the oscillation to the detection of the extremely high-energy neutrino cosmic rays depends on the details of the detectors, and has to be studied regarding specified experiment. Some of these questions have been addressed in a separated work [51], which is focused more on the detection of the relic neutrinos.

3.4.2 Z-Burst Absorption Signatures

After studying the different parameters' contributions to the Z-Burst absorption dip, it is clear that the best case for detecting the Z-Burst absorption dip is that the neutrino mass spectrum is degenerate and the extremely high-energy neutrino cosmic rays are from very localized sources at large redshift. Also, the details of the shape of the source distribution don't affect the Z-Burst absorption dip significantly if the source distribution is relatively localized. This makes the detection of the Z-Burst absorption dip fairly independent of the dynamics that generates the extremely high-energy neutrino cosmic rays.

The "edge" of the Z-Burst absorption dip presents an ideal measurement to determine the absolute mass of neutrino. But it is located at the higher energy end of the spectrum, which will naturally have a much smaller event rate if the spectrum of cosmic ray is power-law like. Another measurement to determine the absolute mass of neutrino is the position of the maximum of the Z-Burst absorption dip. The position of the maximum is determined by the combination of the absolute neutrino mass and the mean location of the source distribution

Table 1: Expected Number of Neutrino Events Per Flavor

	$\sum_\alpha \triangle (N_{\nu_\alpha} + N_{\bar{\nu}_\alpha})$					
energy decade	$10^{21\sim22}$ eV		$10^{22\sim23}$ eV		$10^{23\sim24}$ eV	
year	2008	2013	2008	2013	2008	2013
observ. limit	240	700	30	90	2	5

of the neutrino cosmic rays. The maximum of the Z-Burst absorption is usually locates between $0.2E_Z^{res}$ to $0.7E_Z^{res}$. The mean location of the source distribution can be obtained with astrophysical observations. Even if this information is not available, it is possible to estimate the absolute neutrino mass accurate up to an order of magnitude about the real neutrino mass.

It is also possible to directly check the relic neutrino number density n_0 predicted by the hot Big-Bang cosmology. This approach might be the only possible method to directly verify the prediction of the Big-Bang cosmology in this decade.

3.4.3 Experimental Aspects

The final amount of the observed neutrino cosmic ray events is determined by the observable flux of the neutrino cosmic ray on earth. The current upper limits from the experiments, such as RICE [75], GLUE [76], FORTE [77] and AGASA [52], is shown in Fig. 18. The expected improvement of the future experiments, including ANITA [78], Auger [65], EUSO [62] and SalSA [79], is shown in Fig. 19. These plots are adopted from [51]. The improvement of the future experiments is also summarized in Table. 1.

In the best case scenario for the Z-Burst absorption dip detection, the neutrinos have degenerated mass spectrum with mass of a few 0.2 eV. This is the case for the Relative Observable Spectrum in Fig. 13. The maximum of the Z-Burst absorption dip is located at $E \simeq 5.5 \times 10^{21}$ eV. The depth of the Z-Burst absorption in dip Fig. 13 is about 20%. In order to achieve a 3σ discovery, the required number of observed events at the maximum of the Z-Burst absorption dip is

$$N \simeq (3/20\%)^2 = 225. \tag{12}$$

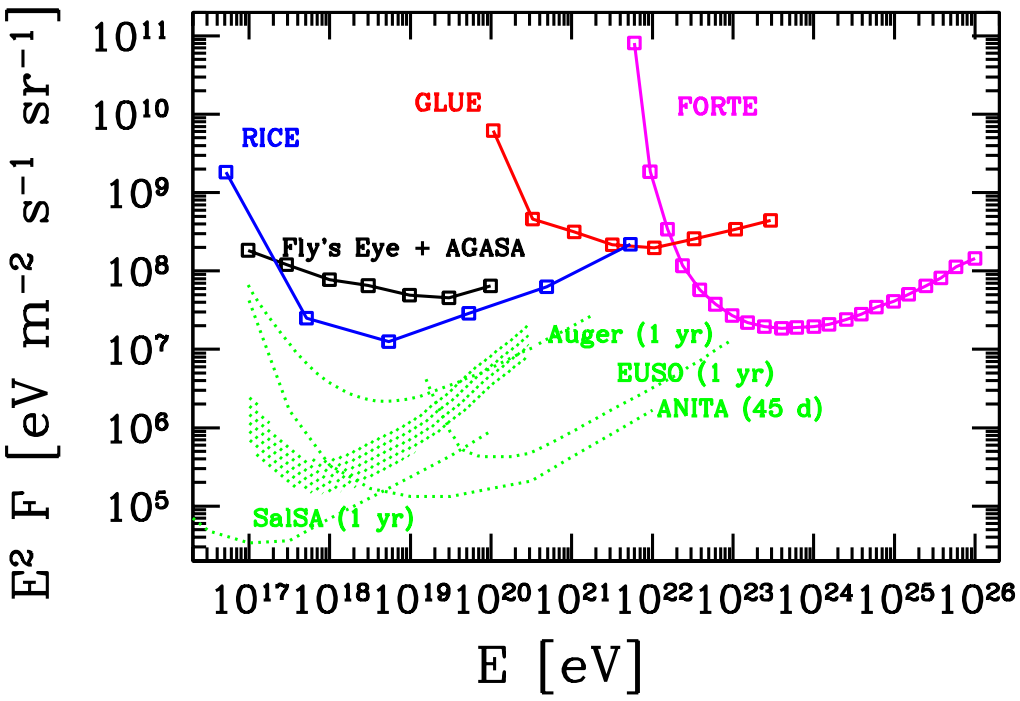

Figure 18: The Current Upper Limit of Neutrino Cosmic Ray Flux

Referring to Table 1, the Z-Burst absorption dip should be detected by the year of 2008. If the heaviest neutrino mass turns out to be two order of magnitude smaller, as suggested by the atmospheric mass gap, the maximum of the Z-Burst absorption dip will locate with $10^{22\sim23}$ eV. It is still possible to detect the Z-burst absorption dip because the total expected number for all neutrino flavors will be $3 \times 90 = 270$ before the year of 2013. So there is still hope to detect the Z-Burst absorption dip in the next decade.

In the worst case scenario, the neutrinos mass spectrum is well separated. This case is plotted in Fig. 12 with the depth of the Z-Burst absorption dips as 6% and the maximum located around 7×10^{21} eV. This will require the number of observed neutrino events for 3σ

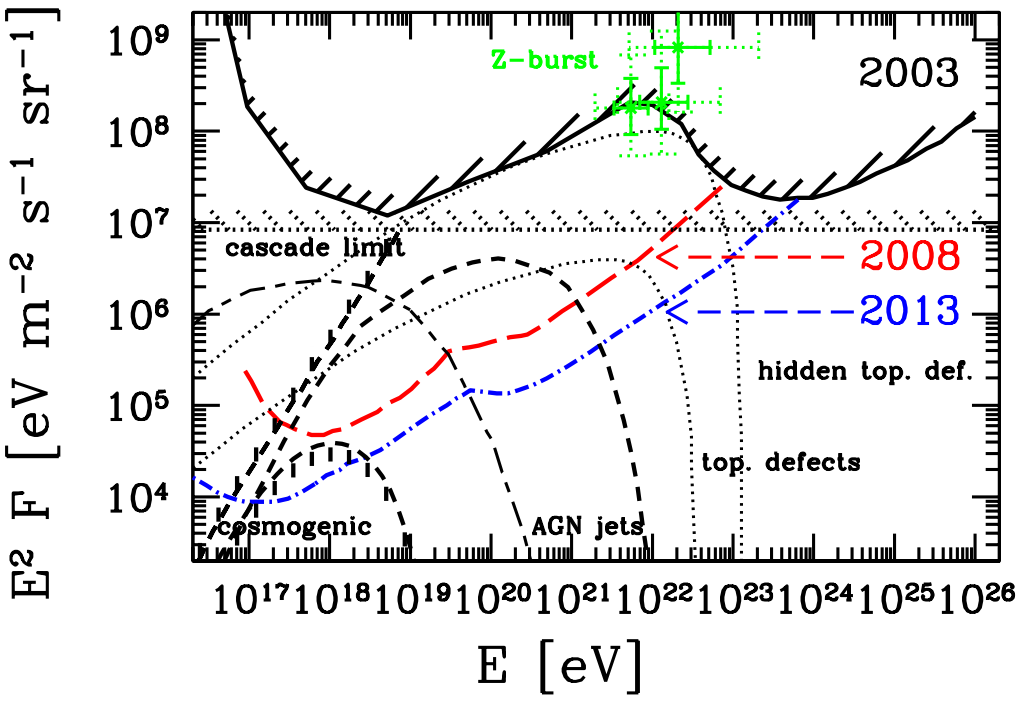

Figure 19: The Improvement of The Future Experiments on Neutrino Cosmic Ray Flux

discovery to be $N \simeq (3/6\%)^2 = 2500$, which will be barely achievable after the year of 2013. It will get much worse if the heaviest neutrino mass turns out to be much smaller than that suggested by the LSND gap.

3.4.4 Conclusion

To conclude this chapter, in the best case scenario with degenerate mass spectrum, it will be possible to detect the Z-Burst absorption dip and to determine the absolute mass of neutrinos in this decade, even if the heaviest neutrino mass is only about 10^{-2} eV as

suggested by the atmospheric mass gap. Together with knowledge of the origin of the neutrino cosmic rays, more accurate neutrino mass measurement can be extracted from the Z-Burst absorption dip in the Relative Observable Spectrum. But the full neutrino mass spectrum cannot be established from the Z-Burst absorption dips, the more accurate neutrino mass square differences from neutrino oscillation experiments are needed.

But for the worst case scenario with well separated neutrino mass spectrum, it will not be possible to achieve a conclusive measurement within this decade, even if the heaviest neutrino has mass of a few 10^{-1} eV as suggested by the LSND gap. In fact, it might be totally out of our reach if the heaviest neutrino mass turns out to be much lighter.

PART TWO
NEUTRINO OSCILLATION

CHAPTER IV

2+2 NEUTRINO OSCILLATION AND SUM RULE

As learned from the previous chapters, the existence of relatively heavy neutrinos of a few 10^{-1} eV's is vital to the detection of Z-Burst absorption dip in this decade. The upper limit of the total mass of the relic neutrinos from the recent observations [66, 68] seems to allow the heaviest neutrino mass to be a few 10^{-1} eV's. The strongest evidence to support a 10^{-1} eV scale neutrino mass is the mass square difference from the combined data analysis of the LSND and KARMEN experiments [80]. The results of the invisible and leptonic width of Z boson determine that there are only 3 active neutrinos [81]. But the inconsistency of the LSND mass gap with the solar and atmospheric mass gaps suggests the existence of the fourth neutrino, which has to be a sterile neutrino.[1] In this chapter, the basics of neutrino oscillation and a specific model of four neutrino oscillation, the (2+2) model, will be discussed. The claimed evidence against this model, especially the Sum Rule of (2+2) model [83], will be investigated in the next chapter through numerical calculation. A partially successful analytical approach is presented in Appendix A.

4.1 Basics of Neutrino Oscillation With Two Neutrino Oscillation

The fact that the neutrino flavor eigenstates are not the same as the neutrino mass eigenstates determines that neutrino beam will oscillate among the flavors when traveling through space. This oscillation can be well illustrated with a simple two neutrino oscillation model.

In this two neutrino oscillation model, the mass eigenspace has two mass eigenvectors $|\nu_j\rangle$ with $j = 1, 2$ as its basis, while the flavor eigenspace has two flavor eigenvectors $|\nu_\alpha\rangle$ with α as one of the two possible flavors, say μ and τ here. The transformation between

[1] An attempt [82] to accommodate the LSND result in a three neutrino model by selective exclusion of some atmospheric data still includes a heavy neutrino mass of 0.2 eV.

these two eigenspaces is described by the unitary transformation matrix

$$U(\theta) = \begin{pmatrix} \cos\theta & -\sin\theta \\ \sin\theta & \cos\theta \end{pmatrix}. \tag{13}$$

The three phases in a general 2×2 unitary matrix have been absorbed in redefinition of the ν fields. The transformation relationship can be formally written as

$$|\nu_j\rangle = U_{\alpha j}|\nu_\alpha\rangle.$$

When the neutrino beam is traveling in vacuum, the evolution of the beam, in the flavor basis, can be described as

$$\begin{aligned} \langle\nu_\alpha|\nu_f(t)\rangle &= \langle\nu_\alpha|e^{-i\mathbb{H}t}|\nu_f(0)\rangle \\ &= \sum_{j,k,\beta}\langle\nu_\alpha|\nu_j\rangle\langle\nu_j|e^{-i\mathbb{H}t}|\nu_k\rangle\langle\nu_k|\nu_\beta\rangle\langle\nu_\beta|\nu_f(0)\rangle. \end{aligned} \tag{14}$$

As the mass eigenstates $|\nu_j\rangle$ are the eigenstates of the free space Hamiltonian $\mathbb{H}$, thus

$$\langle\nu_j|\mathbb{H}|\nu_k\rangle = E_j\delta_{j,k},$$

with this, Eqn. 14 becomes

$$\begin{aligned} \langle\nu_\alpha|\nu_f(t)\rangle &= \sum_{j,k,\beta} U_{\alpha j}e^{-iE_jt}\delta_{j,k}U^*_{j,\beta}\langle\nu_\beta|\nu_f(0)\rangle \\ &= \sum_{j,\beta} e^{-iE_jt}U_{\alpha j}U^*_{j\beta}\langle\nu_\beta|\nu_f(0)\rangle, \end{aligned} \tag{15}$$

where $E_j = \sqrt{m_j^2 + p^2}$ is the energy of the neutrino. For neutrino oscillation experiments, the energy of the neutrino beam $E \simeq p \gg m_j$. Thus $E_j \simeq E + \frac{m_j^2}{2E}$. So Eqn. 15 becomes

$$\langle\nu_\alpha|\nu_f(t)\rangle = \sum_{j,\beta} e^{-i(E+\frac{m_j^2}{2E})t}U_{\alpha j}U^*_{j\beta}\langle\nu_\beta|\nu_f(0)\rangle. \tag{16}$$

If the neutrino beam start with pure muon neutrinos ν_μ, this means $\langle\nu_\mu|\nu_f(0)\rangle = 1$ and $\langle\nu_\tau|\nu_f(0)\rangle = 0$. Thus

$$\langle\nu_\alpha|\nu_f(t)\rangle = \sum_j e^{-i(E+\frac{m_j^2}{2E})t}U_{\alpha j}U^*_{j\mu}.$$

Putting the components of the transformation matrix of Eqn. 13 in to the above equation, the probability to measure tau neutrinos at distance $L = t$ is then

$$\begin{aligned} P_{\nu_\tau}(L) &= |\langle \nu_\tau | \nu_f(L) \rangle|^2 \\ &= \left| -e^{-i(E+\frac{m_1^2}{2E})L} \sin\theta\cos\theta + e^{-i(E+\frac{m_2^2}{2E})L} \cos\theta\sin\theta \right|^2 \\ &= \left(2 - 2\cos\left(\frac{m_2^2 - m_1^2}{2E} L\right)\right) \sin^2\theta\cos^2\theta \\ &= \sin^2\frac{(m_2^2 - m_1^2)L}{4E} \sin^2 2\theta \\ &= \sin^2\frac{\delta m_{21}^2 L}{4E} \sin^2 2\theta. \end{aligned} \tag{17}$$

With the oscillation probability of Eqn. 17, it is easy to reach the following conclusions:

1. The Maximum Oscillation: The maximum probability to detect the other flavor neutrino in the neutrino beams is $\sin^2 2\theta$ when the beam starts with pure neutrinos of one flavor. If the mixing angle θ is $\frac{\pi}{4}$, it is possible to have full conversion from one flavor to the other.

2. The Oscillation Length λ: The oscillation length λ is determine by setting the phase of the oscillation term to π. This leads to

$$\lambda = \frac{8\pi E}{\delta m_{21}^2} = 2.48 \left(\frac{\mathrm{eV}^2}{\delta m_{21}^2}\right) \left(\frac{E}{\mathrm{GeV}}\right) \text{ km}. \tag{18}$$

These results will be very helpful to understand the more complicated oscillation of three or four neutrinos.

4.2 Neutrino Oscillation Experiments

After neutrino oscillations were first confirmed by the Super-Kamiokande experiment in 1998 [15], three types of neutrino oscillation have been studied. These three types of neutrino oscillation will be briefly discussed here.

4.2.1 Solar Neutrino Oscillation

Solar neutrinos are generated by the thermonuclear reactions inside the sun. The sun is well described by the Standard Solar Model [84, 85, 86] in all aspects other than the observed

neutrino flux. This discrepancy is the famous solar neutrino problem [87, 88] that started the whole neutrino oscillation revolution. Among the thermonuclear chain reactions, the main reactions which generate the solar neutrinos are

$$p + p \rightarrow {}^2\mathrm{H} + e^+ + \nu_e, \tag{19}$$

$$p + e^- + p \rightarrow {}^2\mathrm{H} + \nu_e, \tag{20}$$

$${}^8\mathrm{B} \rightarrow {}^8\mathrm{Be}^* + e^+ + \nu_e, \tag{21}$$

$${}^7\mathrm{Be} + e^- \rightarrow {}^7\mathrm{Li} + \nu_e. \tag{22}$$

These reactions will only generate electron neutrinos ν_e, whose energy will fall into the range of 0.1 to 15 MeV. Some of the solar neutrino experiments are able to detect the neutrinos with energy above 0.2 MeV. The solar neutrino experiments fail to observe the electron neutrino flux predicted by the Standard Solar Model. The deficiency in the electron neutrino flux can be explained by electron neutrinos oscillating into, most probably, tau or muon neutrinos. The solar neutrino oscillation is characterized by the solar mass gap δm^2_{sol} and the solar mixing angle θ_{sol}. In the parameter space described by these two parameters, only the large mixing angle (LMA) solution is allowed by the experimental data including the recent SNO and Kamland experiments [89]. The best fits to the solar neutrino experiment data in Reference [90], [91], and [92] give

$$\delta m^2_{sol} = 3.7 \times 10^{-5}\mathrm{eV}^2, \tag{23}$$

$$\tan^2\theta_{sol} = 0.37. \tag{24}$$

4.2.2 Atmospheric Neutrino Oscillation

The atmospheric neutrinos are generated by the high energy cosmic rays bombarding the atmospheric atoms. The most important neutrino producing reactions are the following

$$\pi^\pm \rightarrow \mu^\pm + \nu_\mu(\bar{\nu}_\mu),$$

$$\mu^\pm \rightarrow e^\pm + \nu_e(\bar{\nu}_e) + \bar{\nu}_\mu(\nu_\mu).$$

The measured energies of these muon and electron neutrinos are widely spread from 0.1 GeV up to 10 TeV. Unlike the solar neutrinos, the measured flux of muon neutrinos ν_μ doesn't

offer much helpful information as the original flux of the primary cosmic rays is poorly known. But to a good approximation at low energies, twice as many muon neutrinos ν_μ as electron neutrinos ν_e will be generated. Thus the flux ratio of muon neutrino ν_μ to electron neutrino ν_e, defined as $R_{\mu/e}$, should be 2. The observed ratio $R_{\mu/e}$ is only 0.65 [93]. This deficiency is attributed to the muon neutrino ν_μ's oscillation into the other flavor neutrinos, with tau neutrinos as the top candidate [94]. The parameters for atmospheric neutrino oscillations from the best fits to atmospheric and solar data [95, 96] are

$$\delta m^2_{atm} = 2.4 \times 10^{-3}\text{eV}^2, \tag{25}$$

$$\tan^2\theta_{atm} = 0.66. \tag{26}$$

To achieve the above results, both Solar and Atmospheric neutrino oscillation data are fitted with two neutrino model even there are really three ν's are involved. This is because the other mixing angle is $\theta_{31} \simeq 0$, determined by CHOOZ experiment [97]. This is effectively two neutrino oscillation.

4.2.3 Man-made Neutrino Oscillation Experiments

There are two sources for man-made neutrinos. The first is the accelerator, in which the muon neutrinos are generated when accelerated protons hit matter targets. The energy of these muon neutrinos will be a few 10 MeV. The LSND and KARMEN experiments are designed to detect the appearance of the electron neutrinos in the muon neutrino beam. Among these experiments, the LSND experiment offers a surprisingly big mass gap, which is still the center of heated debates. The second source of the man-made neutrinos is the nuclear reactors. The nuclear fission reactions in these reactors will generate electron anti-neutrinos with energy at the MeV scale. The CHOOZ and KamLAND experiments are designed to detect the disappearance of the electron anti-neutrinos, while the controversial LSND [27] experiment uses a medium energy accelerator at Los Alamos National Lab to produce focused π^+ beams, whose decay produces neutrinos. The combined data of the LSND and the KARMEN experiments determine the parameters of the LSND oscillation [80, 98, 99] as

$$\delta m^2_{LSND} = 0.2 \sim 1\text{eV}^2,$$

$$\sin^2(2\theta_{LSND}) = 10^{-2}.$$

4.3 Four-Neutrino Oscillation's Parameters

The neutrino mass gaps from the solar, atmospheric, and LSND oscillation experiments cannot be reconciled unless a fourth neutrino, the sterile neutrino ν_s, is introduced. This forms the four-neutrino model. The parameters charactering four-neutrino oscillations are discussed next.

4.3.1 Four-Neutrino Mass Spectra

The neutrino oscillation experiments can only measure the values, but not the signs, of the mass square differences of the neutrinos. There are totally six possible neutrino mass spectra with the same three neutrino mass square differences as shown schematically in Fig. 20. Global analysis considering short baseline, solar, and atmospheric neutrinos concludes that both the (3+1) and (2+2) schemes are only viable at very low confidence [100]. But the follow-up works [101, 102], especially the most recent one [103], rule out the (2+2) scheme and leave the (3+1) scheme marginally allowed. But in these global data fits, the two smallest mixing angles are set to zero in order to reduce the number of parameters involved. The contributions of these small mixing angles will be studied, and the possible viability of the (2+2) scheme will be the main focus of the rest of this thesis. In the study of the viability of (2+2) scheme, the normal (2+2) scheme will be used and conclusion will be the same for the inversed (2+2) scheme. In the normal (2+2) scheme, the neutrino mass squares are

$$\begin{aligned} m_2^2 &= m_1^2 + \delta m_{sol}^2, \\ m_3^2 &= m_1^2 + \delta m_{sol}^2 + \delta m_{LSND}^2, \\ m_4^2 &= m_1^2 + \delta m_{sol}^2 + \delta m_{LSND}^2 + \delta m_{atm}^2. \end{aligned} \tag{27}$$

Mixing Angles

The four-flavor mixing of neutrinos is described by six mixing angles and three CP-violating phases. The additional three phases for Majorana neutrinos will not be considered as they don't contribute to the oscillation probabilities. The mass bases are ordered as $\{m_4, m_3, m_2, m_1\}$ with m_4 as the heaviest mass eigenstate, and the flavor bases are ordered as $\{\nu_\mu, \nu_\tau, \nu_s, \nu_e\}$ for our convenience. With this convention, the unitary transformation

matrix that transforms the mass basis to the flavor basis, a product of the six rotation transformation matrices with the six mixing angles, is

$$\mathbb{U} = \mathbb{R}_{23}(\theta_{\tau s})\mathbb{R}_{24}(\epsilon_{\mu\mu})\mathbb{R}_{14}(\epsilon_{\mu e})\mathbb{R}_{13}(\epsilon_{ee})\mathbb{R}_{34}(\theta_{atm})\mathbb{R}_{12}(\theta_{sol}). \tag{28}$$

Here, θ_{sol} and θ_{atm} are the mixing angles dominantly responsible for solar and atmospheric neutrino oscillations, and $\theta_{\tau s}$ is a possibly large angle parameter for the dominant mixing of ν_τ and ν_s. The effects of the CP-violating phases are essentially to change the allowed ranges of the three small mixing angles $\epsilon_{\mu\mu}$, $\epsilon_{\mu e}$ and ϵ_{ee} from $[0, \pi/2]$ to $[-\pi/2, \pi/2]$. So in this work, the CP-violating phases will be replaced by allowing the values of the three small mixing angles to have both the positive and negative signs. Also, the ordering of the six rotation matrix is chosen so that it will be the same as that in Reference [100, 101, 102, 103] when $\epsilon_{\mu e}$ and ϵ_{ee} are set to zero. We do this to facilitate comparison to these prior works. The values of the mixing angles are chosen as following:

1. Solar Neutrino Mixing Angle: $\theta_{sol} = 31^o$ from Eqn. 24.

2. Atmospheric Neutrino Mixing Angle: $\theta_{atm} = 39^o$ from Eqn. 26.

3. Mixing Angle for ν_τ and ν_s: $\theta_{\tau s} \in [0, \pi/2]$ as there is no knowledge of it from experiments.

4. Three Small Mixing Angles: The allowed ranges of the three small mixing angles are correlated. The short-baseline experimental data restricts their values to be in the following range, as derived in [42]:

$$\begin{aligned} \epsilon_{\mu e} &\in [-0.1, 0.1], \\ \epsilon_{\mu\mu} &\in \left[-\sqrt{0.12 - \epsilon_{\mu e}^2}, \sqrt{0.12 - \epsilon_{\mu e}^2}\right], \\ \epsilon_{ee} &\in \left[-\sqrt{0.01 - \epsilon_{\mu e}^2}, \sqrt{0.01 - \epsilon_{\mu e}^2}\right]. \end{aligned}$$

4.4 Matter Effect in Neutrino Oscillation

For neutrinos traveling in the sun and in the earth, the neutrino oscillations will be enhanced by matter through coherent forward scattering [104]. For specific oscillation and

matter density parameters, this enhancement can produce a resonance behavior [105]. The effects that the matter has on the neutrino oscillations is called the MSW matter effect, after the three dominant players in the theoretical formulation of the resonance. The matter can not only enhance but also depress the neutrino oscillations with certain combinations of parameters. The MSW matter effect is described with the matter-induced potential $\mathbb{A}$. In the flavor basis, the matter-induced potential is

$$\mathbb{A} = \frac{\sqrt{2}}{2} G_F \begin{pmatrix} -N_n^X & 0 & 0 & 0 \\ 0 & -N_n^X & 0 & 0 \\ 0 & 0 & 0 & 0 \\ 0 & 0 & 0 & 2N_e^X - N_n^X \end{pmatrix}, \tag{29}$$

where $G_F = 1.17 \times 10^{-5}\text{GeV}^{-2}$ is the Fermi coupling constant just like in Section **??**, N_n^X is the number density of neutrons in the matter, and N_e^X is the number density of electrons. When all the small mixing angles ϵ's are turned on, the MSW matter effect is very important in the solar and atmospheric neutrino oscillations, due to solar matter and Earth matter, respectively. But it will have minimal effect on the Sum Rule when all the small mixing angles ϵ's are set to zero. This contribution of the earth matter effect is studied numerically in the next chapter and analytically in Appendix A.

4.5 Sum Rule and Product Rule of (2+2) Neutrino Model

The Sum Rule of the (2+2) neutrino model was introduced to rule out the (2+2) model [83]. The essence of Sum Rule is that either solar neutrino oscillations or atmospheric neutrino oscillations, or both, will produce sterile neutrinos with a significant probability.

When all the three small mixing angles ϵ's are set to zero, the vacuum mixing matrix in Eqn. 28 becomes

$$\mathbb{U} = \mathbb{R}_{23}(\theta_{\tau s})\mathbb{R}_{34}(\theta_{atm})\mathbb{R}_{12}(\theta_{sol}) = \mathbb{R}_{23}(\theta_{\tau s})\mathbb{U}_{\pm}, \tag{30}$$

with

$$\mathbb{U}_{\pm} = \begin{pmatrix} \cos\theta_{atm} & \sin\theta_{atm} & 0 & 0 \\ -\sin\theta_{atm} & \cos\theta_{atm} & 0 & 0 \\ 0 & 0 & \cos\theta_{sol} & \sin\theta_{sol} \\ 0 & 0 & -\sin\theta_{sol} & \cos\theta_{sol} \end{pmatrix}. \tag{31}$$

This simply means that $\langle\nu_e|\nu_3\rangle = \langle\nu_e|\nu_4\rangle = 0$, and $\langle\nu_\mu|\nu_1\rangle = \langle\nu_\mu|\nu_2\rangle = 0$. The neutrino oscillation probabilities in this case can be denoted by

$$P_{\triangle}(\nu_\alpha \to \nu_\beta) \equiv A_{\triangle}(\nu_\alpha \to \nu_\beta)\sin^2\left(\frac{\delta m^2_{\triangle} L}{4E}\right), \tag{32}$$

Here, $\triangle$ denotes the short baseline (SBL), long baseline (LBL)/atmospheric, or solar scale. $A_{\triangle}$ is the amplitude of the CP-conserving oscillation at each $\delta m^2_{\triangle}$ scale. They are defined as

$$\begin{aligned} A_{SBL}(\nu_\alpha \to \nu_\beta) &= -4\sum_{j=1}^{2}\sum_{k=3}^{4} R^{\alpha j}_{\beta k}, \\ A_{LBL}(\nu_\alpha \to \nu_\beta) &= -4R^{\alpha 3}_{\beta 4}, \\ A_{sol}(\nu_\alpha \to \nu_\beta) &= -4R^{\alpha 1}_{\beta 2}, \end{aligned} \tag{33}$$

with the CP-conserving coefficient $R^{\alpha j}_{\beta k}$ defined as the real part of $(U_{\alpha j}U^*_{\beta j}U^*_{\alpha k}U_{\beta k})$. Also for the disappearance amplitude,

$$A_{\triangle}(\nu_\beta \to \nu_{\not\beta}) = \sum_{\alpha\neq\beta} A_{\triangle}(\nu_\beta \to \nu_\alpha) = 4\sum_{\triangle} |U_{\beta j}|^2 |U_{\beta k}|^2, \tag{34}$$

with $\sum_{\triangle}$ denotes the sum over the appropriate mass states indicated explicitly in Eqn. 33.

From the above results, the non-zero oscillation amplitudes for ν_μ due to atmospheric-scale oscillations are

$$\begin{aligned} A_{atm}(\nu_\mu \to \nu_\tau) &= \sin^2(2\theta_{atm})\cos^2\theta_{\tau s}, \\ A_{atm}(\nu_\mu \to \nu_s) &= \sin^2(2\theta_{atm})\sin^2\theta_{\tau s}, \\ A_{atm}(\nu_\mu \to \nu_{\not\mu}) &= \sin^2(2\theta_{atm}), \end{aligned} \tag{35}$$

while the oscillation amplitudes for ν_e due to solar-scale oscillations are

$$\begin{aligned} A_{sol}(\nu_e \to \nu_\tau) &= \sin^2(2\theta_{sol}) \sin^2 \theta_{\tau s}, \\ A_{sol}(\nu_e \to \nu_s) &= \sin^2(2\theta_{sol}) \cos^2 \theta_{\tau s}, \\ A_{sol}(\nu_e \to \nu_{\not e}) &= \sin^2(2\theta_{sol}). \end{aligned} \tag{36}$$

The oscillation amplitudes listed above will still be of the same form if the matter effects are present. This is because the matrix of the matter-induced potential is diagonal in the flavor basis. The extra matter-induced potential will only change the values of the angles involved here.

When the earth matter is not present, the oscillation amplitudes for ν_μ due to the atmospheric-scale oscillations can simply take the above values. The case with the earth matter effect will be analyzed through numerical calculation in Chapter V and through analytical study in the Appendix A.

But the oscillations the solar neutrinos are very different because the evolution of the neutrinos from the center to the surface of the sun is dominated by matter effects. The solar matter density is not constant, and so the matter-dependent mixing angles change continuously as the neutrinos transit through the solar material. This will possibly affecting non-adiabatic transitions among the mass eigenstates. But for the large mixing angle (LMA) solution of interest in this work, the neutrinos propagate adiabatically from the center to the surface of the sun. Moreover, solar neutrinos with energies above the solar resonance associated with δm^2_{sol} and below the atmospheric resonance associated with δm^2_{atm} will evolve adiabatically to emerge from the sun in a nearly pure $|\nu_2\rangle$ mass eigenstate. As discussed in Reference [42], the solar resonance energy is $E^R_{sol} \leq 4$ MeV and the atmospheric resonance energy is $E^R_{atm} \geq 300$ GeV. The solar neutrinos $|\nu_\odot\rangle$ measure by the Super-Kamiokande and SNO experiments are from the ^8B decay chain, thus have energy within this energy range. For the solar neutrinos measured by these experiments, the approximation $|\nu_\odot\rangle \equiv |\nu_2\rangle$ can be used.

If all three small mixing angle ϵ's are set to zero, from Eqn. 30, it is easy to get

$$|\nu_2\rangle = \cos\theta_{sol}(\sin\theta_{\tau s}|\nu_\tau\rangle + \cos\theta_{\tau s}|\nu_s\rangle) - \sin\theta_{sol}|\nu_e\rangle. \tag{37}$$

From this equation, the oscillation amplitudes for solar neutrinos arriving at the earth in the $|\nu_\odot\rangle \equiv |\nu_e\rangle$ approximation are

$$\begin{aligned} A_{sol}(\nu_\odot \to \nu_\tau) &= \cos^2\theta_{sol}\sin^2\theta_{\tau s}, \\ A_{sol}(\nu_\odot \to \nu_s) &= \cos^2\theta_{sol}\cos^2\theta_{\tau s}, \\ A_{sol}(\nu_\odot \to \nu_{\not e}) &= \cos^2\theta_{sol}. \end{aligned} \tag{38}$$

For solar neutrino oscillation, define the solar ratio as

$$R_{sol} = \left[\frac{P(\nu_\odot \to \nu_s)}{P(\nu_\odot \to \nu_{\not e})}\right]_{sol}, \tag{39}$$

and for atmospheric neutrino oscillation, define the atmospheric ratio as

$$R_{atm} = \left[\frac{P(\nu_\mu \to \nu_s)}{P(\nu_\mu \to \nu_{\not\mu})}\right]_{atm}. \tag{40}$$

Thus, the zeroth order Sum Rule, when the small mixing angle ϵ's are zero and no earth matter effect is present, is

$$\begin{aligned} R_{sol} + R_{atm} &= \left[\frac{P(\nu_\odot \to \nu_s)}{P(\nu_\odot \to \nu_{\not e})}\right]_{sol} + \left[\frac{P(\nu_\mu \to \nu_s)}{P(\nu_\mu \to \nu_{\not\mu})}\right]_{atm} \\ &= \cos^2\theta_{\tau s} + \sin^2\theta_{\tau s} = 1, \end{aligned} \tag{41}$$

and the Product Rule is achieved similarly by defining

$$R'_{sol} = \left[\frac{P(\nu_\odot \to \nu_s)}{P(\nu_\odot \to \nu_\tau}\right]_{sol}, \tag{42}$$

$$R'_{atm} = \left[\frac{P(\nu_\mu \to \nu_s)}{P(\nu_\mu \to \nu_\tau)}\right]_{atm}, \tag{43}$$

combining to yield

$$\begin{aligned} R'_{sol} \times R'_{atm} &= \left[\frac{P(\nu_\odot \to \nu_s)}{P(\nu_\odot \to \nu_\tau)}\right]_{sol} \times \left[\frac{P(\nu_\mu \to \nu_s)}{P(\nu_\mu \to \nu_\tau)}\right]_{atm} \\ &= \cot^2\theta_{\tau s} \times \tan^2\theta_{\tau s} = 1. \end{aligned} \tag{44}$$

It is very important to realized that both the Sum Rule and the Product Rule are not required by any underlying symmetry or principle. Rather, they are accidents of the block-diagonal structure of Eqn. 30, when the small mixing angles ϵ's and the earth matter effect are ignored. It will be shown through the numerical calculation in the next chapter that the small mixing angles ϵ's and the earth matter effect can change the unitary result quite significantly.

4.6 Formalism of (2+2) Neutrino Oscillation in Matter

For neutrinos traveling in matter, the Hamiltonian in the flavor basis is

$$\mathbb{H}_F = \mathbb{U}\frac{\mathbb{M}^2}{2E}\mathbb{U}^\dagger + \mathbb{A}, \tag{45}$$

with

$$\begin{aligned}
\mathbb{M}^2 &= \begin{pmatrix} m_4^2 & 0 & 0 & 0 \\ 0 & m_3^2 & 0 & 0 \\ 0 & 0 & m_2^2 & 0 \\ 0 & 0 & 0 & m_1^2 \end{pmatrix} \\
&= \begin{pmatrix} m_1^2 + \delta m^2_{LSND} & & & \\ +\delta m^2_{sol} + \delta m^2_{atm} & 0 & 0 & 0 \\ 0 & m_1^2 + \delta m^2_{LSND} + \delta m^2_{sol} & 0 & 0 \\ 0 & 0 & m_1^2 + \delta m^2_{sol} & 0 \\ 0 & 0 & 0 & m_1^2 \end{pmatrix} \qquad (46) \\
\mathbb{A} &= \frac{\sqrt{2}}{2} G_F \begin{pmatrix} -N_n^X & 0 & 0 & 0 \\ 0 & -N_n^X & 0 & 0 \\ 0 & 0 & 0 & 0 \\ 0 & 0 & 0 & 2N_e^X - N_n^X \end{pmatrix}. \qquad (47)
\end{aligned}$$

Here, the X can be S standing for the solar matter, EM for the matter of earth mantle, or EC for the core of the earth. As any constant in the Hamiltonian only causes a universal phase shift in the wave function, the common factors m_1^2 in the mass matrix $\mathbb{M}^2$ and $-N_n^X$ in the matter-induced potential matrix $\mathbb{A}$ can be removed. Thus the matrices can be simplified

as

$$\mathbb{M}^2 = \begin{pmatrix} \delta m^2_{LSND} + \delta m^2_{sol} + \delta m^2_{atm} & 0 & 0 & 0 \\ 0 & \delta m^2_{LSND} + \delta m^2_{sol} & 0 & 0 \\ 0 & 0 & \delta m^2_{sol} & 0 \\ 0 & 0 & 0 & 0 \end{pmatrix}, \tag{48}$$

$$\mathbb{A} = \frac{\sqrt{2}}{2} G_F \begin{pmatrix} 0 & 0 & 0 & 0 \\ 0 & 0 & 0 & 0 \\ 0 & 0 & N^X_n & 0 \\ 0 & 0 & 0 & 2N^X_e \end{pmatrix} = \sqrt{2} G_F \begin{pmatrix} 0 & 0 & 0 & 0 \\ 0 & 0 & 0 & 0 \\ 0 & 0 & \frac{N^X_n}{2} & 0 \\ 0 & 0 & 0 & N^X_e \end{pmatrix}. \tag{49}$$

When $N^X_e \simeq N^X_n$, which is true for both the earth and the sun, Eqn. 49 will become

$$\mathbb{A} = \begin{pmatrix} 0 & 0 & 0 & 0 \\ 0 & 0 & 0 & 0 \\ 0 & 0 & \frac{\sqrt{2}}{2} G_F N^X_e & 0 \\ 0 & 0 & 0 & \sqrt{2} G_F N^X_e \end{pmatrix}. \tag{50}$$

In order to study the details of a neutrino beam traveling through matter, the eigenvectors $|\nu^X_k\rangle$ and the corresponding eigenvalues m^X_k of this Hamiltonian $\mathbb{H}$ have to be found. The transformation matrix or the mixing matrix between the eigenbasis in the matter $|\nu^X\rangle$ and the flavor basis $|\nu_\alpha\rangle$ is $\mathbb{U}^X$. It can be composed of the normalized eigenvectors $|\nu^X_k\rangle$ in the flavor basis. This transformation matrix will transform the flavor basis into the matter eigenbasis as

$$|\nu^X\rangle = \mathbb{U}^X |\nu_\alpha\rangle .. \tag{51}$$

The evolution of a neutrino beam of initial state $|\nu_0\rangle$ through matter can be studied as follows. First, the neutrino beam's flavor state $|\nu_0\rangle$ can be decomposed into the eigenstates of the Hamiltonian in the matter $\mathbb{H}^X$. In the diagonal basis of the neutrino will evolve, when it propagates through the matter, as

$$|\nu(L)\rangle = \sum_k e^{-i m^X_k L} \langle \nu^X_k | \nu_0 \rangle | \nu^X_k \rangle . \tag{52}$$

Then the probability to detect neutrinos of flavor ν_α will be

$$P(\nu_0 \to \alpha) = \left| \langle \nu_\alpha | \nu(L) \rangle \right|^2 . \tag{53}$$

Thus the solar ratio and the atmospheric ratio can be computed with these oscillation probabilities with non-zero small mixing angles ϵ's and the earth matter effect.

Both the Sum Rule and the Product Rule are exactly as the zeroth order Sum Rule calculated in Section 4.5.when the three small mixing angles (ϵ's) are zero and the earth matter effect is not included. But when both the small mixing angles ϵ's and the earth matter effect are present, the Sum Rule can be significantly relaxed as shown in the next chapter. Through the study of the Sum Rule and Product Rule of (2+2) neutrino model, both numerically in the next chapter, the contributions of the small mixing angles ϵ's to the solar and atmospheric neutrino oscillations will studied and the viability of the (2+2) model will be investigated. Appendix A contains an analytical study of the (2+2) Sum Rule of simplified special cases.

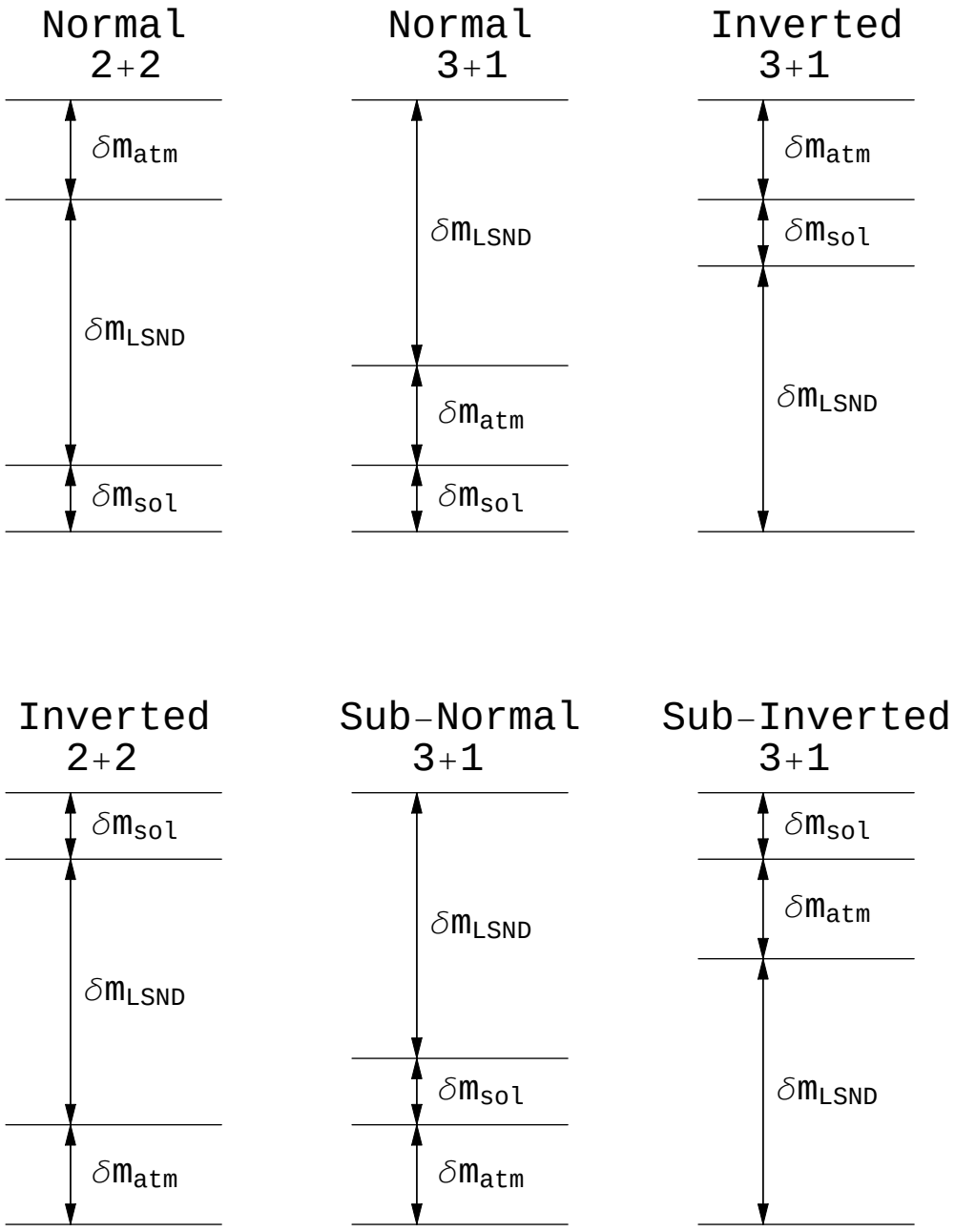

Figure 20: The Six Mass Spectra of 4 Neutrinos

CHAPTER V

NUMERICAL CALCULATION AND RESULTS OF (2+2) SUM RULE

The small mixing angles ϵ's are believed to make negligible contributions to the solar and atmospheric neutrino oscillations. It has been proposed that the Sum Rule of the (2+2) neutrino model, which is exact when all the small mixing angles ϵ's are set to zero, rules out the (2+2) neutrino model [83]. Based on similar belief, recent global fits to the experimental data [100, 101, 102, 103] omit two of the smaller mixing angles, $\epsilon_{\mu e}$ and ϵ_{ee}, and conclude that the (2+2) model is highly disfavored. In this chapter, the Sum Rule of the (2+2) neutrino model with all the small mixing angles ϵ's and the earth matter effect will be calculated through numerical method. The detailed contributions from these small mixing angles ϵ's will also be studied. We will find that the Sum Rule by itself is a poor prognosticator for the fate of the (2+2) model. An analytical approach for a much simplified case will be presented in Appendix A to study the matter effect when all small mixing angles ϵ's are zero.

5.1 Numerical Calculation Procedure

The numerical calculation for the solar and the atmospheric neutrino oscillations will be carried out with a Mathematica© program. In this program, a number of random values between 0 and $\pi/2$ will be chosen for the unrestricted mixing angle $\theta_{\tau s}$. For each value of $\theta_{\tau s}$, a number of random values for the energy within a specified bin will be chosen. For each value of the energy, the procedure described in the previous section will be carried out to get the probabilities. All the probabilities for the energy points will be averaged to get the overall probabilities of the specified energy bin. This method of using random points to get the average is called Monte Carlo average method. The number of energy points chosen is determined by the overall running time and the convergence of the averages. The details for the solar and atmospheric neutrino oscillations are different due to the different energy and different paths involved in the oscillation. These details will be described in the following sections.

5.1.1 Solar Neutrino Calculation

Electron neutrinos are generated at the center of the sun by thermonuclear reactions. Then the neutrinos have to go through the dense solar matter and emerge at the surface of the sun in a nearly pure $|\nu_2\rangle$ mass eigenstate. After this, the neutrinos will hardly oscillate when traveling through the vacuum to reach the earth. When the neutrinos arrive at the earth, after traveling through the solar matter and the distance between the sun and the earth, the mass eigenstates are incoherent. Thus, the density operator of the decoherent neutrinos is diagonal in the mass basis. In the operator notation, it is simply

$$\hat{\rho}^S_{mass} = \sum_j \left|U^S_{ej}\right|^2 |\nu_j\rangle\langle\nu_j|. \tag{54}$$

in the adiabatic approximation. Here, $\mathbb{U}^S$ is the mixing matrix described in Eqn. 51 in the solar matter. Neutrinos emerging from the sun and observed on earth, we name solar neutrinos $|\nu_\odot\rangle$. Thus the probability to detect flavor β among the solar neutrinos will be

$$P(\nu_\odot \to \nu_\beta) = \langle\nu_\beta|\hat{\rho}^S_{mass}|\nu_\beta\rangle = \sum_j \left|U^S_{ej}\right|^2 |U_{ej}|^2 . \tag{55}$$

Here, $\mathbb{U}$ is the mixing matrix in vacuum in Eqn. 28. The product of two classical probabilities, $\left|U^S_{ej}\right|^2 |U_{ej}|^2$, is a result of the decoherence of the neutrino beam. The probability to detect non-electron neutrinos in the solar neutrino is just

$$P(\nu_\odot \to \nu_{\not e}) = 1 - P(\nu_\odot \to \nu_e).$$

The solar density varies exponentially. But as discussed in Section 4.5, the neutrinos evolve adiabatically while traveling from the center to the surface of the sun. It is only the matter density at the center, where they are produced, that enters $\left|U^S_{ej}\right|^2$. This means that the exponentially changing density of the solar material will not affect the neutrino oscillation significantly. For the solar matter at the center, the electron number density is $N^S_e = 6 \times 10^{25}\text{cm}^{-3}$. The solar neutrino energy ranged from 5 MeV to 15 MeV is measured by the Super-Kamiokande experiment. Within this energy range, we find that 10 energy points are enough to achieve good results for the Monte Carlo average method.

So for each chosen value of the mixing angle $\theta_{\tau s}$, 10 random values of energy will be chosen within 5 MeV and 15 MeV. For each energy value, the probability to detect sterile

neutrinos $P(\nu_\odot \to \nu_s)$ and non-electron neutrinos $P(\nu_\odot \to \nu_{\not e})$ will be calculated as described above. Then the ten values of the probabilities will be averaged to get the overall probability in this energy range. In this way the solar ratio R_{sol}, defined by Eqn. 39, can be calculated for each value of mixing angle $\theta_{\tau s}$.

5.1.2 Atmospheric Neutrino Calculation

The calculation for atmospheric neutrinos is more complicated than the solar neutrino because of the higher energy with the atmospheric neutrinos, the more complicated path of the neutrino beam and the more complicated structure of the earth.

Neutrino Beam Direction

The zenith θ_z angle of the neutrino beam is defined as the angle between the direction of the neutrino beam and the earth radius pointing at the experiment site. In the atmospheric neutrino experiment, the final measurement is really an average over a zenith angle bin of certain size. So, the calculation of the neutrino oscillation probabilities has also to be averaged over the zenith angle. In the current work, only the up-going neutrinos with zenith angle between 0 to $\cos^{-1}(0.8) = 36.9^o$ will be considered because these neutrinos have the longest base-line and so have enhanced oscillation probabilities, and are the best experimental test of the sterile/active neutrino ratio in atmospheric data involves the matter effect.

The Structure of Earth

The structure of the earth can be simplified as a dense core, with radius $R_C = 3493$ km, surrounded by a less dense mantle. The radius of the earth is $R_E = 6371$ km. The electron number density in the core is $N_e^{EC} = 6N_A$ cm^{-3}, while the electron number density in the mantle is $N_e^{EM} = 1.6N_A$ cm^{-3}. Here, $N_A = 6.02 \times 10^{23}$ is the Avogadro's Number. For any neutrino beam with zenith angle $\theta_z < \tan^{-1} \frac{R_C}{R_E} \simeq 33^o$, the neutrino beam will travel through the mantle, the core, and the mantle again, as shown in Fig. 21. The distance that the neutrino beam goes through the core is

$$2r_{EC} = 2\sqrt{R_C^2 - \sin^2\theta_z R_E^2}, \tag{56}$$

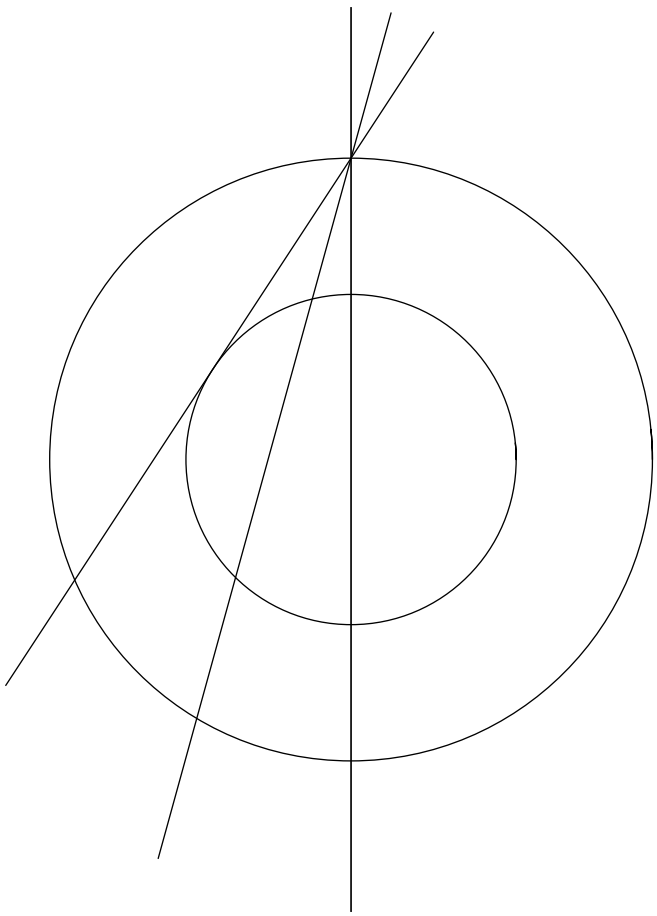

Figure 21: The Neutrino Beam Travel Through the Earth

while the distance the neutrino beam travels through one of the two segments of the mantle is

$$r_{EM} = R_E \cos\theta_z - r_{EC}. \tag{57}$$

So, if the neutrino beam starts from one side of the earth in state $|\nu_\alpha\rangle$, then it will come out of the other side in state

$$\begin{aligned} |\nu_F(\theta_z)\rangle &= \sum_{\beta,l,\gamma,k,\sigma,j} |\nu_\beta\rangle\langle\nu_\beta|\nu_l^{EM}\rangle\langle\nu_l^{EM}|e^{-i\mathbb{H}_l^{EM} r_{EM}}|\nu_l^{EM}\rangle\langle\nu_l^{EM}|\nu_\gamma\rangle \\ &\times \langle\nu_\gamma|\nu_k^{EC}\rangle\langle\nu_k^{EC}|e^{-i\mathbb{H}_k^{EC} 2r_{EC}}|\nu_k^{EC}\rangle\langle\nu_k^{EC}|\nu_\sigma\rangle \\ &\times \langle\nu_\sigma|\nu_j^{EM}\rangle\langle\nu_j^{EM}|e^{-i\mathbb{H}_j^{EM} r_{EM}}|\nu_j^{EM}\rangle\langle\nu_j^{EM}|\nu_\alpha\rangle. \end{aligned} \tag{58}$$

Here, the Greek indexes indicate the flavor basis, and the roman indexes mean the mass basis.

Making use of the transformation matrix of Eqn. 51, Eqn. 58 becomes

$$|\nu_F(\theta_z)\rangle = \sum_\beta U^E_{\beta\alpha}(\theta_z)|\nu_\beta\rangle \tag{59}$$

with the overall unitary evolution matrix for the earth as

$$\mathbb{U}^E(\theta_z) = \left[\mathbb{U}^{EM} e^{-i\mathbb{H}^{EM} r_{EM}} \mathbb{U}^{EM\dagger}\right] \left[\mathbb{U}^{EC} e^{-i\mathbb{H}^{EC} 2r_{EC}} \mathbb{U}^{EC\dagger}\right] \left[\mathbb{U}^{EM} e^{-i\mathbb{H}^{EM} r_{EM}} \mathbb{U}^{EM\dagger}\right]. \tag{60}$$

Here, the propagation matrices $e^{-i\mathbb{H}^X r_X}$ are diagonal, with elements determined by replacing the Hamiltonian $\mathbb{H}^X$ with its eigenvalues. These eigenvalues and the transformation matrices are obtained by finding the eigenvalues and eigenvectors of the Hamiltonian $\mathbb{H}^X$ in matter as described in Section 4.6.

The above calculation is still valid if the neutrino beam does not travel through the core. Setting the distance traveling through the core $2r_{EC} = 0$, the Eqn. 60 becomes

$$\begin{aligned} \mathbb{U}^E(\theta_z) &= \left[\mathbb{U}^{EM} e^{-i\mathbb{H}^{EM} r_{EM}} \mathbb{U}^{EM\dagger}\right] \left[\mathbb{U}^{EC} \mathbb{U}^{EC\dagger}\right] \left[\mathbb{U}^{EM} e^{-i\mathbb{H}^{EM} r_{EM}} \mathbb{U}^{EM\dagger}\right] \\ &= \left[\mathbb{U}^{EM} e^{-i2\mathbb{H}^{EM} r_{EM}} \mathbb{U}^{EM\dagger}\right]. \end{aligned} \tag{61}$$

So as long as the distance through the mantle of the Earth r_{EM} is correct, Eqn. 60 also describes the situation where the neutrino beam travels only through the mantle of the Earth.

Turning to the atmospheric neutrino oscillation, the probability of the muon neutrino to oscillate into sterile neutrino $|\nu_s\rangle$ is

$$P(\nu_\mu \to \nu_s) = \left|\langle\nu_\mu|\mathbb{U}^E|\nu_s\rangle\right|^2 = \left|U^E_{s\mu}\right|^2, \tag{62}$$

and the probability for the muon neutrino to oscillate into non-muon neutrino is

$$P(\nu_\mu \to \nu_{\not\mu}) = 1 - P(\nu_\mu \to \nu_\mu) = 1 - \left|U^E_{\mu\mu}\right|^2. \tag{63}$$

The Fast Oscillation Due to the LSND Mass Gap

When the atmospheric neutrinos have energy ~ 1 GeV, the neutrino oscillation length due to the LSND mass gap, according to Eqn. 18, will be only a few km's. The atmospheric

neutrino oscillation calculation carried out in this work and in the Super-Kamiokande analysis includes energies from a few 10^{-1} GeV to a few hundreds GeV, and zenith angle θ_z from 0 to 37^o. The oscillation lengths L associated with δm^2_{LSND} vary from 1.3×10^4 km to 5.1×10^3 km. These averaging procedures will simply average over a lot periods of the fast oscillation due to the LSND mass gap. Of course, this fast oscillation could be handled by averaging over the energy and the zenith angle. But it force more data points to be taken for the Monte Carlo procedure to converge. In order to reduce the computation cost and time, we set by hand the phases proportional to the LSND mass gap to zero. This is achieved by using projectors to replace the propagation matrix in Eqn. 60, when it is used in Eqn. 62. The projectors are

$$\mathbb{D} = \begin{pmatrix} 1 & e^{i(m_1^X - m_2^X)L_X} & 0 & 0 \\ e^{-i(m_1^X - m_2^X)L_X} & 1 & 0 & 0 \\ 0 & 0 & 1 & e^{i(m_3^X - m_4^X)L_X} \\ 0 & 0 & e^{-i(m_3^X - m_4^X)L_X} & 1 \end{pmatrix}, \tag{64}$$

again, with X represents the core of the earth with EC and the mantle of the earth with EM. For the mantle, $L_{EM} = r_{EM}$. But for the core $L_{EC} = 2r_{EC}$ because the distance inside the core is $2r_{EC}$.

The Range of Atmospheric Neutrino Energy

The atmospheric neutrinos produced by the energetic cosmic rays typically have energy ranged from 0.5 GeV up to 500 GeV. In the Super-Kamiokande experiment, the muon neutrinos ν_μ will interact with the rock below the detector and generate secondary muons, while the electron neutrinos will generate electrons. The Super-Kamiokande detector is a water Cerenkov detector, which can distinguish the muon-like events and the electron-like events by the shape of the rings. The ratio of the muon neutrino flux to the electron neutrino flux can be deduced from the number of the two types of events observed by the Super-Kamiokande detector.

The Cerenkov detector cannot measure the energy of the muons. But when the parent muon neutrinos have energy between 0.5 to 1.5 GeV, the trajectories of the secondary muons will be fully contained within the Super-Kamiokande detector. For the parent muon neu-

trinos with energy between 1.5 to 30 GeV, the trajectories of the secondary muons will be partially contained within the Super-Kamiokande detector, eg. the muon trajectory either starts or ends in the detector. For the parent muon neutrinos with energy between 30 to 500 GeV, the trajectories of the secondary muons will go through the whole detector, eg. the through-going events. Fig. 22 [106] shows the classification of the muon-like events in the Super-Kamiokande detector.

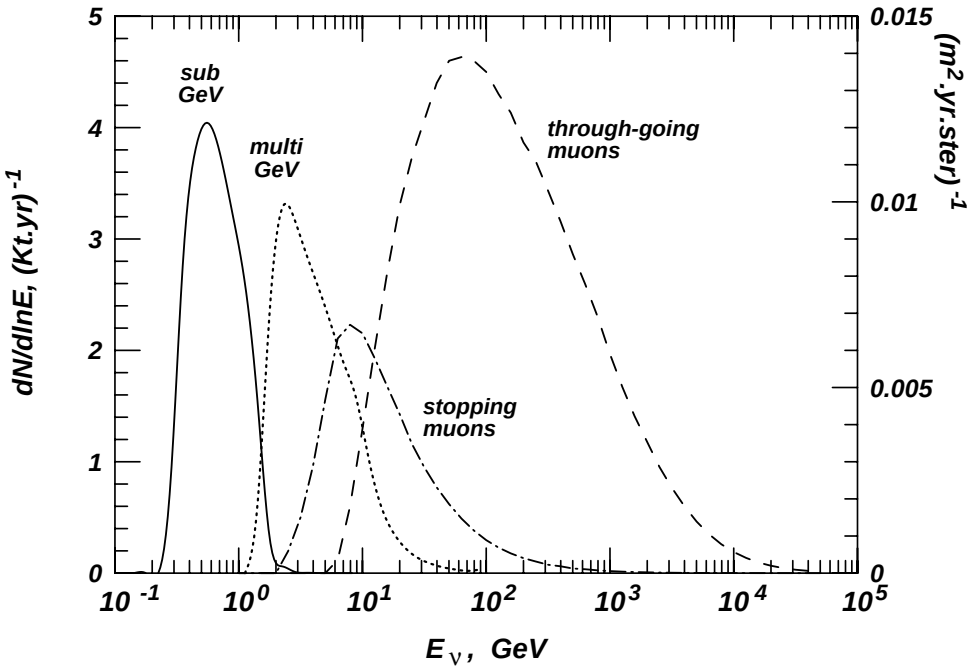

Figure 22: Classification of Super-Kamiokande Neutrino Events

Due to the energy dependence of the MSW matter effect, and the resonant behavior, which can turn small vacuum angles into large matter angles, the small mixing angles ϵ's will definitely have dramatically different roles at different energies. Thus, the investigation will be carried out for different energy bins, the contained energy bin $0.5 \sim 1.5$ GeV, the partially contained energy bin $1.5 \sim 30$ GeV, the through-going energy bin $30 \sim 500$ GeV, and the typical through-going energy bin $50 \sim 150$ GeV to study the energy-dependence of

the small mixing angles' effects.

Brief Walk-through of The Procedure

1. Randomly choose a value for $\theta_{\tau s}$ within $[0, \pi/2]$

2. With this $\theta_{\tau s}$,

   - Randomly choose 10 values for solar neutrino energy within 5 to 15 MeV.

     For each energy, carry out the calculation described in Section 5.1.1 to get the probabilities for $P(\nu_\odot \to \nu_s)$ and $P(\nu_\odot \to \nu_{\not e})$. Then average the 10 values of each of the two probabilities, and form the solar ratio R_{sol} for this value of $\theta_{\tau s}$.

   - Randomly choose 50 values for energy within the specified atmospheric neutrino energy bin.

     For each energy value, randomly choose 10 values of zenith angle θ_z. For each zenith angle, carry out the calculation for atmospheric neutrino oscillation described in Section 5.1.2 to get the probabilities for $P(\nu_\mu \to \nu_s)$ and $P(\nu_\mu \to \nu_{\not\mu})$ for these 10 zenith angle. Then average the values of these 10 probabilities to get the average probability for the energy value. After finish calculating all the 50 values of each of the energy values, average all these 50 probabilities to get the final probabilities for $P(\nu_\mu \to \nu_s)$ and $P(\nu_\mu \to \nu_{\not\mu})$ and form the atmospheric ratio R_{atm} for this value of $\theta_{\tau s}$.

3. Present R_{atm} versus R_{sol} as a scatter-plot to demonstrate the Sum Rule.

4. Repeat the steps above for as many times as needed.

5.1.3 The Exclusion Regions From Experiments

From published works fitting solar and atmospheric oscillation data with (2+2) model [95, 96], with small mixing angles ϵ's ignored, the 90% C.L. and 99% C.L. value for the solar ratio R_{sol} are 0.45 and 0.75, while the 90% C.L. and 99% C.L. for the atmospheric ratio

R_{atm} are 0.17 and 0.26.[1] The allowed values for the solar and atmospheric ratios R_{sol} and R_{atm} are treated as Gaussian distributions centered at $R_{sol} = 0$ and $R_{atm} = 0$ (no ν_s). The combination of these two Gaussian-distributed values generates an elliptical exclusion region, described by

$$\frac{R_{atm}^2}{\sigma_{atm}^2} + \frac{R_{sol}}{\sigma_{sol}^2} = R_{C.L.}^2. \tag{65}$$

Putting in the numbers above, one finds for the 90% C.L. exclusion region, $R_{90\%} = 2.15$, and for the 99% C.L. exclusion region, $R_{99\%} = 3.03$, with $\sigma_{atm} = 0.0957$ and $\sigma_{sol} = 0.0734$.

The 90% and 99% C.L. exclusion regions will be superimposed on the Sum Rule plot. If the Sum Rule point lies inside the exclusion regions, its parameter set is viable. But if the data point lies outside the exclusion regions, its parameter set is definitely not viable. The 90% and 99% exclusion regions will act as visual guides to the Sum Rule plots in the following sections.

5.2 Calculation Results

In this section, the results of my numerical calculations will be shown and briefly discussed. In every one of the plots shown, there are 4000 scatter-points, except for the zeroth order Sum Rule and Product Rule plots which have 500 points. Each of these points corresponds to a value of $\theta_{\tau s}$, which is randomly chosen between 0 to $\pi/2$.

5.2.1 Zeroth Order Sum Rule

500 points for the zeroth order Sum Rule for neutrinos with energy bin 30 GeV to 500 GeV are shown in Fig. 23. Zeroth order Sum Rule means all the small mixing angles ϵ's set to zero. But the earth matter effect is turned on. These 500 data points are plotted against the Sum Rule without matter effect, the blue solid line in Fig. 23. It is obvious that the Sum Rule is nearly exact when all the small mixing angles ϵ's are set to zero but with the earth matter effect turned on. There is no data points inside the 90% exclusion region, and

[1] The data fitting work in [95, 96] are done with all ϵ's set to zero. It is noted that the global fit with the largest small mixing angles $\epsilon_{\mu\mu}$ results expanded exclusion regions. But calculating the exclusion boxes with non-zero ϵ's is a formidable task beyond the scope of this work. So the conclusion from [95, 96] will still be used here.

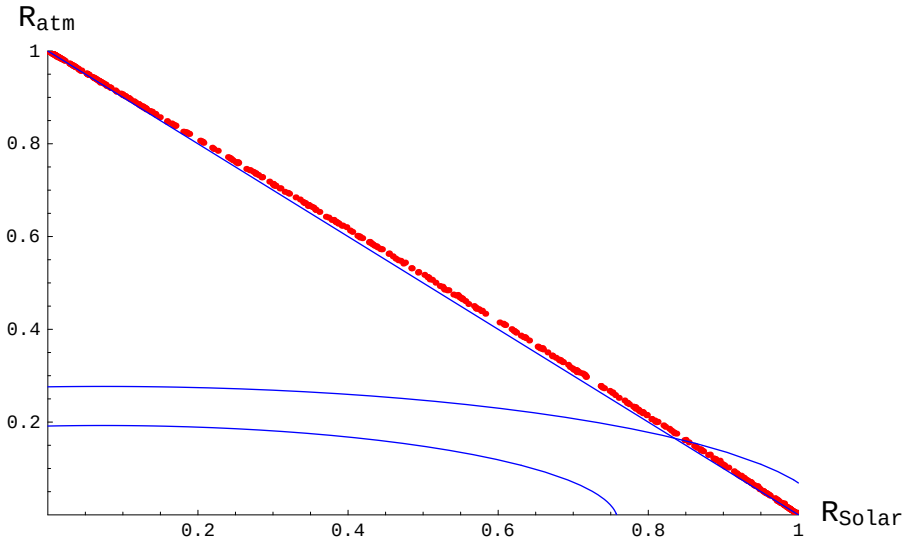

Figure 23: Zeroth Order Sum Rule With Matter Effect

only the data points with $R_{sol} \simeq 1$ are inside the 99% exclusion region. From Eqn. 41 and Eqn. 35, these points correspond to $\theta_{\tau s} \simeq \pi/2$, thus with minimal probabilities to oscillation into sterile neutrinos. Also from Fig. 23, it can be concluded that the small mixing angles ϵ's are essential to the relaxation of the Sum Rule. The presence of earth matter without small mixing angles ϵ's will not cause any obvious relaxation to the Sum Rule. This result will also be investigated in the Appendix A to show the contribution of the earth matter effect, and the slightly deviation of the data points from the zeroth order Sum Rule will be explained.

5.2.2 Sum Rule With Small Mixing Angles and The Earth Matter Effect

In this section, the Sum Rule with all the small mixing angles non-zero and the earth matter effect turned on will be studied. The numerical calculation results are plotted in Fig. 24-27. Two plots are shown in each of these figures. The top one is calculated with the earth matter effect, while the bottom one without the earth matter effect. In each plot of these figures, there are 4000 scattered data points shown together with the 90% and 99%

exclusion regions.

The data points in Fig. 24 are calculated for atmospheric neutrinos with energy between 0.5 to 1.5 GeV, the energy for contained events in Super-Kamiokande experiments. The data points in Fig. 25 are with energy between 1.5 to 30 GeV, the partially contained events, while that data points in Fig. 26 are with energy between 30 to 500 GeV, the through-going events. The data points in Fig. 27 are calculated with the "typical" energy of through-going events.

Based on the results plotted in the figures from Fig. 24 to Fig. 27, the relaxation of the Sum Rule when the small mixing angles ϵ's and the matter effect are included in the neutrino oscillation is evident. At high energy, the Sum Rule can be significantly relaxed that a large fraction of the allowed data points lie within the conservative 90% exclusion region caculated with all ϵ's are zero.

Comparing the top and the bottom plots in figures from Fig. 24 to Fig. 27, the relative significance of the earth matter-effects for the atmospheric neutrino oscillation with the small mixing angles ϵ's is obvious. The earth matter-effects are not significant at low energies, but become more important with increasing energy.

The relaxation of the Sum Rule is also energy dependent. A roughly diagonal band in Fig. 24 and Fig. 25 turns into a butterfly pattern at high energy in Fig. 26 and FIG. 27. This is the result of the energy-dependent matter effects on the oscillation amplitude and length, and of the suppression occurring when oscillation lengths are large compared to the Earth's diameter. While for low energies, the zeroth order Sum Rule provides a good approximation to the (2+2) model with non-zero small mixing angles ϵ's. In this case, $R_{atm} \sim \sin^2\theta_{\tau s} \sim 1 - R_{sol}$. But at high energies, the dependence on $\theta_{\tau s}$ is quite different. As shown by the numerical calculations in this work, $R_{atm} \sim 0$ and $R_{sol} \sim 0$ can be achieved simultaneously, especially at high energy. This means that the sterile neutrino can be hidden from both the atmospheric neutrino oscillation through-going data and the solar neutrino oscillation data.

5.2.3 The Roles of the Individual Small Mixing Angles

Another question of special interest in this work is the different roles of the individual small mixing angles ϵ's. To answer this important question, the Sum Rule is calculated with only one of the small mixing angles ϵ's turned on and with the earth matter effect turn on. The results are plotted in Fig. 28-31. In each one of these figures, the top plot is with only $\epsilon_{\mu\mu}$ as non-zero, the middle plot with only $\epsilon_{\mu e}$ as non-zero, while the bottom plot with only ϵ_{ee} non-zero. Same as the Sum Rule plots in the previous section, calculations are carried out over different energy bins of interests, with Fig. 28 over the energy bin from 0.5 to 1.5 GeV, Fig. 29 over 1.5 to 30 GeV, Fig. 30 over 30 to 150 GeV, and Fig. 31 over 50 to 150 GeV.

Just like in the Sum Rule plots with all the small mixing angles ϵ's are turned on, the effects of the individual small mixing angles ϵ's on the Sum Rule are energy dependent, and become more significant at higher energy. By comparing the bottom plot with only $\epsilon_{ee} \neq 0$ against the other two plots in Fig. 28-31, it is obvious that the non-zero ϵ_{ee} has minimal effects on the Sum Rule both at low energies and high energies. So, the deviation from the zeroth order Sum Rule is mainly caused by the non-zero values of the other two small mixing angles, $\epsilon_{\mu\mu}$ and $\epsilon_{\mu e}$. Also from the comparison, $\epsilon_{\mu\mu}$ has relatively big effects on the Sum Rule than $\epsilon_{\mu e}$, but the contribution from $\epsilon_{\mu e}$ is still too significant to ignore. This result is especially interesting because $\epsilon_{\mu e}$ is set to zero in the global analysis [100, 101, 102, 103]. The $\epsilon_{\mu e}$'s significant effects on the Sum Rule suggest that at least the small mixing angles $\epsilon_{\mu\mu}$ and $\epsilon_{\mu e}$ must be turned on in the global analysis of the neutrino oscillation data. This casts some doubt on the recent claimed exclusions of the (2+2) neutrino model.

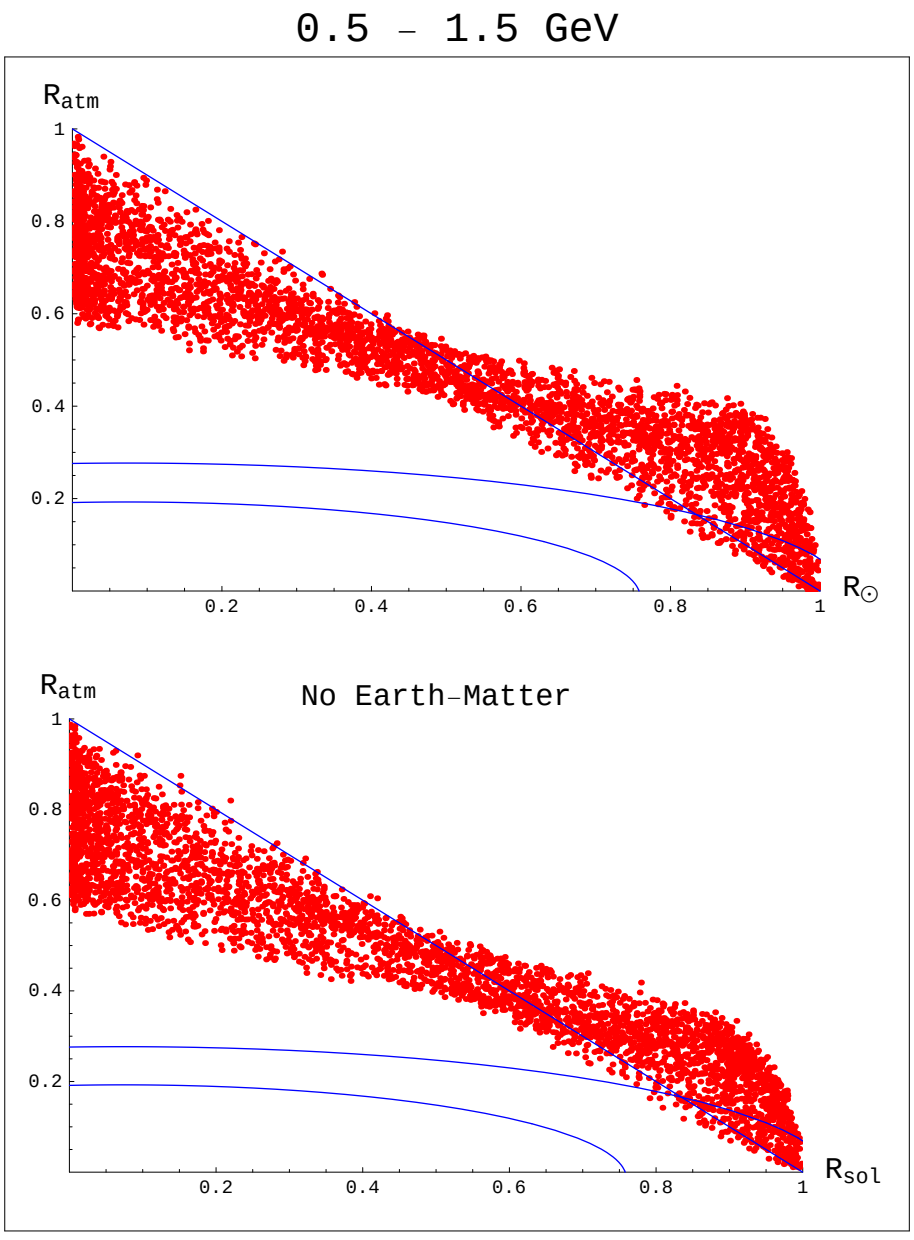

Figure 24: The Sum Rule for 0.5 - 1.5 GeV

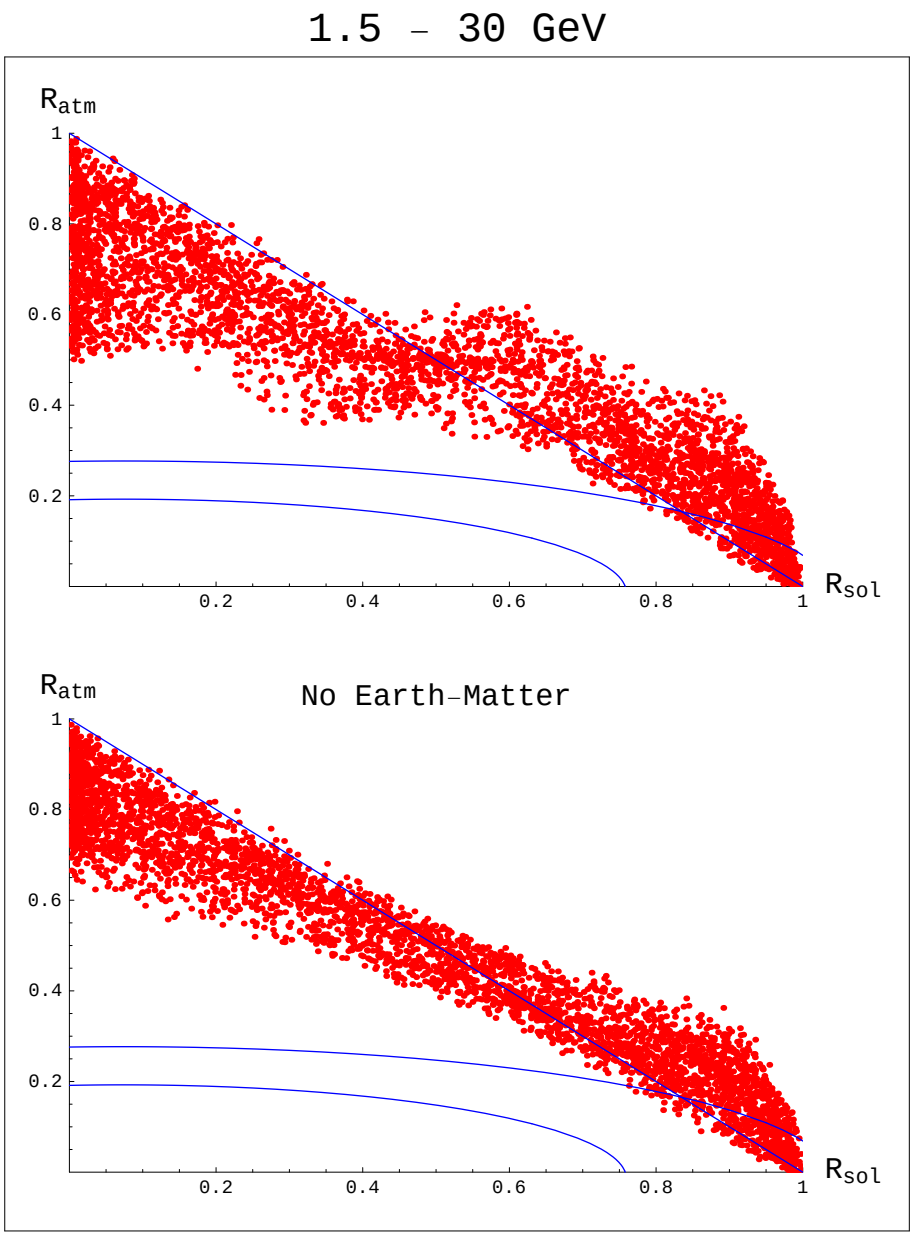

Figure 25: The Sum Rule for 1.5 - 30 GeV

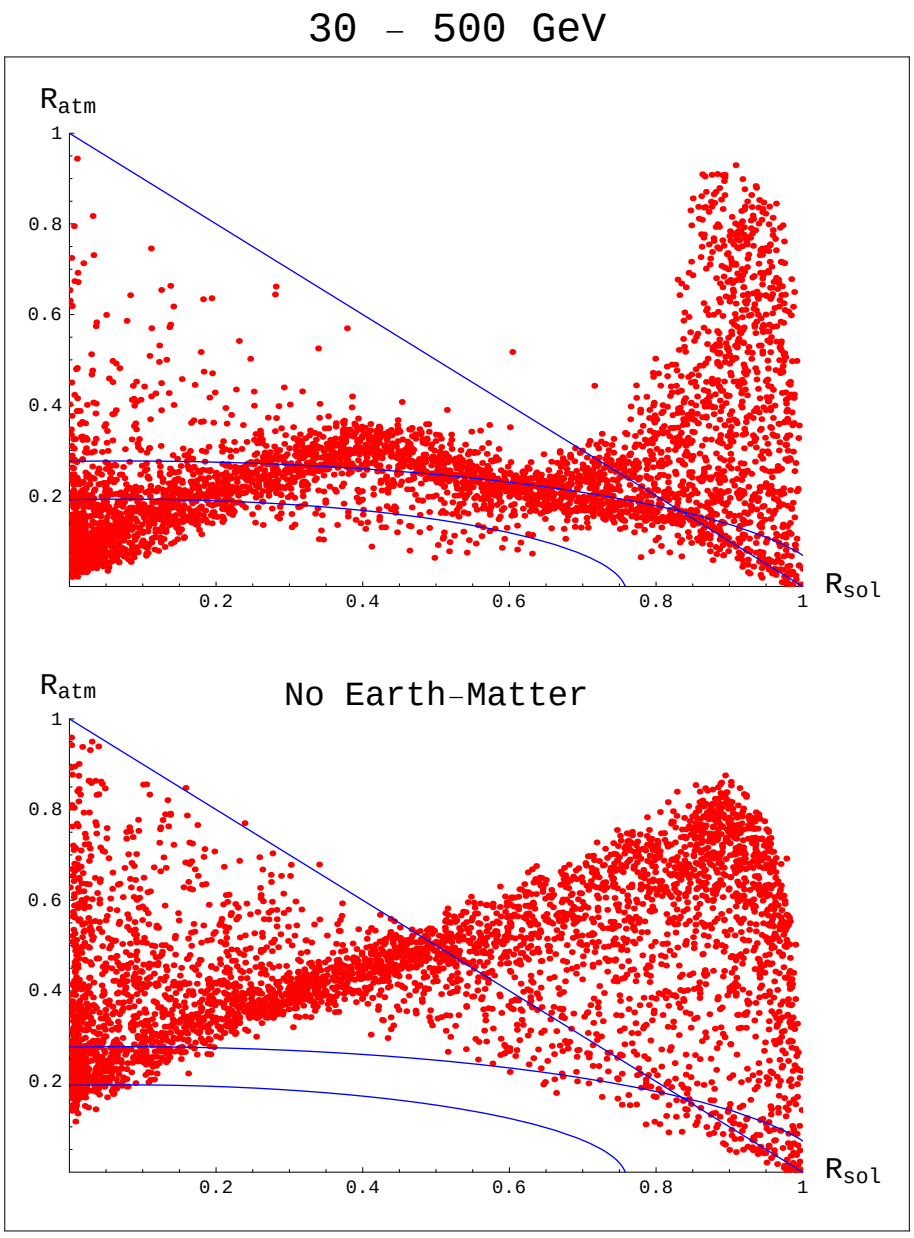

Figure 26: The Sum Rule for 30 - 500 GeV

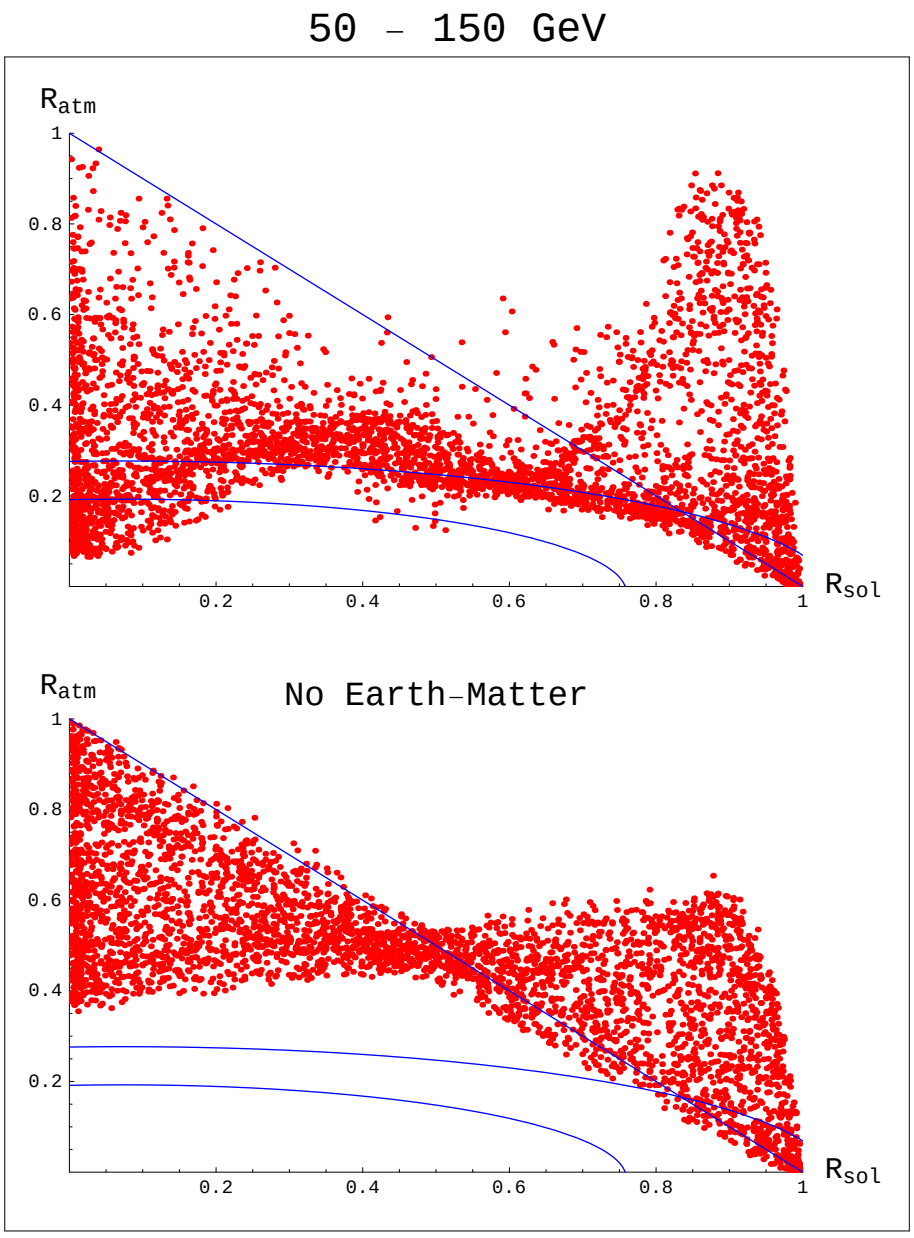

Figure 27: The Sum Rule for 50 - 150 GeV

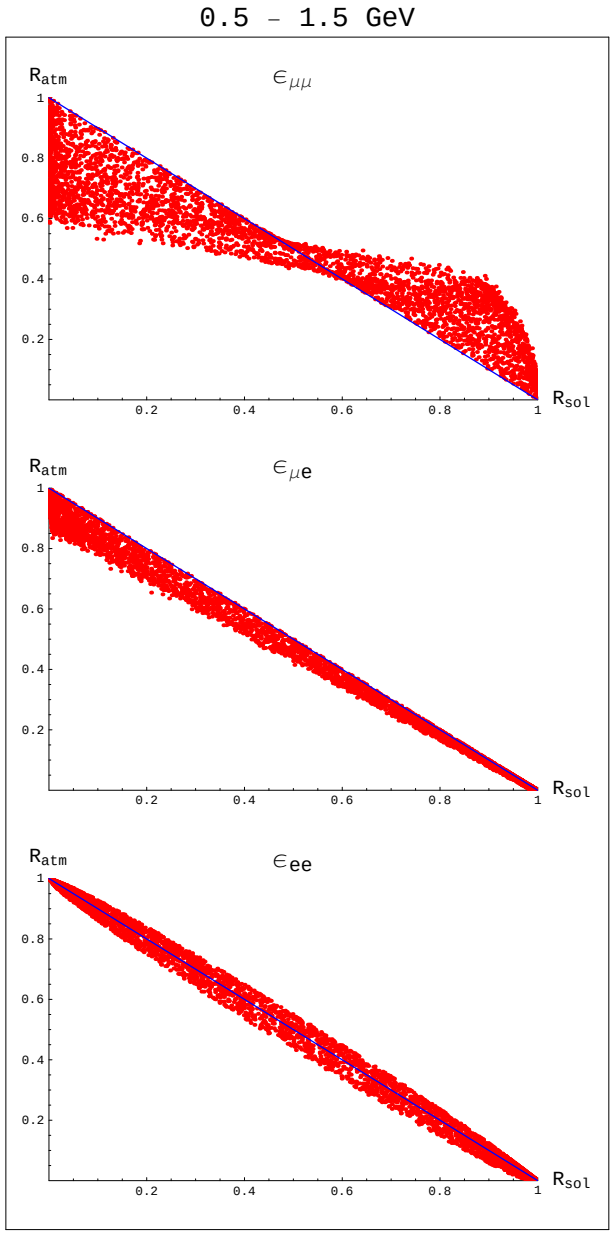

Figure 28: Small Mixing Angles at 0.5 - 1.5 GeV

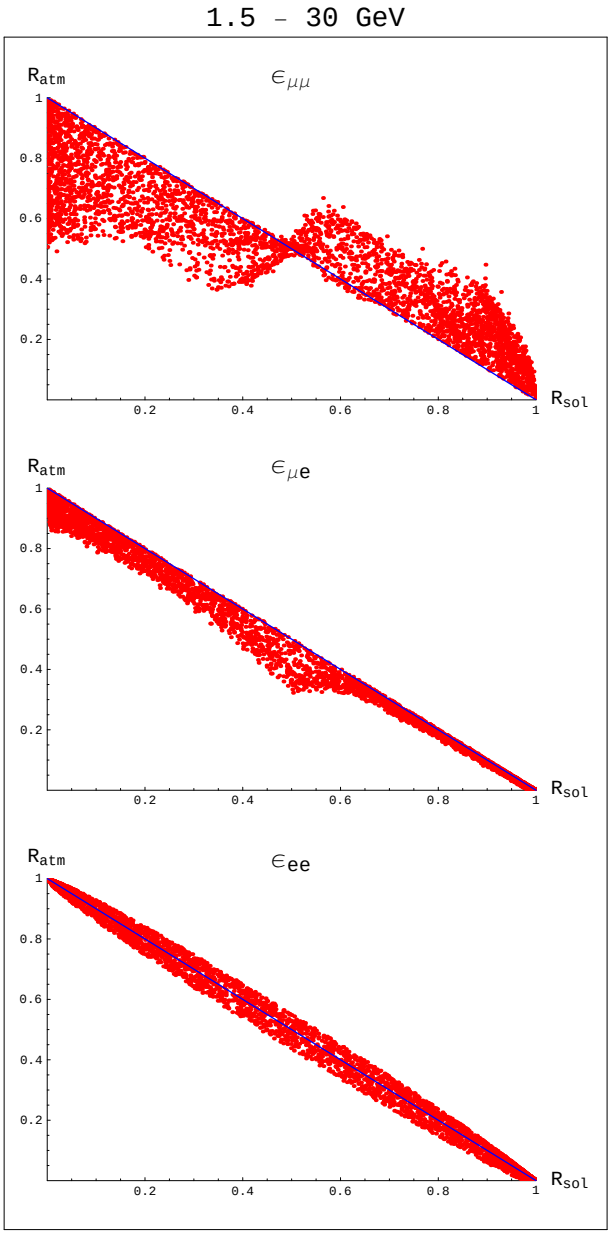

Figure 29: Small Mixing Angles at 1.5 - 30 GeV

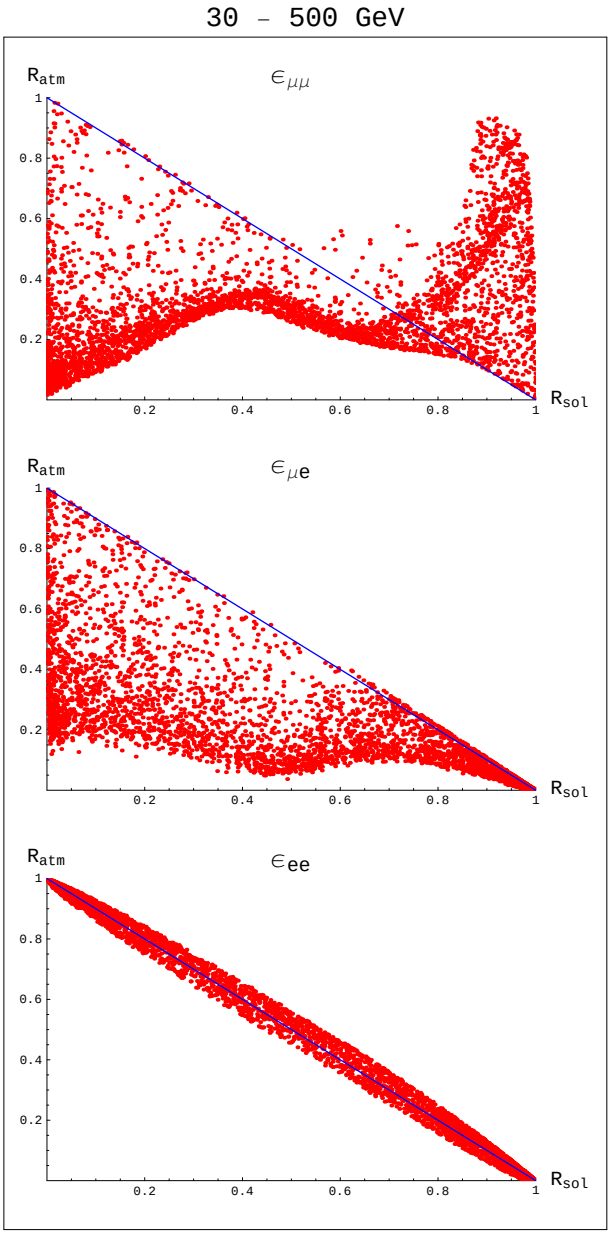

Figure 30: Small Mixing Angles at 30 - 500 GeV

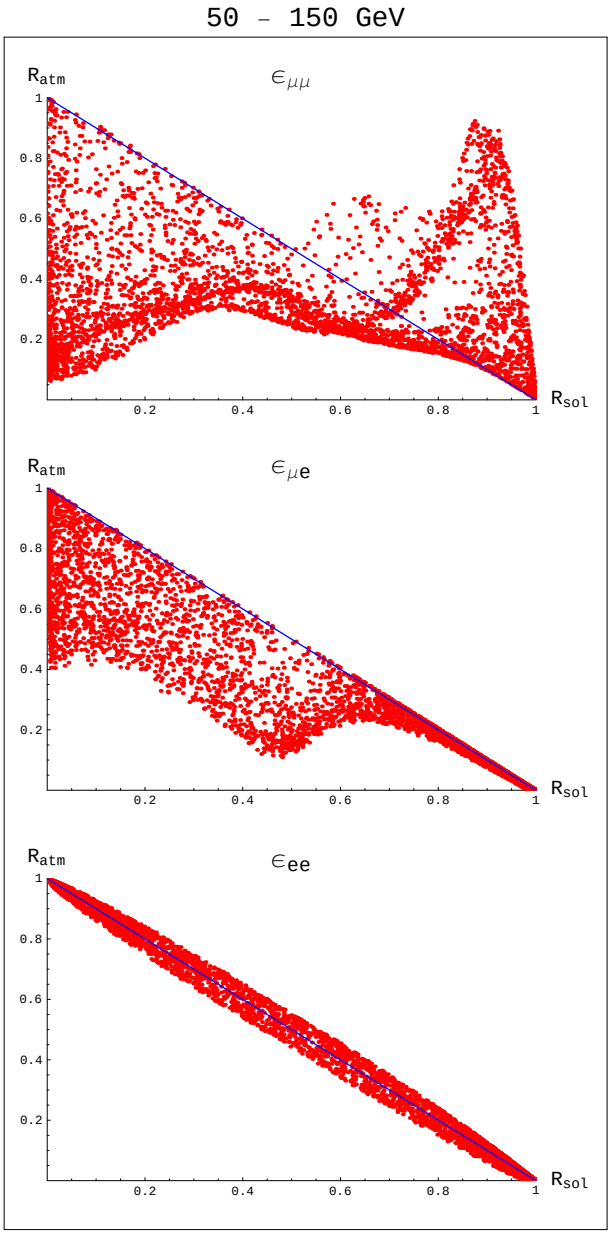

Figure 31: Small Mixing Angles at 50 - 150 GeV

5.2.4 Sum Rule for Anti-neutrinos

When all the small mixing angles ϵ's are neglected, matter effects on the atmospheric ratios are negligible, and so the neutrino and anti-neutrino contributions to the Sum Rule are virtually identical. But with non-zero small mixing angles ϵ's, the contributions of the matter effects become significant and may be different for neutrinos and anti-neutrinos because the sign of the matter potential is reversed for the anti-neutrino. Near a resonance of neutrinos, the anti-neutrinos will not be in resonance, thus the earth matter will affect neutrinos and anti-neutrinos quite differently. But well above a resonance, the earth matter will have the same effect on neutrinos and anti-neutrinos. Whenever the earth matter effects for neutrinos are evident, the same calculation will also be carried out for anti-neutrinos to determine whether the matter effect is any different. For all the energy bins of interests here, the only visible difference between the Sum Rule of neutrinos and anti-neutrinos happens for energy from 1.5 to 30 GeV. The Sum Rule for anti-neutrino plot in this energy bin is shown in Fig. 33. It is obvious that the the anti-neutrinos will not affect the conclusions drawn for the Sum Rule of (2+2) neutrino model. This result hints that the matter induced neutrino oscillation resonances are not playing very significant roles in the atmospheric neutrino oscillations.

5.2.5 Product Rule of (2+2) Neutrino Oscillation

The Product Rule of the (2+2) neutrino oscillation with energy from 50 to 150 GeV is plotted in Fig. 33. The plot on the top is the zeroth order Product Rule, with zeroth meaning all the small mixing angles ϵ's are set to zero. The plot on the bottom is the Product Rule with all the small mixing angles ϵ's and the earth matter effect turned on. It is obvious that the Product Rule is also relaxed significantly by the small mixing angles ϵ's and the earth matter effect.

5.3 Conclusions

In this chapter, numerical calculations of the Sum Rule of the (2+2) neutrino model are performed with the three small mixing angles ϵ's and the earth matter effect turned on. The results show that the combination of the small mixing angles ϵ's, especially two of the larger angles $\epsilon_{\mu\mu}$ and $\epsilon_{\mu e}$, and the matter effect will cause significant relaxation from the Sum Rule.

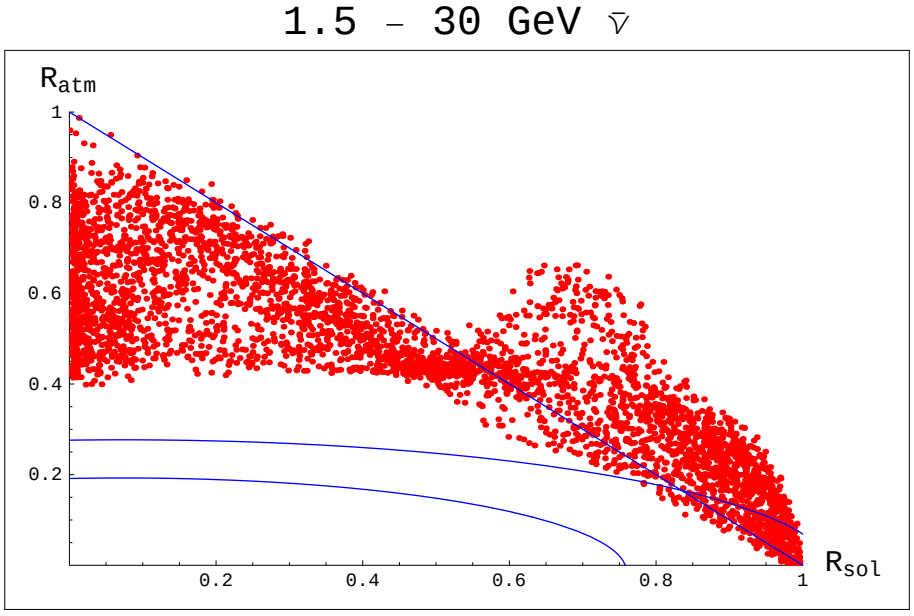

Figure 32: The Sum Rule of Anti-neutrinos of 1.5 - 30 GeV

Among the energy bins of interests, the deviation from the Sum Rule is most significant for energy from 30 to 500 GeV, which corresponds to the range for the through-going events. For the three mixing angles, the mixing angle $\epsilon_{\mu\mu}$ has the most significant contribution to the deviation from the Sum Rule. This justifies the practice of the global data fits [100, 101, 102, 103] to include $\epsilon_{\mu\mu}$ in part of their fitting of LSND data. But the other small mixing angle $\epsilon_{\mu e}$ also has significant contribution to the deviation from the Sum Rule. In certain energy bin, itself can cause enough deviation from the Sum Rule to generate data points within the exclusion regions. The last one of the small mixing angles ϵ_{ee} doesn't have much contribution to the deviation from the Sum Rule. It would not cause any problem to omit ϵ_{ee} in any future global data fitting work. The results here raises questions to the conclusions from those global data fitting works, thus weakens the case that these global data fitting works have against the (2+2) model. In order to rule out the (2+2) model completely, global data fitting with both of the small mixing angles $\epsilon_{\mu\mu}$ and $\epsilon_{\mu e}$ must be carried out.

The Product Rule of (2+2) model is also proposed, and the calculation shows that the Product Rule can also be significantly relaxed when both the small mixing angles ϵ's and

the earth matter effect are present.

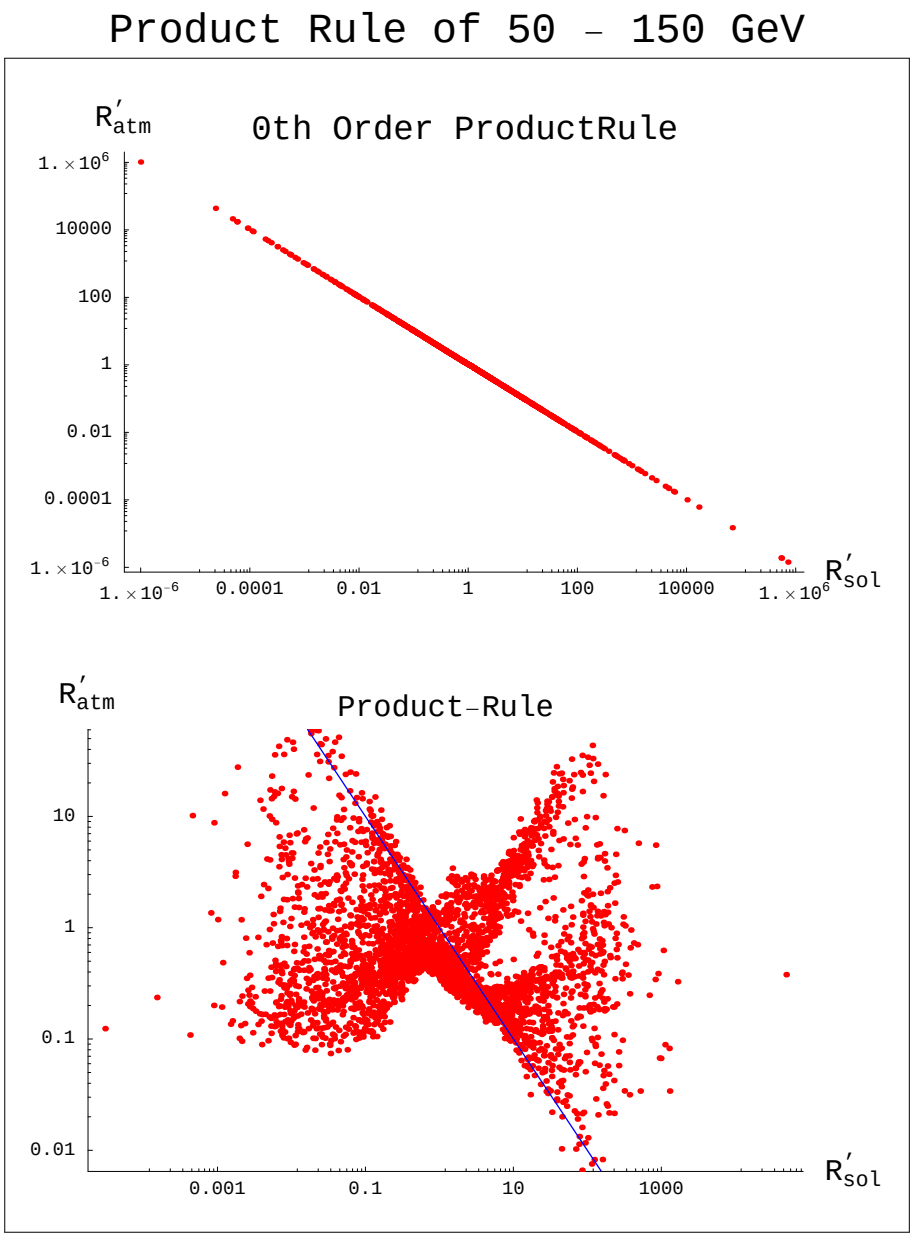

Figure 33: The Product Rules of the (2+2) Model

PART THREE
CONCLUSIONS AND FUTURE STUDY

CHAPTER VI

WHAT HAVE WE LEARNED

We have performed mainly numerical calculations of the Z-Burst mechanism in cosmic-ray physics and the Sum Rule of the (2+2) neutrino model of particle physics. Viability the (2+2) neutrino oscillation model, direct detection of the Big-Bang relic neutrino and measurement of neutrino absolute mass are investigated. The conclusions based on these numerical calculations are discussed in some detail here.

6.1 Viability of Sterile Neutrino and (2+2) Sum Rule

The existence of neutrino mass around 10^{-1} eV is vital for the observation of the Z-Burst absorption dip in this decade. The upper limit of the total mass of relic neutrinos from the WMAP and SDSS [68] allows a neutrino mass above 0.2 eV. The LSND mass gap is the strongest evidence supporting such a mass.

The four-neutrino models and their associated sterile neutrino, required by the LSND data, have been doubted because of recent poor fits to global data and because of a contradiction between data and the Sum Rule of the (2+2) model. In this work, the roles of the three small mixing angles ϵ's and the earth matter effect in the Sum Rule are studied. We use mainly numerical calculations, but include analytic study in Appendix A. From these studies, it is learned that at least two of these small mixing angles, namely $\epsilon_{\mu\mu}$ and $\epsilon_{\mu e}$, can cause the Sum Rule to relax significantly. The third small mixing angle ϵ_{ee} has much less effect on the Sum Rule; thus it can be safely neglected in global data fitting. The relaxation of the Sum Rule raises a question concerning assumptions used in the global data fitting. In particular only one small mixing angle $\epsilon_{\mu\mu}$ is included in the data fitting. With the other small mixing angle $\epsilon_{\mu e}$ included, it might change (2+2) fits, as it changed the Sum Rule. In short, the case against the (2+2) model is weakened by the significant relaxation of the Sum Rule resulting from inclusion of the small mixing angles ϵ's and the earth matter effect. Until global data fitting with both small mixing angles $\epsilon_{\mu\mu}$ and $\epsilon_{\mu e}$ is carried out, the (2+2) model

cannot be ruled out. The four-neutrino model is still a viable solution to the solar, atmospheric and LSND neutrino oscillations. The MiniBooNE experiment [31], already gathering data, will give the final verdict on the validity of the LSND claim.

6.2 Detection of Relic Neutrino and the Neutrino Absolute Mass

The proposal to directly detect the relic neutrino through Z-Burst absorption dips was suggested more than two decades ago [49]. But it has become feasible only recently, due to the progressively larger extremely-high energy neutrino cosmic ray detectors, such as AUGER [65], IceCube [64], ANITA [78], EUSO [62], OWL [63] and SalSA [79].

The detection of the Z-Burst absorption dip faces two difficulties. The first is the extremely-high energy required by the Z-Burst resonance. Even for the heaviest neutrino suggested by the LSND mass gap, and allowed by the WMAP and SDSS data, the cosmic neutrino beam has to have energy well above 10^{21} eV in order to achieve the resonant energy of the Z-Burst. The observation of air shower events with energy above the Greisen-Zatsepin-Kuzmin (GZK) cutoff of 5×10^{19} eV offers hope, if not evidence, of the existence of neutrino cosmic rays energetic enough for the Z-Burst resonance. In fact, the solution of the super-GZK cosmic ray puzzle might lie with the Z-Burst model [59].

The second difficulty faced by detection of the Z-Burst absorption dip is the flux of extremely-high energy neutrino cosmic rays. Cosmic rays typically have a power-law spectrum, which decreases the flux decreased significantly at the very high-energy. This also is probably true for neutrino cosmic rays. Experimental upper limits of extremely high-energy cosmic ray flux from RICE [75], GLUE [76], FORTE [77], and Fly's Eye and AGASA [107] also restrict the possible neutrino flux. The proposed detectors mentioned earlier mitigate this flux problem by making use of very large detector areas or volumes. For example, the EUSO experiment will use part of the earth's atmosphere as detecting media. As shown this work, these experiments make it possible to establish the Relative Observable Spectrum of neutrino cosmic rays, if Nature's flux is not far below present experimental limits.

The observation of the Z-Burst absorption dip in the Relative Observable Spectrum of the neutrino cosmic ray would be direct evidence for the relic neutrino. Measurement of the Z-Burst absorption dip is also one of the most promising methods to measure the absolute

mass of the heaviest neutrino. Either the high energy edge of the Z-Burst absorption dip or the maximum of the absorption dip can be used to deduce the absolute mass of the heaviest neutrino.

The feasibility of the inference of the absolute neutrino mass from the Z-Burst absorption dip also depends on the neutrino cosmic ray source distribution and the neutrino mass spectrum. It is found that the best scenario for the Z-Burst absorption dip is the degenerate mass spectrum with neutrino mass around 10^{-1} eV and with a very distant source distribution localized around a large mean redshift. This situation produces the deepest Z-Burst absorption dip, therefore offering the possibility to detect the Z-Burst absorption dip before the year 2008. The worst case scenario is a well-separated neutrino mass spectrum with very light masses and with a nearby source distribution spread about small mean redshift. This situation will not only push the Z-Burst absorption dip to much higher energy, out of the reach of the proposed detectors, but also produce a Z-Burst absorption dip with only about 1/3 of the depth of the best case scenario. Even with the assumption of the 10^{-1} scale neutrino mass, detection of the Z-Burst dip before the year of 2013 remains difficult. If a much lighter neutrino mass is the choice of the nature, direct detection of the relic neutrino and the measurement of the neutrino absolute mass through the Z-Burst absorption dip will just remain a beautiful theoretical idea without proof.

On the other hand, the four-neutrino models, motivated by the LSND mass gap, support the existence of heavy neutrinos with mass around 10^{-1} eV. This absolute mass is essential for the detection of the Z-Burst absorption dip in the future experiments. Even if the four-neutrino models will be ruled out by future experiments, the atmospheric mass gap still suggests the neutrino absolute mass no less than 0.04 eV. Even with this lighter neutrino mass, the detection of the Z-Burst absorption dip is quite possible in this decade, or during the next decade in the worst case scenario.

6.3 Future Work on the Small Mixing Angles and the Z-Burst Model

It has been proven by this work that the Sum Rule of the (2+2) neutrino model can be significantly relaxed when both the small mixing angles ϵ's and the matter effect are present. Also, it is believed that the inclusion of the small mixing angles, $\epsilon_{\mu e}$ and $\epsilon_{\mu\mu}$, in the global

fitting to the experimental data will improve the viability of the (2+2) neutrino model. But the details of the small mixing angles' contributions are still not clear. These small mixing angles might only change those neutrino oscillation channels which are sub-dominant, as suggested in some recent criticisms [103]. On the other hand, it is also possible that these small mixing angles make the (2+2) model more compatible with the current experiment data. The only way to settle this controversy is to carry out a global fitting of the model to experimental data, with the small mixing angles included.

As for the measurement of the Z-Burst absorption dip in the Relative Observable Spectrum of the neutrino cosmic rays, patience is required as we wait for the proposed detectors to be built and to gather data. With sufficient running time, these detectors will be able to either observe the Z-Burst absorption dip, or provide an upper limit to the heaviest neutrino mass. In the meantime, continued neutrino oscillation experiments will provide better information on the spectrum of the neutrino mass, useful input for the Z-Burst absorption dip calculations.

With the rapid developments in neutrino oscillation experiments and extremely-high energy cosmic ray observatories, the neutrino mass spectrum should be fully identified in the next decade.

APPENDIX A

SMALL MIXING ANGLE $\epsilon_{\mu e}$ AND MATTER EFFECT IN (2+2) NEUTRINO OSCILLATION

It has been shown in Fig. 31 that the small mixing angle $\epsilon_{\mu e}$ together with the earth matter effect can produce data points that deviate very far away from the zeroth order Sum Rule, especially the points with the solar ratio $R_{sol} = 0$ can also have a very small value of the atmospheric ratio R_{atm}. In this section, an analytic study of the atmospheric ratio will be attempted for the case with the other two small mixing angles set to zero, with energy between 50 to 150 GeV, and with the earth matter effect included. The points around $R_{sol} = 0$ with very small value of R_{atm} are the most interesting because they are allowed by the exclusion regions from solar and atmospheric experiment data fittings. The analytic study will focus on this region. In this region, $\theta_{\tau s}$ is close to the maximum value $\pi/2$, because the solar ratio $R_{sol} \simeq \cos^2\theta_{\tau s}$. Through this analytic study, the nature of the contributions of the small mixing angle $\epsilon_{\mu e}$ and the matter effect to the relaxation of the Sum Rule will be revealed. The more general case, with the other two small mixing angles turned on, and with other energy ranges, might be investigated in the future.

A.1 The Mixing Matrix and The Hamiltonian with Earth Matter

When the mass basis is ordered as $\{m_4, m_3, m_2, m_1\}$ with $m_4 > m_3 > m_2 > m_1$ and the flavor basis is ordered as $\{\nu_\mu, \nu_\tau, \nu_s, \nu_e\}$, the mixing matrix in vacuum, Eqn. 28, is

$$\mathbb{U} = \mathbb{R}_{23}(\theta_{\tau s})\mathbb{R}_{24}(\epsilon_{\mu\mu})\mathbb{R}_{14}(\epsilon_{\mu e})\mathbb{R}_{13}(\epsilon_{ee})\mathbb{R}_{34}(\theta_{atm})\mathbb{R}_{12}(\theta_{sol}) \tag{A-1}$$

The definition of the rotation matrices are

$$\mathbb{R}_{12}(\theta) = \begin{pmatrix} 1 & 0 & 0 & 0 \\ 0 & 1 & 0 & 0 \\ 0 & 0 & \cos\theta & -\sin\theta \\ 0 & 0 & \sin\theta & \cos\theta \end{pmatrix}, \quad \mathbb{R}_{13}(\theta) = \begin{pmatrix} 1 & 0 & 0 & 0 \\ 0 & \cos\theta & 0 & -\sin\theta \\ 0 & 0 & 1 & 0 \\ 0 & \sin\theta & 0 & \cos\theta \end{pmatrix},$$

$$\mathbb{R}_{14}(\theta) = \begin{pmatrix} \cos\theta & 0 & 0 & -\sin\theta \\ 0 & 1 & 0 & 0 \\ 0 & 0 & 1 & 0 \\ \cos\theta & 0 & 0 & \cos\theta \end{pmatrix}, \quad \mathbb{R}_{23}(\theta) = \begin{pmatrix} 1 & 0 & 0 & 0 \\ 0 & \cos\theta & -\sin\theta & 0 \\ 0 & \sin\theta & \cos\theta & 0 \\ 0 & 0 & 0 & 1 \end{pmatrix},$$

$$\mathbb{R}_{24}(\theta) = \begin{pmatrix} \cos\theta & 0 & -\sin\theta & 0 \\ 0 & 1 & 0 & 0 \\ \sin\theta & 0 & \cos\theta & 0 \\ 0 & 0 & 0 & 0 \end{pmatrix}, \quad \mathbb{R}_{34}(\theta) = \begin{pmatrix} \cos\theta & -\sin\theta & 0 & 0 \\ \sin\theta & \cos\theta & 0 & 0 \\ 0 & 0 & 1 & 0 \\ 0 & 0 & 0 & 1 \end{pmatrix}.$$

In this analytic work, we consider only the case with $\epsilon_{\mu\mu} = \epsilon_{ee} = 0$ is of interested. Thus,

$$\mathbb{U} = \mathbb{R}_{23}(\theta_{\tau s})\mathbb{R}_{14}(\epsilon_{\mu e})\mathbb{R}_{34}(\theta_{atm})\mathbb{R}_{12}(\theta_{sol}). \tag{A-2}$$

The Hamiltonian in flavor basis, as defined in Eqn. 45 is

$$\mathbb{H}_F = \mathbb{U}\frac{\mathbb{M}^2}{2E}\mathbb{U}^\dagger + \mathbb{A}. \tag{A-3}$$

A.1.1 Transform Into Proper Basis $|\nu_d\rangle$

It will significantly simplify the analytic procedure to find the eigenstates of the Hamiltonian with matter if the mass-squared part of the Hamiltonian, Eqn. A-3, can be transformed into a relative block-diagonal form. The new basis, in which the mass square part of the Hamiltonian is in relative block-diagonal form, is called the proper basis. With this block-diagonal structure, it is possible to carry out perturbation calculation on the Hamiltonian, thus achieve analytic study to certain order of the small off diagonal terms. The transfor-

mation matrix that transforms the flavor basis $|\nu_\alpha\rangle$ into the proper basis $|\nu_d\rangle$ is

$$\begin{aligned}\mathbb{U}_N &= \mathbb{R}_{14}(\epsilon_{\mu e})^\dagger \mathbb{R}_{23}(\theta_{\tau s})^\dagger \\ &= \begin{pmatrix} \cos\epsilon_{\mu e} & 0 & 0 & \sin\epsilon_{\mu e} \\ 0 & \cos\theta_{\tau s} & \sin\theta_{\tau s} & 0 \\ 0 & -\sin\theta_{\tau s} & \cos\theta_{\tau s} & 0 \\ -\sin\epsilon_{\mu e} & 0 & 0 & \cos\epsilon_{\mu e} \end{pmatrix}. \end{aligned} \tag{A-4}$$

The projection of the new proper basis $|\nu_d\rangle$ on to the flavor basis $|\nu_\alpha\rangle$ is

$$\langle \nu_\alpha | d_i \rangle = \left\{ \begin{pmatrix} \cos\epsilon_{\mu e} \\ 0 \\ 0 \\ \sin\epsilon_{\mu e} \end{pmatrix}, \begin{pmatrix} 0 \\ \cos\theta_{\tau s} \\ \sin\theta_{\tau s} \\ 0 \end{pmatrix}, \begin{pmatrix} 0 \\ -\sin\theta_{\tau s} \\ \cos\theta_{\tau s} \\ 0 \end{pmatrix}, \begin{pmatrix} -\sin\epsilon_{\mu e} \\ 0 \\ 0 \\ \cos\epsilon_{\mu e} \end{pmatrix} \right\}. \tag{A-5}$$

In the proper basis, the mass-squared part of the Hamiltonian is relatively block-diagonal. The full Hamiltonian is

$$\begin{aligned}\langle d_i | \mathbb{H} | d_j \rangle &= \langle d_i | \nu_\alpha \rangle \mathbb{H}_F \langle \nu_\beta | d_j \rangle \langle d_j | = \mathbb{U}_N \left(\mathbb{U} \frac{\mathbb{M}^2}{2E} \mathbb{U}^\dagger + \mathbb{A} \right) \mathbb{U}_N^\dagger \\ &= \begin{pmatrix} H_1^{atm} & H_3^{atm} & 0 & 0 \\ H_3^{atm} & H_2^{atm} & 0 & 0 \\ 0 & 0 & H_1^{sol} & H_3^{sol} \\ 0 & 0 & H_3^{sol} & H_2^{sol} \end{pmatrix} + \begin{pmatrix} H_1^A & 0 & 0 & H_6^A \\ 0 & H_2^A & H_5^A & 0 \\ 0 & H_5^A & H_3^A & 0 \\ H_6^A & 0 & 0 & H_4^A \end{pmatrix} \\ &= \begin{pmatrix} H_1^{atm} + H_1^A & H_3^{atm} & 0 & H_6^A \\ H_3^{atm} & H_2^{atm} + H_2^A & H_5^A & 0 \\ 0 & H_5^A & H_1^{sol} + H_3^A & H_3^{sol} \\ H_6^A & 0 & H_3^{sol} & H_2^{sol} + H_4^A \end{pmatrix} \langle d_j |, \end{aligned} \tag{A-6}$$

with

$$H_1^{atm} = \frac{\delta m^2_{atm}\cos^2\theta_{atm} + \delta m^2_{LSND} + \delta m^2_{sol}}{2E},$$
$$H_2^{atm} = \frac{\delta m^2_{atm}\sin^2\theta_{atm} + \delta m^2_{LSND} + \delta m^2_{sol}}{2E},$$
$$H_3^{atm} = \frac{\delta m^2_{atm}}{4E}\sin(2\theta_{atm}), \qquad H_1^{sol} = \frac{\delta m^2_{sol}}{2E}\cos^2\theta_{sol},$$
$$H_2^{sol} = \frac{\delta m^2_{sol}}{2E}\sin^2\theta_{sol}, \qquad H_3^{sol} = \frac{\delta m^2_{sol}}{4E}\sin(2\theta_{sol}),$$
$$H_1^{A} = \sqrt{2}N_eG_F\sin^2\epsilon_{\mu e}, \qquad H_2^{A} = \frac{\sqrt{2}}{2}N_eG_F\sin^2\theta_{\tau s},$$
$$H_3^{A} = \frac{\sqrt{2}}{2}N_eG_F\cos^2\theta_{\tau s}, \qquad H_4^{A} = \sqrt{2}N_eG_F\cos^2\epsilon_{\mu e},$$
$$H_5^{A} = \frac{N_eG_F}{2\sqrt{2}}\sin(2\theta_{\tau s}), \qquad H_6^{A} = \frac{\sqrt{2}}{2}N_eG_F\sin(2\epsilon_{\mu e}).$$

The motivation for going to this proper basis is to transform the Hamiltonian with matter effect into this relative simple structure, in which all the significant terms are within the relative block-diagonal parts and the off diagonal elements are relative smaller than the diagonal elements. In this form, the following discussions of the resonances and the perturbation calculations can be carried out much easier.

A.2 Possible Resonances

Due to the fact that the LSND mass gap δm^2_{LSND} is several orders bigger than the other two mass gaps, there are only two possible resonances in this Hamiltonian.

A.2.1 Atmospheric Resonance

The first resonance involves only the atmospheric mass gap, so it is called the atmospheric resonance. The atmospheric resonance happens between $|d_1\rangle$ and $|d_2\rangle$. For the atmospheric resonance to happen, the two diagonal elements of the sub-block must become equal:

$$H_1^{atm} + H_1^{A} = H_2^{atm} + H_2^{A}, \tag{A-7}$$

or

$$\frac{\sqrt{2}}{2}N_eG_F(\sin^2\theta_{\tau s} - 2\sin^2\epsilon_{\mu e}) = \frac{\delta m^2_{atm}}{2E}\cos(2\theta_{atm}). \tag{A-8}$$

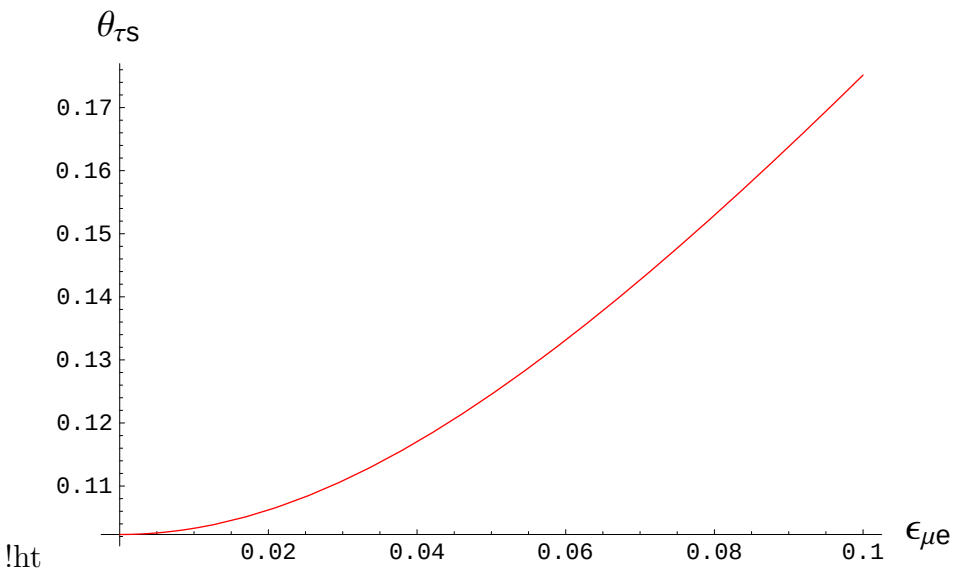

Figure 34: Parameter Values Yielding The Atmospheric Resonance, for $E = 100$ GeV

This leads to

$$\theta_{\tau s} = \sin^{-1}\sqrt{2\sin^2\epsilon_{\mu e} + \frac{\delta m^2_{atm}}{\sqrt{2}EN_eG_F}\cos(2\theta_{atm})}. \tag{A-9}$$

As an example, for $E = 100GeV$ and the other values take from Section 4.3, then the value of $\theta_{\tau s}$ that causes the resonance is within the range of $[0.10, 0.175]$, when the small mixing angle $\epsilon_{\mu e}$ is allowed to take any value within the allowed range $[0, 0.1]$. We show this result in Fig. 34.

These values correspond to the region around $R_{sol} \simeq 1$, when $0.10 \leq \theta_{\tau s} \leq 0.175$, in Fig. 27, which are not of interest here. So this resonance will not be studied in details.

A.2.2 Solar Resonance

The other possible resonance is between $|d_3\rangle$ and $|d_4\rangle$. It will involve only the solar mass gap. Thus it is called the solar resonance. The condition for this resonance to happen is

$$H_1^{sol} + H_3^A = H_2^{sol} + H_4^A, \tag{A-10}$$

or

$$\frac{\sqrt{2}}{2}N_eG_F(2\cos^2\epsilon_{\mu e} - \cos^2\theta_{\tau s}) = \frac{\delta m^2_{sol}}{2E}\cos(2\theta_{sol}). \tag{A-11}$$

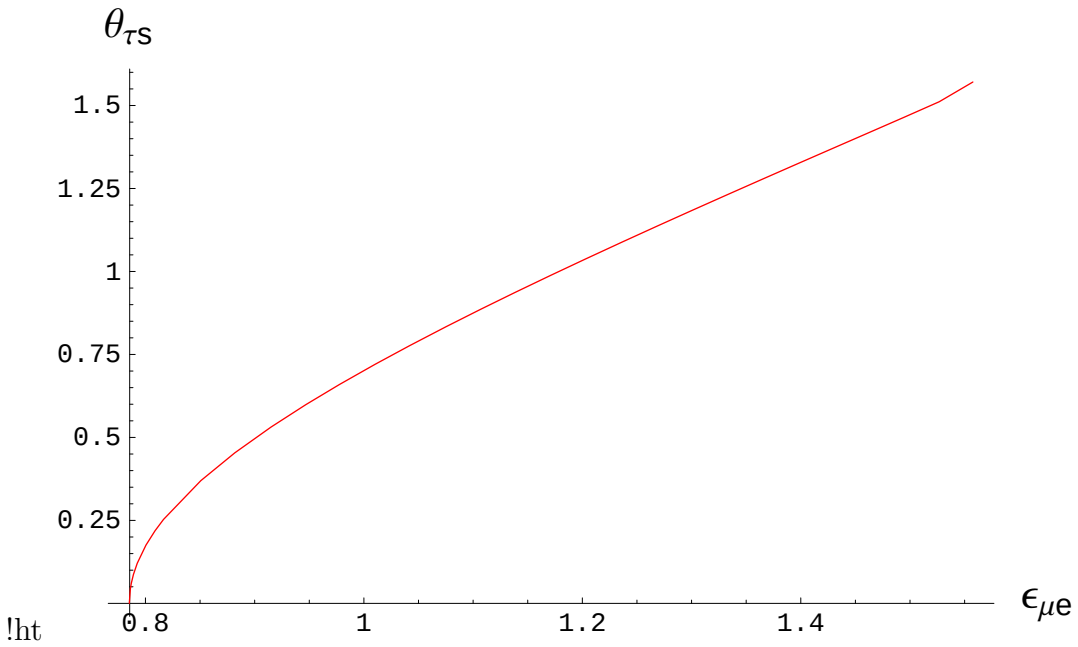

!ht

Figure 35: The Solar Resonance

This leads to

$$\theta_{\tau s} = \cos^{-1}\sqrt{2\cos^2\epsilon_{\mu e} - \frac{\delta m^2_{sol}}{\sqrt{2}EN_eG_F}\cos(2\theta_{sol})}. \qquad \text{(A-12)}$$

With $E = 100GeV$ as an example and the other values take from Section 4.3, the only possible solution to this equation requires $\epsilon_{\mu e} > 0.78$, as plotted in Fig. 35. This resonance does not occur within the allowed range of $\epsilon_{\mu e}$.

A.2.3 Resonances Are Not Essential

In the current study, only one of the small mixing angles $\epsilon_{\mu e}$ is allowed to be non-zero. This non-zero small mixing angle $\epsilon_{\mu e}$ introduces two possible resonances. One is the atmospheric resonance at $\theta_{\tau s} \in [0, 0.175]$, when the energy of the atmospheric neutrino is 100 GeV. The other one is the solar resonance at $\theta_{\tau s} \in [0.78, \pi/2]$ with the same energy. But this solar resonance requires the small mixing angle $\epsilon_{\mu e} > 0.78$, which is outside of the range allowed by the neutrino oscillation experiments. These resonances are between pairs of the proper basis $|\nu_d\rangle$, not the flavor basis $|\nu_\alpha\rangle$. But, the analysis of the resonances in the flavor basis is similar. Looking back to the plot with only $\epsilon_{\mu e}$ non-zero in Fig. 31, it is obvious that

the relaxation of the Sum Rule is not restricted to the region that $R_{sol} \sim 1$, thus it is not coming from the solar resonance. This conclusion is true at least for the data points with large value of $\theta_{\tau s}$, i.e. the data points with smaller values of R_{sol}.

If the other two small mixing angles are turned on, there may be more resonances, which may enhance the relaxation of the Sum Rule of the (2+2) neutrino model. However, other possible resonances will not be discussed here. Instead, we show that resonances are not essential for the relaxation of the Sum Rule of the (2+2) neutrino model.

A.3 Approximations

To simplify the analytic calculation, it will be assumed that the neutrino beam travels through earth with a uniform density given by the core. Also, only the up-going event with $\theta_z = 0$ will discussed, due to a reason to be revealed later in Section A.4.1. Thus, the following values are chosen as typical:

$$\delta m^2_{sol} = 3.65 \times 10^{-5}\ \text{eV}^2, \qquad \delta m^2_{atm} = 2.4 \times 10^{-3}\ \text{eV}^2,$$
$$\delta m^2_{LSND} = 1\ \text{eV}^2, \qquad \theta_{sol} = tan^{-1}\sqrt{0.37} \backsim 0.55 \backsim 31.3^o,$$
$$\theta_{atm} = 0.68 \backsim 5.7^o, \qquad |\epsilon_{\mu e}| \leq 0.1,$$
$$N_A = 6.02 \times 10^{23}, \qquad R_E = 6371\ \text{km},$$
$$N_e = N_n = N_{eEC} = 6N_A/cm^3, \qquad \theta_{\tau s} \gg 0.17,$$
$$E \sim 100\ \text{GeV}.$$

With these typical values, all the elements of the Hamiltonian can be evaluated. They are the following

$$H^{atm}_1 \backsim 5.0 \times 10^{-12}\ \text{eV}, \qquad H^{atm}_2 \backsim 5.0 \times 10^{-12}\ \text{eV},$$
$$H^{atm}_3 \backsim 5.9 \times 10^{-15}\ \text{eV}, \qquad H^{sol}_1 \backsim 1.3 \times 10^{-16}\ \text{eV},$$
$$H^{sol}_2 \backsim 4.9 \times 10^{-17}\ \text{eV}, \qquad H^{sol}_3 \backsim 8.1 \times 10^{-17}\ \text{eV},$$
$$H^{A}_1 \backsim 4.8 \times 10^{-13} \sin^2 \epsilon_{\mu e}\ \text{eV}, \qquad H^{A}_2 \backsim 2.4 \times 10^{-13} \sin^2 \theta_{\tau s}\ \text{eV},$$
$$H^{A}_3 \backsim 2.4 \times 10^{-13} \cos^2 \theta_{\tau s}\ \text{eV}, \qquad H^{A}_4 \backsim 4.8 \times 10^{-13} \cos^2 \epsilon_{\mu e}\ \text{eV},$$
$$H^{A}_5 \backsim 1.2 \times 10^{-13} \sin(2\theta_{\tau s})\ \text{eV}, \qquad H^{A}_6 \backsim 2.4 \times 10^{-13} \sin(2\epsilon_{\mu e})\ \text{eV}.$$

Especially, the typical values of the most interesting terms are

$$N_e G_F \backsim 3.4 \times 10^{-13} \text{ eV}, \qquad \frac{\delta m^2_{sol}}{E} \backsim 3.65 \times 10^{-16} \text{ eV},$$
$$\frac{\delta m^2_{atm}}{E} \backsim 2.4 \times 10^{-14} \text{ eV}, \qquad \frac{\delta m^2_{LSND}}{E} \backsim 10^{-11} \text{ eV}.$$

These typical values will help to identify the small elements in the Hamiltonian with matter, thus make it simple to carry out the perturbation calculation for the analytic study.

The Hamiltonian from Eqn. A-6 can be separated into two parts:

$$\mathbb{H}_0 = \begin{pmatrix} H_1^{atm} + H_1^A & H_3^{atm} & 0 & 0 \\ H_3^{atm} & H_2^{atm} + H_2^A & 0 & 0 \\ 0 & 0 & H_1^{sol} + H_3^A & H_3^{sol} \\ 0 & 0 & H_3^{sol} & H_2^{sol} + H_4^A \end{pmatrix}, \tag{A-13}$$

$$\mathbb{W} = \begin{pmatrix} 0 & 0 & 0 & H_6^A \\ 0 & 0 & H_5^A & 0 \\ 0 & H_5^A & 0 & 0 \\ H_6^A & 0 & 0 & 0 \end{pmatrix}. \tag{A-14}$$

The $\mathbb{W}$ term can be treated as a small perturbation to $\mathbb{H}_0$ if the off diagonal elements in $\mathbb{W}$ are much smaller than the difference between the corresponding diagonal elements in $\mathbb{H}_0$, i.e. if

$$\left|H_1^{atm} + H_1^A - H_2^{sol} - H_4^A\right| = \frac{\delta m^2_{atm} \cos^2\theta_{atm} + \delta m^2_{LSND} + \delta m^2_{sol} \cos^2\theta_{sol}}{2E} + \sqrt{2} N_e G_F \cos(2\epsilon_{\mu e})$$
$$\gg H_6^A = \frac{\sqrt{2}}{2} N_e G_F \sin(2\epsilon_{\mu e}), \tag{A-15}$$

and

$$\left|H_2^{atm} + H_2^A - H_1^{sol} - H_3^A\right| = \frac{\delta m^2_{atm} \sin^2\theta_{atm} + \delta m^2_{LSND} + \delta m^2_{sol} \sin^2\theta_{sol}}{2E} - \frac{\sqrt{2}}{2} N_e G_F \cos(2\theta_{\tau s})$$
$$\gg H_5^A = \frac{N_e G_F}{2\sqrt{2}} \sin(2\theta_{\tau s}). \tag{A-16}$$

We have verified with the numerical calculations that $\mathbb{W}$ can be totally discarded without losing much accuracy for the sterile neutrino oscillation probability $P_{\mu\to s}$, but not for the muon neutrino oscillation probability $P_{\mu\to\mu}$.

A.3.1 Approximate Solution for 2×2 Matrix

For a 2×2 matrix, such as $\begin{pmatrix} a & c \\ c & b \end{pmatrix}$, the eigenvalues and corresponding unnormalized eigenvectors are

$$\frac{a+b-\sqrt{(a-b)^2-4c^2}}{2} : \begin{pmatrix} \frac{a-b-\sqrt{(a-b)^2-4c^2}}{2c} \\ 1 \end{pmatrix},$$
$$\frac{a+b+\sqrt{(a-b)^2-4c^2}}{2} : \begin{pmatrix} \frac{a-b+\sqrt{(a-b)^2-4c^2}}{2c} \\ 1 \end{pmatrix}.$$

When $|a-b| \gg c$, and no matter which of a and b is bigger, the above eigensystem can be approximated up to the order of c^2, after normalization, as

$$a - \frac{c^2}{b-a} : \begin{pmatrix} 1 - \frac{c^2}{2(b-a)^2} \\ -\frac{c}{b-a} \end{pmatrix},$$
$$b + \frac{c^2}{b-a} : \begin{pmatrix} \frac{c}{b-a} \\ 1 - \frac{c^2}{2(b-a)^2} \end{pmatrix}.$$

A.3.2 Atmospheric Block

For the atmospheric block in H_0,

$$\begin{aligned} a =& H_1^{atm} + H_1^A \\ =& \frac{\delta m^2_{atm} \cos^2\theta_{atm} + \delta m^2_{LSND} + \delta m^2_{sol}}{2E} + \sqrt{2} N_e G_F \sin^2 \epsilon_{\mu e} \\ \simeq& \frac{\delta m^2_{LSND}}{2E}, \\ b =& H_2^{atm} + H_2^A \\ =& \frac{\delta m^2_{atm} \sin^2\theta_{atm} + \delta m^2_{LSND} + \delta m^2_{sol}}{2E} + \frac{\sqrt{2}}{2} N_e G_F \sin^2 \theta_{\tau s} \\ \simeq& \frac{\delta m^2_{LSND}}{2E}, \\ b - a =& \frac{N_e G_F (\sin^2\theta_{\tau s} - 2\sin^2\epsilon_{\mu e})}{\sqrt{2}} - \frac{\delta m^2_{atm}\cos(2\theta_{atm})}{2E} \qquad \text{(A-17)} \\ \simeq& \frac{N_e G_F (\sin^2\theta_{\tau s} - 2\sin^2\epsilon_{\mu e})}{\sqrt{2}}, \qquad \text{(A-18)} \\ c =& H_3^{atm} = \frac{\delta m^2_{atm}\sin(2\theta_{atm})}{4E}. \qquad \text{(A-19)} \end{aligned}$$

The approximation from Eqn. A-17 to Eqn. A-18 holds as long as $\sin^2\theta_{\tau s} - 2\sin^2\epsilon_{\mu e} \gg 10^{-2}$, i.e. $\theta_{\tau s} \gg 0.17$. This lower limit on $\theta_{\tau s}$ also guarantee the approximation condition $|a-b| \gg c$, and is consistent with our previous discussion at the end of Section A.2

So, the solutions for the atmospheric block are

$$E_1 = \frac{\delta m^2_{LSND}}{2E} : |E_1\rangle = \begin{pmatrix} 1 - U^2_{atm}/2 \\ -U_{atm} \end{pmatrix}, \tag{A-20}$$

$$E_2 = \frac{\delta m^2_{LSND}}{2E} : |E_2\rangle = \begin{pmatrix} U_{atm} \\ 1 - U^2_{atm}/2 \end{pmatrix}, \tag{A-21}$$

with

$$U_{atm} = \frac{\sin(2\theta_{atm})\delta m^2_{atm}}{2\sqrt{2}EN_eG_F(\sin^2\theta_{\tau s} - 2\sin^2\epsilon_{\mu e})}. \tag{A-22}$$

Another relation we will use is

$$E_2 - E_1 \simeq b - a \simeq \frac{1}{\sqrt{2}} N_e G_F(\sin^2\theta_{\tau s} - 2\sin^2\epsilon_{\mu e}). \tag{A-23}$$

$$\tag{A-24}$$

A.3.3 Solar Block

For the solar block in H_0,

$$\begin{aligned} a =& H_1^{sol} + H_3^A = \frac{\delta m^2_{sol}\cos^2\theta_{sol}}{2E} + \frac{\sqrt{2}}{2} N_e G_F \cos^2\theta_{\tau s} \\ \simeq& \frac{\sqrt{2}}{2} N_e G_F \cos^2\theta_{\tau s}, \end{aligned} \tag{A-25}$$

$$\begin{aligned} b =& H_2^{sol} + H_4^A = \frac{\delta m^2_{sol}\sin^2\theta_{sol}}{2E} + \sqrt{2} N_e G_F \cos^2\epsilon_{\mu e} \\ \simeq& \sqrt{2} N_e G_F \cos^2\epsilon_{\mu e}, \end{aligned} \tag{A-26}$$

$$\begin{aligned} b - a =& \frac{N_e G_F(2\cos^2\epsilon_{\mu e} - \cos^2\theta_{\tau s})}{\sqrt{2}} - \frac{\delta m^2_{sol}\cos(2\theta_{sol})}{2E} \\ \simeq& \frac{N_e G_F(2\cos^2\epsilon_{\mu e} - \cos^2\theta_{\tau s})}{\sqrt{2}}, \\ c =& H_3^{sol} = \frac{\delta m^2_{sol}\sin(2\theta_{sol})}{4E}. \end{aligned} \tag{A-27}$$

The approximation in Eqn. A-25 is valid as long as $\cos^2\theta_{\tau s} \gg 10^{-3}$, i.e. $\frac{\pi}{2} - \theta_{\tau s} \gg 0.03$. The approximation in Eqn. A-26 is always valid, as $\epsilon_{\mu e} < 0.1$ from the experimental limit. The

approximation in Eqn. A-27 is valid as long as $2\cos^2\epsilon_{\mu e} - \cos^2\theta_{\tau s} \gg 10^{-4}$. As $\epsilon_{\mu e} < 0.1$, this is always true. So, the solutions for the solar block are

$$E_3 = \frac{\sqrt{2}}{2} N_e G_F \cos^2\theta_{\tau s} : |E_3\rangle = \begin{pmatrix} 1 - U_{sol}^2/2 \\ -U_{sol} \end{pmatrix}, \tag{A-28}$$

$$E_4 = \sqrt{2} N_e G_F \cos^2\epsilon_{\mu e} : |E_4\rangle = \begin{pmatrix} U_{sol} \\ 1 - U_{sol}^2/2 \end{pmatrix}, \tag{A-29}$$

with

$$U_{sol} = \frac{\sin(2\theta_{sol})\delta m_{sol}^2}{2\sqrt{2}EN_eG_F(2\cos^2\epsilon_{\mu e} - \cos^2\theta_{\tau s})}. \tag{A-30}$$

Other relations to be used are

$$E_4 - E3 = \frac{N_e G_F(2\cos^2\epsilon_{\mu e} - \cos^2\theta_{\tau s})}{\sqrt{2}},$$

$$E_1 - E_3 \simeq E_1 - E_4 \simeq E_2 - E_3 \simeq E_2 - E_4 \simeq \frac{\delta m_{LSND}^2}{2E}.$$

A.3.4 Overall Transformation Matrix

Based on the eigensystems from the above calculations in Section A.3.3 and Section A.3.2, it is very easy to construct the transformation matrix between the diagonalized basis $|d_i\rangle$ and the energy basis $|E_i\rangle$. The result is

$$\begin{aligned} \mathbb{U}_{ed} &= \langle E_j | d_m \rangle \\ &= \begin{pmatrix} 1 - U_{atm}^2/2 & -U_{atm} & 0 & 0 \\ U_{atm} & 1 - U_{atm}^2/2 & 0 & 0 \\ 0 & 0 & 1 - U_{sol}^2/2 & -U_{sol} \\ 0 & 0 & U_{sol} & 1 - U_{sol}^2/2 \end{pmatrix}. \end{aligned} \tag{A-31}$$

So, the transformation matrix between the flavor basis $|\nu_\alpha\rangle$ and the energy basis $|E_i\rangle$ is:

$$\begin{aligned} \mathbb{U}_{ef} &= \langle E_i | d_m \rangle \langle d_n | \nu_\alpha \rangle = U_{ed} U_N \\ &= \begin{pmatrix} (1 - U_{atm}^2/2)\cos\epsilon_{\mu e} & -U_{atm}\cos\theta_{\tau s} & -U_{atm}\sin\theta_{\tau s} & (1 - U_{atm}^2/2)\sin\epsilon_{\mu e} \\ U_{atm}\cos\epsilon_{\mu e} & (1 - U_{atm}^2/2)\cos\theta_{\tau s} & (1 - U_{atm}^2/2)\sin\theta_{\tau s} & U_{atm}\sin\epsilon_{\mu e} \\ U_{sol}\sin\epsilon_{\mu e} & -(1 - U_{sol}^2/2)\sin\theta_{\tau s} & (1 - U_{sol}^2/2)\cos\theta_{\tau s} & -U_{sol}\cos\epsilon_{\mu e} \\ -(1 - U_{sol}^2/2)\sin\epsilon_{\mu e} & -U_{sol}\sin\theta_{\tau s} & U_{sol}\cos\theta_{\tau s} & (1 - U_{sol}^2/2)\cos\epsilon_{\mu e} \end{pmatrix}. \end{aligned} \tag{A-32}$$

A.3.5 Final State From Initial $|\nu_\mu\rangle$ Through Earth

From the above transformation matrix, Eqn. A-32, the initial state of the muon neutrino in the energy basis is

$$\langle E_i|\nu_\mu(0)\rangle = \mathbb{U}_{ef}\begin{pmatrix}1\\0\\0\\0\end{pmatrix} = \begin{pmatrix}(1-U_{atm}^2/2)\cos\epsilon_{\mu e}\\ U_{atm}\cos\epsilon_{\mu e}\\ U_{sol}\sin\epsilon_{\mu e}\\ -(1-U_{sol}^2/2)\sin\epsilon_{\mu e}\end{pmatrix}. \tag{A-33}$$

Thus the final state of the neutrino after traveling through the earth, with constant core density, is

$$\langle E_i|\nu_\mu(R)\rangle = \begin{pmatrix}e^{-iE_1R}(1-U_{atm}^2/2)\cos\epsilon_{\mu e}\\ -e^{-iE_2R}U_{atm}\cos\epsilon_{\mu e}\\ -e^{-iE_3R}U_{sol}\sin\epsilon_{\mu e}\\ -e^{-iE_4R}(1-U_{sol}^2/2)\sin\epsilon_{\mu e}\end{pmatrix}. \tag{A-34}$$

Converting this back to the flavor basis, one gets

$$\begin{aligned}\langle\nu_\alpha|\nu_\mu(R)\rangle &= U_{ef}^\dagger\langle E_i|\nu_\mu(R)\rangle\\ &= \begin{pmatrix}(1-U_{atm}^2/2)^2\cos^2\epsilon_{\mu e}e^{-iE_1R} - U_{atm}^2\cos^2\epsilon_{\mu e}e^{-iE_2R}\\ -U_{sol}^2\sin^2\epsilon_{\mu e}e^{-iE_3R} + (1-U_{sol}^2/2)^2\sin^2\epsilon_{\mu e}e^{-iE_4R}\\ \cdots\\ -(1-U_{atm}^2/2)U_{atm}\sin\theta_{\tau s}\cos\epsilon_{\mu e}(e^{-iE_1R}-e^{-iE_2R})\\ -(1-U_{sol}^2/2)U_{sol}\cos\theta_{\tau s}\sin\epsilon_{\mu e}(e^{-iE_4R}-e^{-iE_3R})\\ \cdots\end{pmatrix}.\end{aligned} \tag{A-35}$$

Finally, the desired oscillation amplitudes are obtained:

$$\begin{aligned}A_\mu &= (1-U_{atm}^2/2)^2\cos^2\epsilon_{\mu e}e^{-iE_1R} - U_{atm}^2\cos^2\epsilon_{\mu e}e^{-iE_2R}\\ &\quad -U_{sol}^2\sin^2\epsilon_{\mu e}e^{-iE_3R} + (1-U_{sol}^2/2)^2\sin^2\epsilon_{\mu e}e^{-iE_4R},\end{aligned} \tag{A-36}$$

$$\begin{aligned}A_s &= -(1-U_{atm}^2/2)U_{atm}\sin\theta_{\tau s}\cos\epsilon_{\mu e}(e^{-iE_1R}-e^{-iE_2R})\\ &\quad -(1-U_{sol}^2/2)U_{sol}\cos\theta_{\tau s}\sin\epsilon_{\mu e}(e^{-iE_4R}-e^{-iE_3R}).\end{aligned} \tag{A-37}$$

A.4 Oscillation Probability From $|\nu_\mu\rangle$ to $|\nu_s\rangle$

The neutrino oscillation probability from $|\nu_\mu\rangle$ to $|\nu_s\rangle$ is

$$\begin{aligned}
P_{\mu\to s} =& A_s \cdot A_s^* \\
=& \big[(1-U_{atm}^2/2)U_{atm}\sin\theta_{\tau s}\cos\epsilon_{\mu e}(e^{-iE_1R}-e^{-iE_2R}) \\
&+(1-U_{sol}^2/2)U_{sol}\cos\theta_{\tau s}\sin\epsilon_{\mu e}(e^{-iE_4R}-e^{-iE_3R})\big] \\
&\times\big[(1-U_{atm}^2/2)U_{atm}\sin\theta_{\tau s}\cos\epsilon_{\mu e}(e^{iE_1R}-e^{iE_2R}) \\
&+(1-U_{sol}^2/2)U_{sol}\cos\theta_{\tau s}\sin\epsilon_{\mu e}(e^{iE_4R}-e^{iE_3R})\big] \qquad \text{(A-38)} \\
=& 2(1-U_{atm}^2/2)^2U_{atm}^2\sin^2\theta_{\tau s}\cos^2\epsilon_{\mu e}\,[1-\cos(E_1-E_2)R] \\
&+2(1-U_{sol}^2/2)^2U_{sol}^2\cos^2\theta_{\tau s}\sin^2\epsilon_{\mu e}\,[1-\cos(E_4-E3)R] \\
&+\frac{1}{2}(1-U_{sol}^2/2)(1-U_{atm}^2/2)U_{sol}U_{atm}\sin(2\theta_{\tau s})\sin(2\epsilon_{\mu e}) \\
&\times[\cos(E_1-E_4)R-\cos(E_1-E_3)R-\cos(E_2-E_4)R+\cos(E_2-E_3)R]\,. \qquad \text{(A-39)}
\end{aligned}$$

From Eqn. A-28, A-29, A-20 and A-21, one has

$$E_4-E_1\simeq E_4-E_2\simeq E_3-E_1\simeq E_3-E_2\simeq\frac{\delta m^2_{LSND}}{2E}.$$

So, the last term in Eqn. A-39 can be neglected, because fast oscillations related to $\frac{\delta m^2_{LSND}}{2E}$ vanish when average on energy and oscillation path. Also, any terms of order higher than the second order of U_{sol} and U_{atm} can be neglected. Thus, the probability of $|\nu_\mu\rangle$ oscillation to $|\nu_s\rangle$ is, to a good approximation,

$$\begin{aligned}
P_{\mu\to s} &= 4U_{atm}^2\sin^2\theta_{\tau s}\cos^2\epsilon_{\mu e}\sin^2\frac{(E_2-E_1)R}{2}+4U_{sol}^2\cos^2\theta_{\tau s}\sin^2\epsilon_{\mu e}\sin^2\frac{(E_4-E_3)R}{2} \\
&= \frac{\sin^2(2\theta_{atm})\delta m^4_{atm}\sin^2\theta_{\tau s}\cos^2\epsilon_{\mu e}}{2(EN_eG_F)^2(\sin^2\theta_{\tau s}-2\sin^2\epsilon_{\mu e})^2}\sin^2[\frac{N_eG_FR}{2\sqrt{2}}(\sin^2\theta_{\tau s}-2\sin^2\epsilon_{\mu e})] \\
&+ \frac{\sin^2(2\theta_{sol})\delta m^4_{sol}\cos^2\theta_{\tau s}\sin^2\epsilon_{\mu e}}{2(EN_eG_F)^2(2\cos^2\epsilon_{\mu e}-\cos^2\theta_{\tau s})^2}\sin^2[\frac{N_eG_FR}{2\sqrt{2}}(2\cos^2\epsilon_{\mu e}-\cos^2\theta_{\tau s})]. \qquad \text{(A-40)}
\end{aligned}$$

A.4.1 Average Over Energy and Zenith Angle

There is a common factor of $\frac{1}{(EN_eG_F)^2}$ with the probabilities in Eqn. A-40. The average over neutrino energy of this factor is given by

$$\frac{1}{E_{max}-E_{min}}\int_{E_{min}}^{E_{max}}\frac{1}{E^2}dE=\frac{1}{E_{max}E_{min}}=\frac{1}{E^2_{eff}}, \qquad \text{(A-41)}$$

with $E_{eff} = \sqrt{E_{max}E_{min}}$. For the typical through-going energy range from 50 to 150 GeV, $E_{eff} = \sqrt{7500} = 87$ GeV. In the following calculation, $E_{eff} = 100$ GeV will be used for simplicity.

For the average over the zenith angle θ_z, or equivalently, the length through the earth R in Eqn. A-40 is not so easy to handle. The angular range is from $\cos\theta_z = 0$ to $\cos\theta_z = 0.8$, corresponding to lengths from $R = 2R_E = 12742$ km to $R = 1.6R_E = 10194$ km. This leads to phase changes for the terms in Eqn. A-40 up to a maximum of

$$0.4 N_e G_F R_E = 4.4. \tag{A-42}$$

A phase change of this scale is not large enough to be simply averaged out. So, a fixed traveling length through earth, $R = 2R_E$, will be used in the following discussion.

A.4.2 Approximation To the Order of $\epsilon_{\mu e}^2$

As $|\epsilon_{\mu e}| \leq 0.1$, valid approximations are

$$\begin{aligned} \sin\epsilon_{\mu e} &\simeq \epsilon_{\mu e}, \\ \cos\epsilon_{\mu e} &\simeq 1 - x^2/2. \end{aligned} \tag{A-43}$$

Also, as $\theta_{\tau s} \gg 0.17$, it can be shown that

$$\begin{aligned} \sin^2[\frac{N_e G_F R}{2\sqrt{2}}(\sin^2\theta_{\tau s} - 2\sin^2\epsilon_{\mu e})] &\simeq \sin^2[\frac{N_e G_F R}{2\sqrt{2}}\sin^2\theta_{\tau s}] \\ \sin^2[\frac{N_e G_F R}{2\sqrt{2}}(2\cos^2\epsilon_{\mu e} - \cos^2\theta_{\tau s})] &\simeq \sin^2[\frac{N_e G_F R}{2\sqrt{2}}(2 - \cos^2\theta_{\tau s})] \qquad \text{(A-44)} \\ &\simeq \sin^2[\frac{N_e G_F R}{2\sqrt{2}}(2 - \cos^2\theta_{\tau s})] \qquad \text{(A-45)} \end{aligned}$$

Putting these approximations into Eqn. A-40, and dropping any term of order higher than $\epsilon_{\mu e}^2$, one finds

$$\begin{aligned} P_{\mu\to s} &= \frac{\sin^2(2\theta_{atm})\delta m_{atm}^4 \sin^2\theta_{\tau s}\left(1 + \frac{4-\sin^2\theta_{\tau s}}{\sin^2\theta_{\tau s}}\epsilon_{\mu e}^2\right)}{2(EN_eG_F)^2\sin^4\theta_{\tau s}} \sin^2[\frac{N_e G_F R}{2\sqrt{2}}\sin^2\theta_{\tau s}] \\ &+ \frac{\sin^2(2\theta_{sol})\delta m_{sol}^4 \cos^2\theta_{\tau s}\epsilon_{\mu e}^2}{2(EN_eG_F)^2(1+\sin^2\theta_{\tau s})^2} \sin^2[\frac{N_e G_F R}{2\sqrt{2}}(2 - \cos^2\theta_{\tau s})] \end{aligned} \tag{A-46}$$

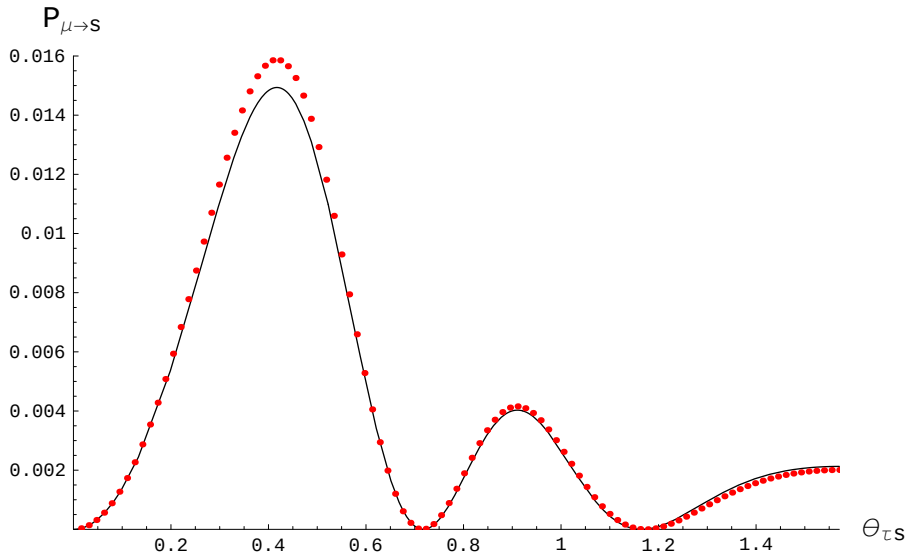

!ht

Figure 36: The Approximate Analytical $P_{\mu\to s}$ Compared with the Exact Numerical Result

Omitting terms of order $\epsilon_{\mu e}^2$, this becomes

$$P_{\mu\to s} = \frac{\sin^2(2\theta_{atm})\delta m_{atm}^4}{2(EN_eG_F)^2\sin^2\theta_{\tau s}}\sin^2[\frac{N_eG_FR}{2\sqrt{2}}\sin^2\theta_{\tau s}]. \qquad \text{(A-47)}$$

Fig. 36 shows the above result compared to the numerical results calculated with the same parameter settings. From Fig. 36, it is obvious that the approximate analytical $P_{\mu\to s}$ is very close to the exact numerical result with the same parameter settings. Thus, the non-zero $\epsilon_{\mu e}$ has very small effect on the sterile neutrino probability $P_{\mu\to s}$. Thus, the significant relaxation from the zeroth order Sum Rule is really due to the effect of the small angles on the muon neutrino probability $P_{\mu\to\mu}$, thus the on muon neutrino to non-muon neutrino probability, $P_{\mu\to\not\mu}$.

Another note worth mentioning here is the seemingly good agreement between the approximate result and the numerical result at small $\theta_{\tau s}$ in Fig. 36. As discussed in Section A.2, an atmospheric resonance will happen around $\theta_{\tau s} \sim 0.17$. Thus the above approximate approach should be valid only for the region $\theta_{\tau s} \gg 0.17$. So the near-perfect agreement with the numerical result around $\theta_{\tau s} \sim 0.17$ must be purely good luck. The more valuable result of this section is agreement within the region $\theta_{\tau s} \gg 0.17$, the interesting region in this study

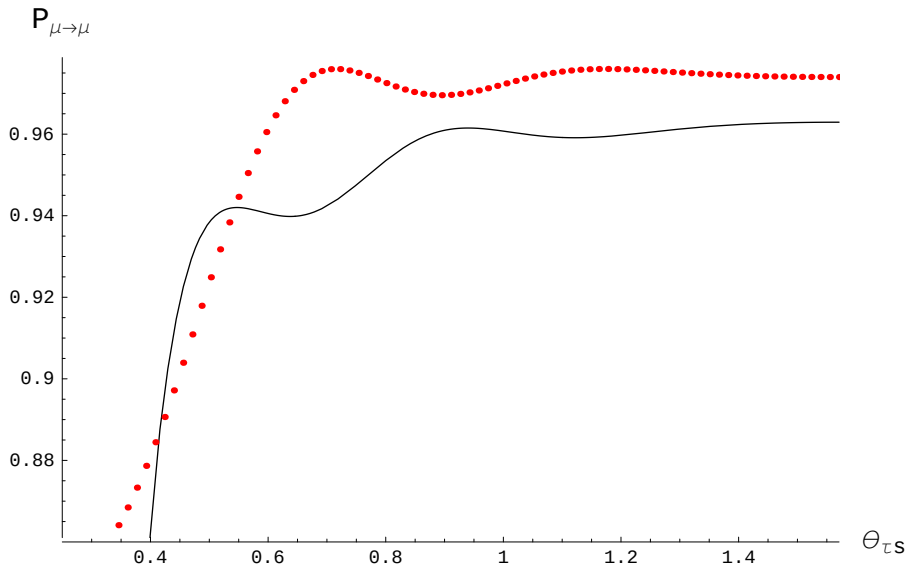

!ht

Figure 37: The Approximate Analytical $P_{\mu\to\mu}$ Compared with Exact Numerical Result

because the most significant relaxation of the Sum Rule happens within this region.

A.5 Muon Neutrino Oscillation Probability

From Eqn. A-36, the muon neutrino survival probability is

$$\begin{aligned} P_{\mu\to\mu} &= A_\mu \cdot A_\mu^* \\ &= \left\{(1-U_{atm}^2/2)^2\cos^2\epsilon_{\mu e}e^{-iE_1R} - U_{atm}^2\cos^2\epsilon_{\mu e}e^{-iE_2R}\right. \\ &+ \left.(1-U_{sol}^2/2)^2\sin^2\epsilon_{\mu e}e^{-iE_4R} - U_{sol}^2\sin^2\epsilon_{\mu e}e^{-iE_3R}\right\} \times C.C. \end{aligned} \tag{A-48}$$

Without any further approximation, Eqn. A-48 is plotted against the numerical results in Fig. 37, with the same parameters as in Fig. 36. It is seen that the zeroth order perturbation calculation for the Hamiltonian in matter here is not accurate enough for the muon neutrino survival probability. In order to achieve acceptable accuracy, the first order perturbation theory calculation has to be carried out. Nevertheless, some useful information can be extract here, without going into the first order perturbation calculation, Eqn. A-48 is still

accurate when $\epsilon_{\mu e} = 0$. In this limit, Eqn. A-48 becomes

$$P_{\mu\to\mu} = \left\{(1 - U_{atm}^2/2)^2 e^{-iE_1R} - U_{atm}^2 e^{-iE_2R}\right\} \times C.C. \tag{A-49}$$

and

$$\begin{aligned} U_{atm} &= \frac{\sin(2\theta_{atm})\delta m_{atm}^2}{2\sqrt{2}EN_eG_F\sin^2\theta_{\tau s}} \sim \frac{1.23\times10^{-8}}{\sin^2\theta_{\tau s}}, \\ E_2 - E_1 &= \frac{1}{\sqrt{2}}N_eG_F\sin^2\theta_{\tau s}. \end{aligned} \tag{A-50}$$

This gives a muon neutrino survival probability

$$\begin{aligned} P_{\mu\to\mu} &= (1 - U_{atm}^2/2)^2 - U_{atm}^4 - 2(1 - U_{atm}^2/2)^2 U_{atm}^2 \cos\left[(E_2 - E_1)R\right] \\ &= 1 - 2U_{atm}^2\left(1 + \cos\left[(E_2 - E_1)R\right]\right) \\ &+ U_{atm}^4\left(\frac{5}{2} + \cos\left[(E_2 - E_1)R\right]\right) - \frac{1}{2}U_{atm}^6 + \frac{1}{16}U_{atm}^8 \\ &\simeq 1 - 4U_{atm}^2\sin^2\left(\frac{E_2 - E_1}{2}R\right) + U_{atm}^4\left(\frac{5}{2} + \cos\left[(E_2 - E_1)R\right]\right). \end{aligned} \tag{A-51}$$

In the last step, the terms with order higher than U_{atm}^4 are dropped. Thus the non-muon neutrino oscillation probability is

$$\begin{aligned} P_{\mu\to\not\mu} &= 1 - P_{\mu\to\mu} \\ &= 4U_{atm}^2\sin^2\left(\frac{E_2 - E_1}{2}R\right) - U_{atm}^4\left(\frac{5}{2} + \cos\left[(E_2 - E_1)R\right]\right) \\ &= \frac{\sin^2(2\theta_{atm})\delta m_{atm}^4}{2(EN_eG_F)^2\sin^4\theta_{\tau s}}\sin^2\left(\frac{E_2 - E_1}{2}R\right) \\ &- \frac{\sin^4(2\theta_{atm})\delta m_{atm}^8}{64(EN_eG_F)^4\sin^8\theta_{\tau s}}\left(\frac{5}{2} + \cos\left[(E_2 - E_1)R\right]\right) \\ &= \frac{\sin^2(2\theta_{atm})\delta m_{atm}^4}{2(EN_eG_F)^2\sin^4\theta_{\tau s}}\sin^2\left(\frac{N_eG_FR}{2\sqrt{2}}\sin^2\theta_{\tau s}\right) \\ &- \frac{\sin^4(2\theta_{atm})\delta m_{atm}^8}{64(EN_eG_F)^4\sin^8\theta_{\tau s}}\left(\frac{5}{2} + \cos\left[\frac{N_eG_FR}{\sqrt{2}}\sin_{\tau s}^{\theta}\right]\right). \end{aligned} \tag{A-52}$$

Ignoring the last term is ignored in Eqn. A-52 for the moment, the non-muon oscillation probability is

$$P_{\mu\to\not\mu} = \frac{\sin^2(2\theta_{atm})\delta m_{atm}^4}{2EN_eG_F\sin^2\theta_{\tau s}}\sin^2\left(\frac{1}{2\sqrt{2}}N_eG_F\sin^2\theta_{\tau s}R\right). \tag{A-53}$$

Combining this with Eqn. A-47, the zeroth order perturbation calculation result of atmospheric ratio is

$$R_{atm} = \frac{P_{\mu\to s}}{P_{\mu\to\not\mu}} \simeq \sin^2\theta_{\tau s}. \tag{A-54}$$

This is exactly the atmospheric ratio for the zeroth order Sum Rule without matter effect discussed in Section 4.5. If the last term in Eqn.A-52 is not ignored, the value of $P_{\mu\to\not\mu}$ will be slightly smaller. Thus, the atmospheric ratio R_{atm} will be slightly bigger than the value of the zeroth order Sum Rule without matter, as in Eqn.A-54. This is exactly the reason why the zeroth order Sum Rule with matter, plotted in Fig.23, is slightly above the zeroth order Sum Rule without matter.

A.6 Conclusion

Through the analytic study in this section, it is proved that the small mixing angle $\epsilon_{\mu e}$ can introduce possible resonances into the oscillation when the matter effect is present. The same will probably be true for the other two small mixing angle $\epsilon_{\mu\mu}$ and ϵ_{ee}. These resonances will enhance the relaxation of the Sum Rule, but we find that they are not very significant. For the case with $\epsilon_{\mu e}$ non-zero, the relaxation from the zeroth order Sum Rule is the significant change of the muon neutrino oscillation probability caused by $\epsilon_{\mu e}$. Non-zero $\epsilon_{\mu e}$ can make the atmospheric ratio R_{atm} very small, thus can relax the Sum Rule significantly. The details of the muon probability change caused by $\epsilon_{\mu e}$ are worth more detailed study in the future.

Also, through the analysis in this section, it is proved that the Sum Rule is still a very good approximation when all the small mixing angles ϵ's are sent to zero and the matter effect is present. The presence of matter will cause the value R_{atm} to increase only slightly, thus explaining the tiny difference between the zeroth order Sum Rule with matter and the zeroth order Sum Rule without matter in Fig. 23.

REFERENCES

[1] E. W. Kolb and M. S. Turner, Redwood City, USA: Addison-Wesley (1990) 547 p. (Frontiers in physics, 69).

[2] The Wilkinson Microwave Anisotropy Probe (WMAP), http://map.gsfc.nasa.gov/.

[3] The Two Degree Field Galaxy Redshift Survey (2dFGRS), http://magnum.anu.edu.au/ TDFgg/.

[4] Sloan Digital Sky Survey (SDSS), http://www.sdss.org/.

[5] A. Dekel et al., Potent reconstruction from mark iii velocities, astro-ph/9812197, 1998.

[6] C.-P. Ma, Neutrinos and dark matter, astro-ph/9904001, 1998.

[7] J. R. Primack and M. A. K. Gross, Hot dark matter in cosmology, astro-ph/0007165, 2000.

[8] Z. Fodor, S. D. Katz, and A. Ringwald, JHEP **06**, 046 (2002).

[9] W. Pauli, *Rapp. Septieme Conseil Phys.*, Solvay, Brussels (Gautier-Villars, Paris, 1934)(1933).

[10] J. Chadwick, Nature **129**, 312 (1932).

[11] C. L. Cowan, F. Reines, F. B. Harrison, H. W. Kruse, and A. D. McGuire, Science **124**, 103 (1956).

[12] G. Danby et al., Phys. Rev. Lett. **9**, 36 (1962).

[13] K. Kodama et al., Phys. Lett. **B504**, 218 (2001).

[14] J. Davis, Raymond, D. S. Harmer, and K. C. Hoffman, Phys. Rev. Lett. **20**, 1205 (1968).

[15] T. Kajita, Nucl. Phys. Proc. Suppl. **77**, 123 (1999).

[16] B. T. Cleveland et al., Astrophys. J. **496**, 505 (1998).

[17] The Sudbury Neutrino Observatory (SNO), http://www.sno.phy.queensu.ca/.

[18] GALLEX Collaboration, http://www.mpi-hd.mpg.de/nuastro/gallex.html.

[19] Gallium Neutrino Observatory (GNO), http://www.lngs.infn.it/site/exppro/gno/Gno_home.htm.

[20] The RuSsian-American Gallium Experiment (SAGE),
http://ewiserver.npl.washington.edu/SAGE/SAGE.html.

[21] T. S. Experiment,
http://hepunx.rl.ac.uk/soudan2/.

[22] A. Monopole and C. R. O. (MARCO),
http://hep.bu.edu/ macro/.

[23] CERN Dortmund Heidelberg Saclay (CDHS),
http://knobloch.home.cern.ch/knobloch/cdhs/cdhs.html.

[24] Y. Declais et al., Nucl. Phys. **B434**, 503 (1995).

[25] CHOOZ Collaboration,
http://www.pi.infn.it/chooz/.

[26] KamLAND Collaboration,
http://www.awa.tohoku.ac.jp/html/KamLAND/index.html.

[27] the Liquid Scintillating Neutrino Detector (LSND),
http://www.neutrino.lanl.gov/LSND/.

[28] Super-Kamiokande Collaboration,
http://www-sk.icrr.u-tokyo.ac.jp/doc/sk/index.html.

[29] M. B. Smy, Nucl. Phys. Proc. Suppl. **118**, 25 (2003).

[30] KEK to Kamioka Long Baseline Experiment,
http://neutrino.kek.jp/.

[31] The Mini Booster Neutrino Experiment (miniBooNE),
http://www-boone.fnal.gov/.

[32] Main Injector Neutrino Oscillation Search (MINOS),
http://www-numi.fnal.gov/.

[33] M. Colless et al., The 2df galaxy redshift survey: Final data release, 2003.

[34] K. N. Abazajian, Astropart. Phys. **19**, 303 (2003).

[35] S. Hannestad, JCAP **0305**, 004 (2003).

[36] J. Bonn et al., Nucl. Phys. Proc. Suppl. **110**, 395 (2002).

[37] Karlsruhe Tritium Neutrino (KATRIN) Experiment,
http://www-ik.fzk.de/tritium/.

[38] F. Schwamm, AIP Conf. Proc. **605**, 461 (2002).

[39] S. M. Bilenky, A. Faessler, and F. Simkovic, The majorana neutrino masses, neutrinoless double beta decay and nuclear matrix elements, hep-ph/0402250, 2004.

[40] H. Paes and T. J. Weiler, Absolute neutrino masses: Physics beyond sm, double beta decay and cosmic rays, hep-ph/0205191, 2002.

[41] H. Paes and T. J. Weiler, Absolute neutrino mass update, hep-ph/0212194, 2002.

[42] H. Paes, L. Song, and T. J. Weiler, Phys. Rev. **D67**, 073019 (2003).

[43] G. B. Mills, Nucl. Phys. Proc. Suppl. **91**, 198 (2001).

[44] A. Aguilar et al., Phys. Rev. **D64**, 112007 (2001).

[45] A. Strumia, Phys. Lett. **B539**, 91 (2002).

[46] S. Pakvasa and J. W. F. Valle, Proc. Indian Natl. Sci. Acad. **70A**, 189 (,204).

[47] V. Barger, D. Marfatia, and A. Tregre, Neutrino mass limits from sdss, 2dfgrs and wmap, hep-ph/0312065, 2003.

[48] G. Bhattacharyya, H. Paes, L. Song, and T. J. Weiler, Phys. Lett. **B564**, 175 (2003).

[49] T. J. Weiler, Phys. Rev. Lett. **49**, 234 (1982).

[50] T. J. Weiler, Astrophys. J. **285**, 495 (1984).

[51] B. Eberle, A. Ringwald, L. Song, and T. J. Weiler, Relic neutrino absorption spectroscopy, hep-ph/0401203, 2004.

[52] S. Yoshida et al., AGASA Collaboration, Astropart. Phys. **3**, 105 (1995).

[53] D. J. Bird et al., HiRes Collaboration, Astrophys. J. **441**, 144 (1995).

[54] M. A. Lawrence et al., Haverah Park Collaboration, J. Phys. G **17**, 733 (1991).

[55] J. N. Bahcall and E. Waxman, Phys. Lett. B **556**, 1 (2003).

[56] M. Vietri, D. De Marco and D. Guetta, Astrophys. J. **592**, 378 (2003).

[57] T. Jacobson, S. Liberati and D. Mattingly, Phys. Rev. D **67**, 124011 (2003).

[58] C. Barbot and M. Drees, Astropart. Phys. **20**, 5 (2003).

[59] T. J. Weiler, Astropart. Phys. **11**, 303 (1999).

[60] H. Päs and T. J. Weiler, Astropart. Phys. **11**, 303 (1999).

[61] S. M. Bilenky, C. Giunti, J. A. Grifols and E. Masso, Phys. Rept. **379**, 69 (2003).

[62] Extreme Universe Space Observatory, http://www.euso-mission.org/.

[63] Orbiting Wide-angle Light-collectors,
http://owl.gsfc.nasa.gov/.

[64] IceCube,
http://icecube.wisc.edu/.

[65] Pierre Auger Observatory,
http://www.auger.org/.

[66] D. N. Spergel et al., Astrophys. J. Suppl. **148**, 175 (2003).

[67] K. Hagiwara et al. (Particle Data Group, http://pdg.lbl.gov), Phys. Rev. D **D66**, 010001 (2002).

[68] M. Tegmark et al., Cosmological Parameters from SDSS and WMAP, arXiv:astro-ph/0310723, 2004.

[69] G. V. Kulikov et al., JETP **35**, 635 (1958).

[70] M. Nagano and A. A. Watson, Rev. Mod. Phys. **72**, 689 (2000).

[71] K. L. Adelberger, C. C. Steidel, A. E. Shapley, and M. Pettini, Astrophys. J. **584**, 45 (2003).

[72] C. Steidel, K. Adelberger, M. Giavalisco, M. Dickinson, M. Pettini, and M. Kellogg, Galaxy clustering at $z \sim 3$, astro-ph/9805267, 1998.

[73] W. R. Mathematica, http://www.wolfram.com.

[74] W. L. Freedman and M. S. Turner, Rev. Mod. Phys. **75**, 1433 (2003).

[75] I. Kravchenko, Recent results from the rice experiment at the south pole, astro-ph/0306408, 2003.

[76] P. W. Gorham et al., Experimental limit on the cosmic diffuse ultra-high energy neutrino flux, astro-ph/0310232, 2003.

[77] N. G. Lehtinen, P. W. Gorham, A. R. Jacobson, and R. A. Roussel-Dupre, Phys. Rev. **D69**, 013008 (2004).

[78] ANtarctic Impulse Transient Array,
http://www.ps.uci.edu/ãnita.

[79] P. Gorham et al., Nucl. Instrum. Meth. **A490**, 476 (2002).

[80] E. D. Church, K. Eitel, G. B. Mills, and M. Steidl, Phys. Rev. **D66**, 013001 (2002).

[81] K. H. et al., Physical Review D **66**, 010001+ (2002).

[82] D. C. Latimer and D. J. Ernst, Three-neutrino model analysis of the world's oscillation data, nucl-th/0310083, 2003.

[83] O. L. G. Peres and A. Y. Smirnov, Nucl. Phys. **B599**, 3 (2001).

[84] J. N. Bahcall, Phys. Rev. Lett. **12**, 300 (1964).

[85] J. N. Bahcall, Scientific American **221**, 28 (1969).

[86] J. N. Bahcall and M. H. Pinsonneault, What do we (not) know theoretically about solar neutrino fluxes?, astro-ph/0402114, 2004.

[87] J. N. Bahcall, Phys. Rev. Lett. **23**, 251 (1969).

[88] J. N. Bahcall and J. Davis, Raymond, An account of the development of the solar neutrino problem, PRINT-81-0484 (IAS,PRINCETON).

[89] P. C. de Holanda and A. Y. Smirnov, JCAP **0302**, 001 (2003).

[90] P. C. de Holanda and A. Y. Smirnov, Phys. Rev. **D66**, 113005 (2002).

[91] A. Strumia, C. Cattadori, N. Ferrari, and F. Vissani, Phys. Lett. **B541**, 327 (2002).

[92] A. Bandyopadhyay, S. Choubey, S. Goswami, and D. P. Roy, Phys. Lett. **B540**, 14 (2002).

[93] Y. Fukuda et al., Phys. Rev. Lett. **81**, 1562 (1998).

[94] S. Fukuda et al., Phys. Rev. Lett. **85**, 3999 (2000).

[95] M. C. Gonzalez-Garcia, M. Maltoni, and C. Pena-Garay, Phys. Rev. **D64**, 093001 (2001).

[96] M. C. Gonzalez-Garcia, M. Maltoni, and C. Pena-Garay, (2001).

[97] M. Apollonio et al., Phys. Lett. **B466**, 415 (1999).

[98] C. Athanassopoulos et al., Phys. Rev. Lett. **81**, 1774 (1998).

[99] C. Athanassopoulos et al., Phys. Rev. **C58**, 2489 (1998).

[100] M. Maltoni, T. Schwetz, and J. W. F. Valle, Phys. Rev. **D65**, 093004 (2002).

[101] M. Maltoni, T. Schwetz, M. A. Tortola, and J. W. F. Valle, Nucl. Phys. **B643**, 321 (2002).

[102] M. Maltoni, T. Schwetz, M. A. Tortola, and J. W. F. Valle, Phys. Rev. **D67**, 013011 (2003).

[103] M. Maltoni, T. Schwetz, M. A. Tortola, and J. W. F. Valle, Nucl. Phys. Proc. Suppl. **114**, 203 (2003).

[104] L. Wolfenstein, Phys. Rev. **D17**, 2369 (1978).

[105] S. P. Mikheev and A. Y. Smirnov, Sov. J. Nucl. Phys. **42**, 913 (1985).

[106] T. K. Gaisser, Nucl. Phys. Proc. Suppl. **87**, 145 (2000).

[107] L. A. Anchordoqui, J. L. Feng, H. Goldberg, and A. D. Shapere, Phys. Rev. **D66**, 103002 (2002).